THE CITY COLLEGE

CITY UNIVERSITY OF NEW YORK

NEW YORK, N.Y. 10031

Technical Report

The Influence of Initial and Surface Boundary Conditions on a Model-Generated January Climatology

Kwok-Fung Wu

August 1981

NASA, Goddard Space Flight Center

Grant NGR 33-013-086

J. Spar, Prinicipal Investigator

Contents

Abstract

The influence on a model - generated January climate of various surface boundary conditions, as well as initial conditions, has been studied by using the GISS coarse-mesh climate model.

Four experiments - two with water planets, one with flat continents, and one with mountains - were used to investigate the effects of initial conditions , and the thermal and dynamical effects of the surface on the model generated-climate. However, climatological mean zonal-symmetric sea surface temperature (SST) is used in all four runs over the model oceans. Moreover, zero ground wetness and uniform ground albedo except for snow are used in the last two experiments.

Ensemble means and their differences were used for evaluation. The statistical significance of the results were determined by using the student's t-test. In addition, spherical harmonic analysis was employed for further comparison.

Initial conditions appear to represent a minor problem in climate simulation, if the first few months of the model-generated climate are discarded

The addition of continental surfaces results in a strong thermal influence in the lower troposphere together with mass exchanges between continents and oceans.

With the orography included in the last run, the model produces both beneficial and detrimental effects as compared with the observed climatology.

Introduction

As discussed by Spar (1981) ,general circulation models (GCM's) including the GISS coarse-mesh (8x10 degrees) climate model (Hansen,et al.,1980),are often used to perform "prescribed change" experiments in which the atmospheric response to some alteration in solar radiation, surface boundary conditions ,or atmospheric composition is calculated.In such experiments,the specified change is usually some perturbation of the basic constraints on the system, and the computed response of the model may be weaker than the background noise.

The analysis of these experiments would undoubtedly be aided by a better understanding of the ways in which the primary climatological controls combine and interact to generate the basic climatic state . It is also of interest to examine the influence of initial conditions on the model climate simulations.

Using both space and time averaging of the model's output in the analysis ,we may learn how certain characteristics of the large scale motion depend on surface conditions,even though the model contains certain defects.

There are still many fundamental questions in general circulation theory ,e.g.: What is the role of the semi-permanent centers (polar cyclones and subtropical anticyclones) ? Why are they located where they are ? How are the strengths and positions of the mean planetary waves and Hadley cells affected by the

distribution of mountains and land ? How do the troposphere and stratosphere respond to suface conditions in general?

Numerical climate models provide a tool that may help to answer those questions . In fact, many numerical experiments have been performed to improve our understanding of the theory of the general circulation in the last two decades. For example, Kasahara and Washington (1971) and Manabe and Terpstra (1974), have carried out numerical simulations to evaluate the thermal and dynamical effects of orography on the general circulation of the atmosphere. Of course, there are limits on how well the GCM can imitate the real world but it is of interest to investigate the GISS climate models' response to the various kind of surface conditions.

In this study,an attempt is made to compute the contributions of various surface boundary conditions to the monthly mean states generated by the 7- layer,8x10 GISS climate model(Hansen et.,1980).

For the purpose of the study,such obvious climate controls as the shape and rotation of the earth,the solar radiation,and the dry composition of the atmosphere are fixed, and only the surface boundary conditions are altered in the various climate simulations.

Model description

The GISS model of the global atmosphere is a three-dimensional primitive equation model using spherical geometry. The model numerically solves the simultaneous equations for conservation of mass , energy , and momentum, and the equation of state. The numerical differencing schemes for the dynamics are based on the work of Arakawa, with a time step of 15 minutes. Radiative heating and cooling are computed with a semi-implicit spectral integration which is accurate throughout the troposphere and stratosphere and includes all significant atmospheric gases, aerosols, and cloud particles. Cloud cover is computed by the model. Convection mixes moisture, sensible heat, and horizontal momentum in the vertical direction based on a model which permits penetration to an arbitrary height. The ground temperature is computed with a method which provides realistic simulation of both the diurnal variation of temperature and seasonal heat storage. Ground moisture is computed with a two layer model; the wetness of the upper layer responds rapidly to evaporation and precipitation while the deeper layer has a water holding capacity appropriate for the root zone of the regional vegetation. Snow depth is computed over land and ice with a simple mass budget model. Fluxes of sensible heat, moisture, and momentum between the surface and atmosphere are obtained from a drag-law formulation which employs a parameterization of the Monin-Obukhov similarity functions. Sea surface temperature and sea ice coverage are specified seasonally-

varying boundary conditions.

The model uses a grid of 24 points of latitude by 36 points of longitude, or about 8 x 10 degrees. This coarse horizontal resolution results in computing times an order of magnitude less than normally employed in general circulation models, allowing simulations of long time periods. To compensate for the great distance between grid points, the specified surface condition for each grid point represents appropriate fractions of land and ocean. Interactions between the surface and the atmosphere (radiation, momentum transfer, and latent and sensible heat fluxes) are computed separately for each surface type.

The seven vertical layers use a sigma coordinate, so that the ground is a coordinate surface. The top of the dynamically active portion of the atmosphere is fixed at 10 mb; the atmosphere above is radiatively interactive with the lower levels, with the temperature profile above 10 mb determined by radiative equilibrium.

The GISS climate model(version 660) is used to run four experiments in which the dynamic,radiation,and condensation routines use about 40%,30%,12% respectively of the total computing time. It takes approximately 2 hours of c.p.u time on a 360/95 IBM computer for a monthly simulation,while the surface routine consumes only from 3-4% of the computing time.
It is already well known that the model's surface temperature is too high in the summer hemisphere and too cold in the winter hemisphere over the continents.

Experiments and purpose

Four[1] perpetual January experiments were carried out using the GISS coarse mesh model. The model is operated at a fixed solar declination, specifically that of January 15, initialized on January 1 and allowed to simulate either 15 or 25 sucessive Januaries without going through the annual cycle. Furthermore, the results of the first 2 months of the first two experiments and the first 5 months of the last two runs are discarded as transients.

(1) Water planet experiment (run 1).

The first run is with a simple surface boundary condition with no land or continents, but with sea ice caps (3m thick) over the Arctic and Antartic. A fixed set of zonally uniform sea surface temperature(SST) at each grid latitude is prescribed by zonal averaging of the climatological monthly mean SST for January.

The model is initialized with monthly mean zonal values of the atmospheric history variables, including winds, taken from an earlier 5-year model climate simulation (Christidis and Spar, 1981) except for the surface pressure which is assigned a globally uniform initial value of 1010 mb. The model is run for 15 Januaries.

---

1 Six experiments have been conducted. This paper describes the first four experiments. The effects of surface physics and zonal asymmetry of the SST on the model generated climate are discussed by Cohen (1981).

(II) Water planet experiment (run 0)

The second run uses the same surface boundary conditions as run 1 ,but different initial condtions. The model is initialized with globally uniform mean values of sigma level specific humidities and temperatures,as well as a constant surface pressure (1010 mb) and zero wind.This is referred to as a " spin up " experiment. The model is again run for 15 'anuaries.

(III) Flat continents experiments (run 2)

The third run is a step closer to the real world by superimposing geographically realistic but topographically flat continents on the water planet with zero elevation above sea level, uniform roughness length (0.3 m), zero water storage capacity, and uniform surface albedo (0.14). The zonal distribution of sea ice and SST remain unchanged over the oceans.The initial conditions are the same as the water planet spin up experiment, and the model is run for 25 months.

(IV) Mountains experiment (run 3)

The fourth run is with a relatively realistic smooth topography in the model. The ground albedo is still kept uniform over the continents,except where snow is calculated , and the water storage capacity in this mountain run is also zero.

The model in this case is initialized not only with a state of rest, but also with completely dry isothermal atmosphere (273 K) so that the model takes some time to generate its own humidity and temperature distributions. The run is for 25 Januaries.

By differencing the two water planet ensemble means of horizontal and vertical fields, we can evaluate how much the initial conditions influenced the model climate. Next, the ensemble mean difference between 'flat continents' and 'water planet', which are based on identical initial conditions ,represents the influence of the flat land surface on the model climate. Finally the ' mountain ' run minus ' flat continents ' run reflects the role of topography on the model-generated climate.

Method of data analysis

The horizontal fields that we have used for analysis are divided into two parts . Part i includes the horizontal maps of 500 millibar (mb) height (G500), sea level pressure (SLP), the mean temperature in the layers between 1000-850 mb(T10-8) and 850-700mb (T8-7), and the surface air temperature (SAT). In part ii , the sensible heat flux, evaporation, low cloud cover and precipitation are shown. In addition, meridional cross sections of zonal means of temperature and the three components of the winds are illustrated.

To supplement the subjective analysis of these fields, the spectral components of the first three horizontal maps of part i listed above are examined using the method of spherical harmonic analysis described in Christidis and Spar (1981). Tables 1 and 2 list the degree (n) and order (m) of the ten leading harmonics (with the exception of the 0,0 component, which represents the global mean value) of SLP, G500 and T10-8 for runs 1, 0, 2, and 3. For the n,m-th harmomic, m is the zonal (longitudinal) wave number,while n-m represents the number of nodal parallels. Also tabulated are the amplitude (A), in physical units, and the phase angle (b), in

degrees, of each harmonic.

As in Chervin (1980a,b) , the results are analyzed by computing ,for each experiment,ensemble means and ensemble standard deviations of the 13 or 20 Januaries. These statistics are then used to calculate,with the standard student's t-test, the confidence levels at which the ensemble means of each pair of experiments can be judged to be significantly different. For details and definitions, see Cohen (1981).

Contour maps and cross-sections of significance level are then plotted with contour lines of .01, .05 , and multiples of 0.10. On these maps and cross-sections, large continuous areas where the differences between the ensemble means are significant at the 1% level appear as clear areas, and areas where the difference are not significant i.e.,where the "signal" cannot be seen through the "noise", are generally covered with closely spaced contour lines in multiples of .10. In a few cases ,small clear areas appear in regions that show no statistically significant difference, necessitating numerical labels on the contour lines.

The maps and cross-sections of significance levels should be examined in conjunction with the maps of differences between ensemble means, since there can , of course ,be no statistical significance where the means are exactly equal. Statistical significance is a result of a difference between two ensemble means that is large compared to the ensemble standard deviations; therefore, there can be some cases where differences too small to be physically interesting are nevertheless statistically significant, and some cases where very large difference are not significant.

Table 1

Comparison of dominant spherical harmonic components

(See text for details)

Sea-level pressure (mb)

run 1			run 0			run2			run3		
n,m	A	b	n,m	A	b	n,m	A	b	n,m	A	b
4,0	9.6	180	4,0	8.9	180	4,0	10.0	180	1,0	11.4	0
2,0	7.1	180	2,0	6.7	180	2,0	5.6	180	4,0	7.4	180
6,0	3.6	0	6,0	3.4	0	1,1	5.3	165	1,1	7.0	167
6,0	3.4	0	6,0	3.3	0	3,2	5.2	230	2,0	6.9	0
8,0	3.0	180	1,0	2.8	180	4,4	4.2	305	3,2	5.0	233
1,0	3.0	180	3,0	2.3	180	5,4	3.6	136	4,4	4.7	295
10,0	1.1	0	5,0	2.0	0	3,3	3.6	265	3,0	4.6	0
11,0	1.1	0	10,0	1.2	0	2,2	3.6	154	5,4	4.5	124
18,0	0.9	180	18,0	1.0	180	2,1	3.3	96	5,2	4.4	127
5,0	0.7	0	7,0	1.0	0	3,0	3.2	180	8,0	4.3	0

500 mb height (meters)

run 1			run 0			run2			run3		
n,m	A	b	n,m	A	b	n,m	A	b	n,m	A	b
2,0	791	180	2,0	785	180	2,0	885	180	2,0	836	180
1,0	129	180	1,0	132	180	1,0	293	180	1,0	264	180
4,0	82	180	4,0	78	180	4,0	96	160	4,0	95.6	180
7,0	45	180	7,0	37	180	8,0	55	180	6,0	73	0
8,0	39	180	8,0	36	180	7,0	49	180	8,0	44	180
6,0	31	180	6,0	32	180	6,0	49	0	7,0	43	180
6,0	29	0	6,0	27	0	3,0	34	180	6,2	39	38
15,0	21	0	15,0	20	0	15,0	25	0	5,2	39	31
5,0	15	180	10,0	14	0	4,2	24	20	7,2	32	45
10,0	13	0	9,0	13	180	7,1	23	85	5,3	31	236

Table 2

Comparison of dominant spherical harmonic components

(See text for details)

Temperature between 1000 and 850 mb (K)

run 1			run 0			run2			run3		
n,m	A	b	n,m	A	b	n,m	A	b	n,m	A	b
2,0	35.7	180	2,0	35.6	180	2,0	46.	180	2,0	46.7	180
1,0	6.0	180	1,0	6.0	180	1,0	17.6	180	1,0	19.4	180
7,0	4.1	180	7,0	4.0	180	3,2	5.5	38	3,0	6.2	180
5,0	3.5	180	5,0	3.5	180	4,4	5.0	124	4,4	5.5	113
8,0	3.0	180	3,0	3.0	180	6,0	4.6	180	1,1	5.3	5.3
3,0	3.0	180	8,0	2.9	180	1,1	4.4	344	3,2	5.2	55
4,0	2.3	180	4,0	2.2	180	4,2	4.1	359	5,4	4.8	320
15,0	2.2	0	15,0	2.2	0	7,0	3.9	180	8,0	4.7	180
17,0	1.9	0	17,0	1.9	0	3,3	3.7	104	4,1	4.6	274
14,0	1.8	0	14,0	1.8	0	3,1	3.4	246	5,2	4.3	319

I. The effects of initial conditions on water planet experiments: differences between run 0 and run 1

The evolution of the two water planet climatologies has been described by Spar (1981) . In this paper we discuss the mean climatic states which have been averaged from the last 13 months of each water planet experiment.

Horizontal fields (part 1)

Although both runs began with different initial states, briefly one (#1) with winds and meridional gradients(but uniform surface pressure) and the other (#0) with a horizontally uniform state of rest, as mentioned previously, the results indicate that the model generates almost the same climatologies for the two runs. All mean variables generally show a predominately zonal symmetric character, as expected from the forcing by zonal symmetric surface boundary conditions (the fixed zonal SST and uniform ice caps), although, waves and cells are found on the individual January maps.

The mean sea level pressure (SLP) maps of run 0 and run 1 (fig. 1a) show general agreement in the zonal mass distributions, although, there is more cellular structure in run 1 than in run 0, probably due to the mutual adjustment of the initially unbalanced surface winds and pressure in run 1. Likewise, standard deviations of SLP computed from the 13 individual monthly data of run 1 (fig.1b) show higher magnitudes(more fluctuations) than run 0 .Differences between the two fields are shown in the difference map (fig. 1c) for the two runs,where dashed lines indicate positive differences (higher SLP) and dotted lines denote negative differences (lower SLP). The differences are generally

less than 3 or 4 mb.Student's t-test shows generally no statistical significance for the differences between the means, except for a few grid points in the Southern Hemisphere.

Meridional profiles of the zonal mean SLP for both runs are shown in figure 1d.(Run 1 is indicated by solid lines,while asterisks denote run 0.) One can see the general agreement between the two runs with a broad ,near-equatorial low pressure belt centered at 4 N, subtropical highs,subpolar lows and an Antarctic high in both runs. The minor differences between the two runs can be seen especially over the polar ice caps. The climatological observed zonal mean SLP profile is also shown in the same figure(heavy dash curve). As can be seen, there is generally good agreement of the water planet SLP profile with the observed in most of the tropics, although the magnitude is slightly lower.

Other mean horizontal variables , For example , geopotential height of 500 mb (G500) and 700 mb surfaces , and mean layer temperatures for both runs , also show predominantly zonal symmetric structures. As noted by Spar(1981), those fields remain nearly constant during the 15 months of run 1.Figures 1e-1f display the meridional profiles of the zonal means of G500, the surface air temperature (SAT) and SST,and the layer temperature (T8-7), respectively, for both runs. The 500mb surface, in agreement with the temperature profile, shows a maximum height over the warm tropics and decreasing heights toward the cold polar regions for both runs. The strength of the westerlies in both hemispheres (as indicated by the gradient of geopotential) is about the same , but the northern westerlies occupy a broader region.

The mean zonal SST in figure 1e indicated by '$' signs is the fixed surface boundary condition for all three experiments. Note that the gradient of SST in the Northern Hemisphere is greater than that of the Southern Hemisphere.However, it decreases at around 60N, and the SST at 67N reaches a minimum of 3.8°C which is 4 degree C warmer than at the same latitude in the Southern Hemisphere. The mean surface air temperatures for both runs (denoted by the solid lines for $1 and asterisks for $0) parallel the SST,especially over the Southern Hemisphere,but are generally cooler than SST. For example, at 67N, the SAT is about 4°C cooler than the SST,indicating strong sensible heat flux from the ocean to the atmosphere. Another striking feature in fig.1e is the sharp decline of SAT of more than 30 degrees C between the ocean and the northern polar ice cap. At higher levels over the Nothern Hemisphere a more gentle temperature gradient (fig. 1e) is found from the middle latitudes to the pole, while the sharp temperature drop between the ocean and the ice boundary is reduced to less than 10°C in the layer 850-700mb.

The mean difference maps for T8-7 and G500. (figs.1f to 1g) both reflect features similar to those found on the SLP map (fig. 1c). The surface air temperature differences (fig.1g) appear only over the winter ice cap, and these are not statistically significant. Overall,the standard deviations of all these variables show generally higher values than their mean differences. Thus,the student's t-tests are similar to that of SLP with no statistical significance in general.

Spherical harmonic analysis

For further objective comparison of horizontal fields, spherical harmonic analysis was employed. Table 1 displays the first ten leading harmonics of SLP and G500, and Table 2 shows those for the layer temperature from 1000-850 mb.

For both run 1 and 0, only zonal harmonics are found among the ten leading harmonics, which confirms the dominant zonal symmetric character of the water planet climatology. Both runs generate very similar large scale structures. For SLP (Table 1) the (4,0) and (2,0) are the first two leading harmonics, both with 180 degrees phase, representing the equatorial low pressure, two subtropical highs, and polar lows and the difference between the poles and equator, respectively. Also the first 4 leading harmonics of SLP are nearly the same for the two runs , and 5 of the 6 remaining harmonics appear in both runs with the same phases and, with the exception of (5,0), nearly the same amplitude. For the T10-8 , all 10 harmonics are virtually identical for the two runs, while for G500, the same is true for 9 of the first 10 terms. Except for SLP, the 1,0 harmonic appears as either the second or third leading harmonic, indicating the warm Southern Hemisphere.

As discussed previously, the relatively warm ocean temperature at 67N provides a considerable amount of surface heat flux to the atmosphere in this region, as shown in figure 1h for both runs. Relatively minor peaks can also be seen in both subtropical highs. Overall, in the absence of any land surface, sensible heat flux from the surface seems to be a very small quantity in the water planet experiments, due to the rapid adjustment of SAT to SST. On the other hand, evaporative heat flux from the ocean surface is a major source of energy. From the meridional profile of zonal mean surface evaporation (fig. 1h) , strong evaporation takes place around 27N, where sinking air of the subtropical high is relatively dry. Transported by the surface trade winds to the equatorial region, this moisture condenses out as it ascends, and the latent heat released helps to drive the Hadley cell, as is well known. It should also be mentioned that the amount of long wave thermal energy radiated from the surface is also considerable . Unlike evaporation, which dominates mainly over much of the tropics, it plays an important role everywhere, especially in the Southern Hemisphere where evaporation and sensible heat flux are small.

The mean zonal precipitation profile (fig.1i) indicates a band of maximum rainfall over 4N where the SST is a maximum, in agreement with the results of Manabe et al. (1974). A secondary precipitation maximum is found over 35N where the model generates some transient eddies. A third band of convective rainfall can also be seen over 67N. It is interesting to compare this water planet zonal precipitation with the climatological precipitation over the Pacific Ocean as recently calculated by Dorman and Bourke (1979) (fig. 1i). Although their data is for the whole winter season rather than Jan-

mary alone, one can see the similarity of the band of maximum precipitation at around 4N. The mean difference of precipitation (fig.1j) between two runs is generally less than a millimeter per day in the Northern Hemisphere and almost zero everywhere in the Southern Hemisphere, with no statistical significance.

Meridional cross-sections

Mean meridional cross-sections of the temperature (in degrees C) of run 0 and 1 respectively, are shown in figure 1k . There are no apparent differences between the two temperature cross-sections. As noted by Spar (1981),the temperature cross-sections exhibit some of the defects of the model simulation. The tropical tropopause is too low and too warm. However, the tropospheric structure of the model atmosphere is not unrealistic. The difference between the two cross-sections(fig.1l), shows temperature differences close to zero in most of the troposphere. Differences of 1 °C can be found in both polar regions, but the high variances of both runs result in no statistical significance in those regions. Nevertheless,in higher southern latitudes (e.g., near 51S) temperature difference of 0.5 °C can be found near the 500 mb level.This is the same zonal area where large residual differences are located, as seen earlier in the mean difference maps.The student's t-test verified the existence of significance for the differences in this area.Therefore, a time series of temperatures at this point was made to see whether this zonal mean difference could be due to the difference of the first few months. As can be seen from figure 1l ,at the end of the first month run 0 (solid line) shows a warmer temperature (more than 2 °C higher) than run 1. After 2 months,the two temperatures are much closer,and it seems reasonable to have deleted the first 2 months as transients

before averaging. However,oscillations begin to occur after the 7th month. With zonal mean differences of 2 °C appearing in the 9th and 15th months, both curves tend to return to the condition of the first month.Thus ,this may indicate, at least over the 15 perpetual January period from which the 13-year mean was computed, that the effect of initial states may be of some minor importance in the climate simulation.

Meridional cross-sections of the zonal wind (in tenths of meters per second,abbr. m/sec) for run 0 and 1 are shown in fig. 1m. Solid lines indicate westerly components.From inspection, the two cross-sections show considerable similarity,with the exception of the equatorial easterlies which appear in the stratosphere of run 1. The mean difference cross-sections (fig.1n),shows differences of 6 m/sec in this region.The standard deviations of run 1 (fig.1n) in this region are generally less than 3m/sec, and the differences are found to be statistically significant over this area. A time series of the mean zonal wind at 32 mb over the Equator is plotted and shown in figure 1o . Run 1 (dashed line) was initialized with excessively strong equatorial stratospheric easterlies as compared to run 0 (solid line), as indicated by the results for the first month. It took almost 5 Januaries for the zonal winds in run 1 to reach a magnitude close to that of run 0. Furthermore, there are indications that in both runs, the easterlies tend to diminish further in the last 3 months of simulation.

Cross-sections of the zonal mean meridional wind components (in units of tenths of m/sec)for run 0 and 1 are shown in figure 1p. Solid curves are drawn for positive (southerly) components and dotted curves for negative (northerly) components. The convergence of the low-level trade winds toward an ITCZ at 4N and divergence aloft clearly defines the Hadley cell.The circulation in the northern part

of the cell is more uniform and stronger than that in the south. A weak convergence at the surface can also be seen over 67N where the subpolar low is located. The mean difference of the two meridional wind cross-sections (fig. 1q) shows generally a small difference, mostly at the surface, and also some minor variations in the Hadley circulation over the tropics.

The mean cross-sections of vertical wind for run 0 and run 1 are shown in figure 1r. One can see clearly the strong upward motion (solid curves) at 4N and a strong sinking motion (dotted curves) in the northern tropics and subtropics for both runs. However, much weaker sinking is found in the southern branch where the air is prevented from further subsidence because of strong diabatic heating as well as a weak low level surface convergence at 27S. The zonal mean difference cross-section of vertical motion (fig. 1q) again shows only a minor change in the Hadley cell, as well as in the polar region, as a result of different initial conditions. The maximum differences are generally an order of magnitude smaller than the maximum vertical velocities themselves. Again, student's t-test shows no significant difference.

II. The thermal effects of flat dry continents: differences between run 2 and run 0

As described by Spar (1981),the model in the perpetual January mode produces excessive snow accumulation over the continents of the Northern Hemisphere,as well as a somewhat unrealistic continental snow line, especially in run 2 . However,the later does stablize between about 30N and 45N and the model does not produce catastrophic glaciation of the Northern Hemisphere. Thus ,the averaging of the last 20 months of run 2 may be used to represent the mean climatology of the flat dry continents model.

Horizontal fields (part 1)

In higher latitudes north of 65N over continents, the SAT of run 2 (fig. 2a) shows a band of extremely cold temperature (-40 °C), the result of no insolation and insufficient warm advection. Over northern Greenland, temperature as low as -55 degrees can be seen. The snow line on the northern continents corresponds to approximately the zero (°C) isotherm (solid lines) of the SAT. The accumulation of snow on the flat dry continents has significantly increased the ground albedo, as compared to the water planet, by 10% over 35N to almost 70% at higher latitudes. In contrast, temperatures as high as 35 °C can be found over the tropical and southern continents due to direct heating of the ground. Over the oceans, the SAT map shows generally zonal isotherms ,which indicate the strong influence of the SST.

The layer temperature from 1000-850mb (not shown) reflects a similar pattern. In general, over the ocean,the temperature of this layer is a few degrees (e.g., 3 °C) colder than SAT. Conversely,temperatures more than 10 °C higher than SAT are found over the cold

northern continents, indicating a very stable lapse rate,while over southern continents, temperatures at least 3°C higher than SAT are found. In the higher layer from 850-700mb , the horizontal T8-7 gradient (fig. 2a) in the Northern Hemisphere,is much weaker than in the lower layer. However, the warming influence of the tropical and southern continents has spread over the adjacent ocean, as can be seen by the 285K isotherm.This warming is mainly due to the flow around the southern subtropical highs at the 700 or 500 mb level. Here ,energy in the form of latent and sensible heat is transported from land to ocean. As the hot continental air flows over relatively cool ocean low clouds form over many parts of the ocean.

Further evaluation of the thermal influence of the flat dry continents can be made using the temperature difference maps for SAT and T8-7 in figures 2b to 2c ,which are accompanied by maps illustrating the significance levels of the mean differences. We can clearly see the warmer temperatures over the southern continents and colder temperatures over the continents of the Northern Hemisphere. Furthermore,the significance maps for both levels indicate that significant differences exist over the continents. The temperature differences over the northern continents decrease markedly with increasing height,but the influence of the cold Eurasian land mass on T8-7, which extends eastward off the coast of Japan, is greater than that of North America. The thermal influence of the continents over the Southern Hemisphere oceans, noted above with respect to SAT,also appears in the mean difference and significance maps for T8-7. For example, significant mean differences of about +2 °C cover the South Atlantic as well as many parts of the Pacific and Indian Oceans.

Without orographic effects, the SLP of run 2 (fig.2d) shows a relatively weak pressure gradient and a generally smooth pattern.The Canadian and Siberian highs are centered around 35N,where the latter has a maximum SLP of 1025 mb and extends eastward to the ocean. A small but weak Aleutian low is detectable in the Bering Strait, and the Icelandic low,with central pressure about 995 mb,stretches from west of Iceland to western Scandinavia.Both lows are confined to the southern boundary of the north rn polar ice cap. Low SLP is found over all three warm southern continents,where low level convergence from the ocean takes place. At the same time, divergence aloft, which transports air masses back to the adjacent oceans, maintains the subtropical highs over the southern oceans.

The mass exchange between the continents and oceans can best be examined in terms of the mean difference of SLP (Fig.2e) and the corresponding significance map.Again, the dominant features of a Siberian high, southern continental lows,and subtropical highs are all reflected in these maps. However,the Canadian high is very weak and barely significant over much of the area. Furthermore, a tongue of significantly negative pressure difference of 4 mb extends from south west of Iceland towards the northeast, and stretches eastward over much of the northern polar ice cap. Also an area of significantly lower pressure can be found over the cool ocean west of the United States.

The mean zonal SLP profile of run 2 (dashed lines) is shown in figure 1d. As compared with run 0 (asterisks), it shows slightly higher pressure north of 30N and lower pressure over the northern polar region, as discussed earlier. The continental heating effect has also induced a generally lower pressure over the southern tropics, with the minimum shifted to around 20S. This SLP profile is

still much too low in higher northern latitudes,while the reverse is true over higher southern latitudes, as compared to the observed SLP. The locations of maximum subtropical high pressure in both hemispheres generated by the model (both run 0 and 2) are slightly poleward of the observed peaks, and the northern subtropical high is still relatively low.

The 500 mb heights in run 2 (fig. 2d) show a generally zonal symmetric character outside the tropics in both hemispheres. A very weak trough over Japan and also a weak ridge over the north Atlantic Ocean can barely be seen. The southern subtropical highs centered over the three continents now extend over much of the oceans, as discussed earlier. Unlike the 700 mb surface, the subtropical highs at 500mb are generally weaker and broken into individual cells. The hydrostatic effects of the cold northern (winter)continents and warm southern (summer) continents on the 500 mb surface are reflected in the mean difference and significance map (fig.2f). The decrease (increase) in 500mb height over northern (southern) continents results in stronger westerlies in both hemispheres. Significant warm effects over the tropical and southern oceans are also reflected in this 500mb height difference map.

Spherical harmonic analysis

With the presence of longitudinal variations, zonal wave numbers (m) greater than zero are expected to appear in the spherical harmonic analysis. However, from the calculations for SLP,G500 and T10-8 (Tables 1 and 2), the first two or more leading harmonics are basically the same as for the water planet runs and are still dominated by the zonal symmetric components (m equal to zero) despite the increased influence of small scale cellular patterns.

For SLP of run 8, the same (4,0 and 2,0) zonal symmetric harmonics (both with a phase of 180 degrees) are still the two leading harmonics as in run 0. Under the influence of mass exchanges between the continents and oceans, zonal wave numbers of 1,2,3,and 4 have begun to appear among the rest of the seven leading harmonics. For example, the third harmonic (1,1), represents the dominance of the Asiatic anticyclone, followed by the (3,2) harmonic which indicates the Siberian and Canadian high pressure cells, with reversal of phase in the Southern Hemisphere. Preceded by two harmonics with zonal wave number of 4 ,the (3,3) harmonic reflects the 3-cell structure in the Southern Hemisphere. Finally, the tenth harmonic component is a zonal symmetric harmonic (3,0) with phase angle 180 degrees , which reflects the relatively high pressure around Antarctica and a relatively low pressure over the Arctic.

For G500, the order of the first three leading harmonics, (2,0), (1,0), (4,0), remains the same as in run 0. But the large scale effect of cold continents in the Nothern Hemisphere, together with heating over the tropics , has dramatically increased the amplitudes of these harmonics. From the fourth to eighth harmonics of run 2, all are zonal symmeiric components.These are generally the same harmonics as in run 0 except for some change in order as well as increasing magnitude. Not until the ninth harmonic,(4,2), in the table of G500 is there any reflection of the weak long wave troughs and ridges in the Northern Hemisphere. Thus, we can conclude that the influence of flat dry continents on G500 is very weak.

Similarly, the first two harmonics of T10-8 in run 2 are still the same zonally symmetric components as in run 0.For example, the (2,0) harmonic reflects the temperature contrast between the poles and equator, and the (1,0) represents the temperature difference between the two hemispheres. As we can see from the table,

the extremely cold Northern Hemisphere in run 2 results in a tripling of the amplitude of the (1,0) harmonic. The third largest harmonic (3,2) indicates the zonal pattern of two relatively warm oceans and two cold continents in the Northern Hemisphere, but with a reversal of phase in the Southern Hemisphere. This is followed by the (4,4) harmonic which indicates four relatively warm and cold meridional bands with no nodal parallels.

In run 2, sensible heat flux (fig. 2g) is another energy source when continental surfaces are introduced. South of 30N, all continents contribute significant amounts of sensible heat, except for Antarctica. In northern high latitude continents, surface air temperatures are generally higher than the ground temperatures, resulting in no sensible heat transfer to the atmosphere. For example, in northern Siberia and Greenland, SAT (not shown) is even 2 °C higher than the ground temperature. On the other hand, extremely cold polar air from the Siberian and Canadian highs flowing over the relatively warm oceans causes strong upward sensible heat flux along the east coasts of the northern continents. Over Iceland and the Bering Sea, the SAT is even 4 °C colder than the ocean temperature. Thus ,more sensible heat is released from ocean surfaces to feed and maintain the Icelandic and Aleutian lows.

In run 2, a third of the surface area of the water planet is now occupied by a dry flat surface with no evaporation and no water storage. Obviously, the global hydrological cycle has been modified dramatically,especially over the Northern Hemisphere. Similar to the sensible heat flux, the evaporation is restricted to certain geographical locations (fig 2g).Strong enhanced evaporation takes place over the western parts of both the North Pacific and Atlantic Oceans, where dry, cold air originates from the Siberian and Canadian highs. However, the evaporation over the northwestern Pacific is far more intense (9 mm/day) and a tongue of high evaporation extends across the northern Pacific along 30N. In the water planet runs, this latitude zone is also where the highest evaporation (5mm/day) took place.

In general, evaporation is high over the tropical oceans. Strong oceanic evaporation can also be found over the western edge of the southern continents at around 30S where dry subsidence takes place in the subtropical highs. Figure 2i shows the mean difference and significance of the evaporation between run 2 and 0. The positive evaporation change off the east coast of the U.S is generally insignificant ,as a result of the weaker influence by the Canadian high as compared to the colder and drier Siberian high. But the increase of 2 mm/day in evaporation is significant over the higher northern latitudes of the Atlantic Ocean. Finally, an increase (decrease) of oceanic evaporation over the west (east) coasts of the southern continents around 30S can be seen, as noted above.

The low cloud cover (in percent) generated by the flat continents model is shown in figure 2h . Over the tropical and southern continents,formation of low clouds is completely supressed.This may be due to the low level stability which the model generates,as discussed earlier, as well as to the absence of soil moisture and evaporation. Over the oceanic areas, on the other hand, 40 percent or more low cloud cover can be found along the coastal regions on both sides of the tropical and southern continents. Low clouds appear over the Pacific Ocean southwest of Peru, in the Gulf of Guinea, southwest of the Canary Islands in the Atlantic, and south of Indonesia. All these regions are located downstream of areas of maximum oceanic evaporation.

Over the South Atlantic Ocean and South of 25S in both the Pacific and Indian Oceans, large areas of 20% or more stratus cloud can be found, associated with relatively warm moist air flowing over the cooler oceans. Within these low clouds regions, latent heat of

condensation is released to the surroundings when the clouds are formed. Clouds also alter the heating and cooling due to absorption, reflection and scattering of solar and thermal radiation. For instance, the difference and significance maps of the planetary albedo (not shown) indicate a significant 5% increase over the low cloud regions in the Southern Hemisphere. In compensation for the loss of short wave radiation,the low clouds trap long-wave thermal radiation below as well as sensible heat carried by the circulation from the continents .The net thermal effect of the low clouds is a slight warming of the lower atmosphere.

Over the tropical Pacific and Indian Oceans, very little low cloud cover is seen, while in higher latitudes of the Northern Hemisphere, low cloud cover of 30% or more can be found over the oceans as well as on the snow covered continents.

The difference and significance maps (fig. 2j) also reflect the general increase of low cloudiness over the entire globe,except for the negative effect of the tropical and southern continents. Highly significant increases of low cloud cover over oceanic regions around latitude 30S can be found,e.g. north of New Zealand,south of Australia,and southeast of Madagascar and Brazil. A 25% increase of the low cloud cover can also be found over the Great Lakes region in North America. Evaporation from the snow surface may also contribute to the significant increase of the low cloud cover over Eurasia and North America. Strong evaporation over the Aleutian region and south of the Icelandic low also results in more low cloud cover over the ocean. Furthermore, cool moist oceanic air flowing over cold northern continental coastal and inland areas causes stratus clouds to form, for example, over Alaska and around the Baltic Sea.

In general, the continental surfaces not only create monsoonal

mass exchanges with the oceans ,but also cause the formation of clouds which interact with the energy and hydrological cycles of the climate system.

The mean daily precipitation map of run 2 (fig.2h) shows generally dry conditions, with rainfall less than 2 mm/day,over the continents in the Northern Hemisphere. In contrast,enhanced precipitation areas are found over the adjacent oceans in the northwestern part of both the Pacific and Atlantic oceans, extending in a northeasterly direction to higher latitudes over the Aleutian and Icelandic regions. Similar to the evaporation pattern in the Northern Hemisphere, a tongue of precipitation (4 mm/day) stretches across the Pacific Ocean at around 35N. Heavy convective precipitation of more than 8 mm/day is found over the equatorial Amazon in South America with the rainbelt elongated to the southeastern coast of Brazil.The NW to SE orientation of this rainbelt is a direct result of warm moist air from the Northern Hemisphere meeting cooler air flowing around the subtropical high off the coast of Chile.(Note that the Andes are absent in run 2, otherwise, there would be a diverting effect on the flow.) Two rainfall maxima can also be seen just to the north and south of the Equator in Africa. In Australia, a small area of moderate precipitation can also be found south of the Gulf of Carpentaria. Over the tropical Pacific and Indian Oceans, precipitation up to 4mm/day is found.

The difference and significance maps of precipitation (fig.2k) show clear statistical significance for the positive precipitation differences over South America,but somewhat lower significance levels for the differences over Africa and Australia. A dry zone is also seen over the southern continents around 25S because of the subtropical high presure areas. The model did produce realistic

features such as the dry Horn of east Africa (Somalia) and the dry Sahara desert. The enhanced precipitation east of Japan and south of the Aleutian and Icelandic lows are all significant. Over the equatorial Atlantic and Pacific ocean regions, the existence of the flat dry continents seems either to suppress precipitation or to move it southward from the maximum rainfall zone which is located at 4N on the water planet. This effect can also be seen in the zonal profile of precipitation (fig. 11).

Meridional cross-sections

The meridional temperature cross-section of run 2 (fig.21) is qualitatively similar to that of run 0 under direct visual comparison. However, the difference and significance cross-sections (fig. 2m) reveal numerous areas of significant difference. The low level continental cold source of northern high latitudes is clearly seen and supports the horizontal temperature fields discussed earlier. Furthermore ,temperatures 2 to 4 ^{o}C cooler can also be found over the northern polar stratosphere in run 2 .Over the southern tropics, significant warming below 600mb is seen, mainly the result of strong ground heating as well as latent heat release , both of which are smaller on the water planet.

At higher levels, the thermal influence has gradually propagated both southward and upward,and is related to the southern Hadley circulation. The colder northern continents have caused the troposphere and tropopause to lower and cool around 35N in run 2 , while warming up to 3 ^{o}C has taken place in lower stratosphere. This warming is mainly due to strong adiabatic compression of sinking air from high levels where the northern Hadley cell converges with a weak stream of northerly wind from high latitudes.

The mean cross-section of zonal wind for run 2 is shown in figure 21. With the presence of the flat continents,dominant easterlies are now found over much of the tropics,increasing in speed with height. The existence of the easterlies has also created a strong gradient of zonal winds in the southern tropics,while the location of the maximum westerly jet still remains at 31S as in the water planet. In the Northern Hemisphere,the zonal westerlies are generally stronger at high latitudes.

Again, the influence of the heat and cold sources on the zonal circulation may best be illustrated by the difference and significance cross-sections (fig. 2n).The strong westerlies at latitude 31S and 16N are readily seen to be the result of warm tropical continents, although the northern circulation is somewhat less significant. At 16S, a significant difference of 16m/sec is found. This is mainly caused by a reversal in direction,with easterlies induced by land in run 2 replacing the westerlies in run 0. The adiabatic warming region (35N), as discussed in the temperature difference cross-section, also causes weaker stratospheric westerlies in agreement with the thermal wind relationship. Furthermore, the cooler stratosphere and colder troposphere have strengthened the westerlies significantly in the Northern Hemisphere.

The cross-section of meridional wind of run 2 (fig.2o) shows a shift of low level convergence from 4N in run 0 to around 16S.Thus the principal effect of the flat continents is to induce the ITCZ to move southward over the heated land surfaces. The symmetric pattern of the Hadley circulation found in the water planet run is now broken into a dominant northern cell, which extends farther south, and a weak southern branch. In northern high latitudes,

around 70N,the surface southerly wind of run 0 is missing in run 2. This is mainly due to the cancellation between the southerly winds over the continents and the northerly winds over the ocean. In the lower stratosphere near 55N a northerly wind is found.In connection with the low level convergence at 65N (also see the cross-section of vertical wind), this forms part of a weak indirect circulation.

The difference cross-section of meridional wind for run 0 and 2 is shown in figure 2p. The solid isotachs indicate stronger southerly (weaker northerly) wind and the reverse is shown by dotted isotachs. Clearly, the southward shift of the ITCZ is generally significant. In the stratosphere over 55N - 70N, a band of significantly stronger northerly wind (8 cm/sec) is found (not seen in the difference cross-section), and again this is an indication of the indirect circulation of run 2.

Unlike the vertical velocity cross-section for the water planet, with a single ascending column at 4N and with maximum speed of 6.6 cm/sec, the cross-section of run 2 (fig. 2o) shows two distinct ascending branches of the Hadley circulation,one at 4N and the other at 12S. However,the maximum upward speed for both branches is reduced by almost half compared to run 0 due to the zonal averaging of the rising motion over land and the descending motion over the adjacent oceans. The southern branch of the ascending region is wider than the northern branch, and much of the air in the lower convergence level originates from the trade winds of the Northern Hemisphere. (Also see the meridional wind cross-section.) Aloft, much of the air mass is diverted back to the north, enhancing the strong dominant circulation of the northern Hadley cell. To the north, the rising motion in the northern branch is due to the heating of the African continent and small portion of the tropical

oceans. Weaker ascending motion can also be seen at 67 degrees over both hemispheres where the subpolar lows are located.

The mean difference and significance cross-sections (fig.2q) clearly indicates a southward shift of the Hadley cell. Dotted lines denote either weaker rising or stronger sinking motion and solid lines either stronger rising or weaker sinking motion. The significance of stronger ascending motion in the southern branch and stronger descending motion to the south (at 35S) is clearly seen. Weaker rising motion in the northern Hadley cell and weaker sinking motion at 25N are all reflected in the difference cross-section.

III. The thermal and dynamical effects of terrain and mountain barriers: differences between run 3 and run 2

In this experiment (#3), realistic topography is incorporated into the coarse-mesh model. Figure 3a illustrates the topography of the model in geopotential meters. It may be helpful to distinguish the terrain effects into two types. First, the general uplift of continents above sea level, or " plateau " effect , produces elevated cold (winter,high latitude) and warm (summer,low latitude) sources. Second, there are mountain barrier effects,which may be further subdivided according to the orientation of the mountains into north-south "Cordilleran" barriers to zonal flow and east-west "Alpine-Himalayan" barriers to meridional flow.

The dry isothermal initialization of this experiment may hinder somewhat the evaluation of the orographic effect when compared to run 2. However, as we shall see, after several months, the model seems to forget its initial state. Averaging the last 20 months of the mountain experiment thus provides a climatology that is comparable with that of run 2.

Horizontal fields (part i)

Figures 3a to 3b display the surface air temperature (in °C) and layer temperatures from 1000-850 mb and from 850-700 mb (both in K) of run 3. At the surface , the most obvious difference is seen over Antarctica where the ground albedo (not shown) ,as compared to run 2, increased by almost 30%. In the layer 1000-850 mb,the T10-8 of run 3 shows a pattern similar to that of run 2, but more irregular, with wave-like isotherms and high temperature

gradients over Asia, North America and Greenland. It must,of course, be noted that much of the Hamalayas, the Tibetan plateau, Greenland, and the Sierra, Andes, and Rocky mountain barriers are higher than this layer,so that T10-8 in those areas has no physical meaning,and represents only an artificial extrapolation based on the surface air temperature. Unlike T10-8, the irregular pattern and temperature gradient of T8-7 has diminished gradually. Again, it must be recognized that some mountainous areas lie above the 700mb level. Nevertheless, the effects of the elevated heat sources of the Andes, African highlands and Australia,together with their influence over the tropical oceans , can be found by comparison of the T8-7 isotherms of runs 3 and 2 (figs 3b and 2a).

Further understanding of the role of topography in redistributing the thermal sources and sinks can be obtained from an examination of the difference and significance maps of SAT,T10-8, and T8-7 (figs. 3c to 3e ,respectively) for run 3 and 2. In figure 3c ,significantly cooler SAT is found over the southern continents due to the high elevation.For instance, in South America a temperature difference of -5 ^{o}C over Peru is due to the high altitude of the Andes. However,a large temperature difference (-4 ^{o}C) is also found in southern Brazil at a lower elevation. A significant increase of convective precipitation and a 15% increase of cloud cover due to the topography are found in this region.Thus , the reduction of the insolation is probably the main cause of the cooling in this area. That these cooling effects are confined to the surface layers may be inferred from the difference and significance maps of T10-8 and T8-7 (figs. 3d and 3e), which show practically no significant differences between runs 3 and 2.

Negative SAT differences are also found from central to southern Africa, where the magnitude of cooling is slightly greater than in the Andes. This is probably a result of the larger area coverage of the African highlands, despite the lower elevation. Similarly, small but detectable cooling of SAT can also be found in the elevated northwestern part of Australia.

It is interesting to note that the belt of cooler SAT is not located over the Ethiopian highlands of Africa (see topography map, fig.3a) but appears farther north in the Sudan. Again, this surface cooling may be explained by referring to the surface winds of run 3 (fig.3f), which indicate a more northerly flow of cooler air from the Mediterranean Sea.That this is a surface feature can be seen by comparing it with the maps for T10-8 and T8-7 , where no significant differences appear. On the other hand, the elevated heat source of the Ethiopian highland to the south is vividly seen in these two layers, and it also extends westward to the southern Sahara desert.

From the difference maps of T10-8 and T8-7, the Andes region of South America is seen to be the most intense elevated heat source among the three southern continents. With the presence of orography, there is a significant westward spreading of the thermal influence to the adjacent oceans at around 25S over the three southern continents , which is related to the circulation around the subtropical highs.Farther south, around 35S, eastward spreading of heating effects over the ocean can be found on the east side of the continents as a result of the westerlies.

Over the Himalayas , including Tibet, the SAT difference map indicates a high elevated cold source, surrounded by areas of warmer

temperatures. For example, in eastern China , a positive SAT difference of 6 °C is found. This is apparently an indirect effect of the Himalayas,which cause the Siberian high to shift to the north. Consequently, the anticyclonic flow is now onshore in run 3 over the south-eastern China (see surface wind of run 2 and 3). For much the same reason, higher values of SAT and T8-7 can be found to the north and west of the Tibetan Plateau in run 3. The snow cover in the northern part of Afghanistan is absent in run 3. Furthermore, this high elevated region has experienced an increase of convective cloud of more than 10%.

Farther north over the continents, the SAT and layer temperatures show significantly colder temperatures partly due to higher elevation in Siberia, the Sierras, and Greenland. In addition, the mountain barriers also act to block warm advection, so that even lower level surfaces also show colder temperatures. Again, the fact that the initialization may have caused a minor residual effect needs to be considered. Finally , significantly warmer values of SAT,T10-8, and T8-7 can be seen over Alaska and around Iceland,where warm advection from the oceans to the south is taking place.

As pointed out earlier,the isothermal and,more importantly, dry initialization for run 3 certainly has an impact on the model-generated climatology. Insufficient moisture and clouds, during the first few months ,cause extremely cold temperatures to develop over much of the high northern latitudes. However, with advection of moisture and heat, from lower latitudes later on, these initially cold conditions undergo a change. In order to see how the initial state affects the later months, time series of T10-8 were made for several grid points. Particularly, those along latitude 67N will be

shown,further subdivided into 3 major groups :(i) northwest(170W) and northeast (150W) of Alaska,(ii) extreme northwestern USSR or east of Scandinavia (longitudes of 30E and 50E), and (iii) northern and northeastern Siberia (longitudes 100E,120E,140E,160E). Regions (i) and (ii) are shown in figure 3g and region (iii) in figure 3h. Dashed lines denoted run 2 and solid line represent run 3 at the same grid points. The topography of all the grid points lies below the 850 mb level for run 3.

In the first month of run 2, a monthly mean T10-8 close to 270K is found in all three regions along 67N (including those grid points not shown in the figure), a direct result of the relatively warm moist initialization. In the following two months ,temperatures in all three regions fell by more than 15K ,except for the location at 30E of region (i), where the change was smaller because of its location in open water. During the rest of the run, all locations exhibit realistic interannual fluctuations with temperatures colder than the first month.

In the first month of run 3 , a more erratic and colder temperature distribution is found under the influence of the dry isothermal initial condition, as well as topography. For example, a large temperature difference can be found between the location of regions (i) and (ii). However, a more uniform temperature of around 260K can be seen in region (iii) in the first month. Starting in the second or third month of run 3 , all grid points show a sudden cooling, but most dramatically over region (iii) with a 30K to almost 50K drop. However, in the following months,temperatures in all regions start to climb steadily. In region(i), slightly warmer temperatures than in run 2 can be seen as the effect of warm

advection from the Aleutian low , while in region(ii) and (iii), temperatures are either colder or cooler than in run 2. In region (iii) over northern Siberia, large amplitude fluctuations are found.

From the small data sample shown above,it is apparent that the dry isothermal initialization of run 3 does result in very rapid radiational cooling in high northern latitudes during the first two months of the model history,while in run 2, the moist isothermal initialization allows a smaller cooling rate to take place. However, after the first two months of run 3, as evaporation moistens the model atmosphere , the temperature rises rapidly. Within a few months, the temperature of run 3 , like that of run 2, begins to fluctuate around a long-term mean value that is well below the initial temperature , but considerably warmer than the extremely low temperature reached in the second or third month. Thus , it appears that the long-period average temperature of the model atmosphere after the first few months is virtually independent of the initial state.

The sea-level pressure map for run 3 (fig.3i) shows a more irregular pattern and larger gradients than run 2. With orography, the Siberian high is now shifted northeastward and broken into cells over the elevated cold areas. Similarly, the Canadian high has also migrated to the northwest . Unrealistic high SLP appears over Greenland,probably due to the method of reduction to SLP. A weak but closed cold low can be found in the southeastern Gulf of Alaska. The Icelandic and Aleutian lows are now located to the south of Greenland and over the Kamchatka Peninsula,respectively. Although the Aleutian low is more intense and better organized than in run 2, the pressure is still somewhat higher than observed.

Over Antarctica, low SLP is seen between longitudes zero and 90E, where the highest elevation is found.In the tropical Pacific and Indian Oceans, SLP is generally lower than in run 2. This small difference does not appear in the difference map (fig.3j), but its significance is clearly seen. In addition, the colder temperature of run 3 in northern high latitudes is also reflected in the higher pressure on the difference map. Similarly, the retreat of the Siberian high to the north and its replacement by a generally lower SLP have resulted in a total decrease of SLP of more than 8 mb in southern Asia. The significant sea level pressure decreases over the elevated African highlands and the Andes are also well depicted.

The mean zonal SLP profile of run 3 is shown in figure 1d and denoted by the number 3. In the tropics, the elevated heat source has lowered the SLP relatively to the water planet and flat continents experiments, and thus farther from the observed values. (Even allowing water storage and evaporation to take place over the continents still only raises the pressure slightly in the tropics.) On the other hand, It is very encouraging to see the increase in SLP in the Northern Hemisphere in run 3,which brings it closer to the observed profile.However, the presence of the arbitrary northern ice cap has made the polar pressure somewhat too high. The magnitude of the subtropical high in both hemispheres is in better agreement with the observed pressure profile, but still too far poleward, especially in the north .Finally, a serious model problem can be found in southern polar latitudes (e.g. 67S) where the SLP of the model is much too high compared to the observed profile, even with orography.

With topography included, the 500mb map of run 3 (fig. 3i) shows many wave-like structures in contrast to the more zonal symmetric character of run 2. For example, perturbations can be found over the high elevated area of Antarctica. In southern high latitudes, the pattern of G500 is basically similar to that of run 2 because of the strong influence of the oceans. Nevertheless, small "wiggles" in the pattern can be seen off the coast of Chile in run 3.

Among the southern continents, the G500 over South America is lower than over Australia and Africa due to a much lower SLP. This can be seen in the difference and significance maps (fig 3k). In contrast to the broken southern subtropical high pressure cells in run 2, a more organized large scale structure can be found over the Pacific and Indian oceans in run 3. The hydrostatic effect of the warm continents spreading on both sides of the oceans, as discussed earlier, is also reflected in the G500 difference map.

Recently ,Kasahara (1980) has reviewed the influence of orography on the general circulation of the troposphere. Figure 31 (after Kasahara) is a schematic representation of two types of blocking pattern, taken from Kikuchi (1970). Kasahara noted that the blocking high and diffluent structures could be caused by large scale topography as well as land-sea temperature contrast. In G500 of run 3 , a diffluent structure resembling that of figure 31 appears over the Himalayas complex with a high closed contour to the north and a low to the south. The strong westerlies here have split into two streams, one towards the north and the other to the south of the Tibetan plateau, in agreement with observational studies. To the southwest of this region, waves can be seen over India. Furthermore,

the elevated thermal influence of the Himalayas complex is reflected in the significant difference in fig. 3k . A similar diffluent pattern with no closed contour can also be seen in southern Greenland.

With orography (but zonal SST) in run 3, the model has generated a diffluent structure in the Gulf of Alaska, with a warm ridge in the north(over the continent)and cold trough to the south (over the ocean). The trough is just to the north of the cold low,which was mentioned in the discussion of the SLP map. This is a quasi-barotropic feature, and the pattern extends up to the 300mb surface. Such a diffluent structure appears to be related to a trough formed on the leeward side of the Himalayas complex (over Japan), and results in a transport of warm air downstream towards high northern latitudes. Subsequently, a warm high or ridge built up over Alaska. Thus, the process leading to the diffluent structure may be an indirect orographic effect, involving also the land-sea temperature contrast.

In northern polar latitudes , significant positive differences of G500 can be seen , e.g., over Greenland and the northern ice cap, despite the colder temperature of run 3 in these regions. The reason for the higher G500 is the higher SLP of run 3 in these areas,except south of Iceland and Alaska where warming takes place. In Siberia and central Canada, on the other hand , negative difference of G500 are found due to the extremely cold temperatures, but only a portion of the area shows significance.

Spherical harmonic analysis

As seen in the horizontal fields, the orography diverts the zonal flow into meridional motions and also affects the atmosphere thermally through the elevated heat and cold sources. One might therefore expect the spherical harmonic analysis of run 3 to show a few new dominant harmonics, although many of the major characteristics may be retained in the global harmonic structure of SLP, G500 (table 1) and T10-8 (Table2).

For SLP of run 3, the dominant (1,0) harmonic again indicates the excess of mass in the the Northern Hemisphere. The (4,0) harmonic ranks a step lower,with smaller amplitude,than in run 2,but still reflects the subtropical highs and equatorial low as dominant features of the SLP structure. The polar-equatorial difference represented by the (2,0) harmonic in run 3 has a reveral of phase which reflects the high SLP in the winter hemisphere together with a slightly lower pressure in the tropics. Furthermore, high SLP in the northern polar region and relatively low pressure in mid latitudes can also be seen from the (3,0) harmonic,which is 7th in run 3 and 10th in 2 ,with 180 degree phase difference indicating relatively low pressure in the northern polar region in run 2.

The slightly enhanced amplitude of the Asiatic anticyclone in run 3 is shown by the (1,1) harmonic which still remains the 3rd leading harmonic as in run 2,while the (3,2) ,(4,4) and (5,4) harmonics which follow exhibit similar or slightly larger magnitudes.The (3,3) harmonic, reflecting 3 longitudinal waves or

cells,which appears as 7 th harmonic in run 2, is no longer among the ten leading harmonics of run 3 when topography is included.

For G500, the first 3 leading harmonics of run 3 are similar to those of run 2 except that smaller amplitudes are found in the (2,0) and (1,0) terms.This is a reflection of the higher SLP in the northern polar region which causes a higher G500 and thus a decrease of the amplitude.The following leading harmonics of G500 in run 3, (7,0) and (6,0), show a decrease of magnitude. However,the most interesting is the (6,0) harmonic,which jumps up to 4th place in run 3 from 6th place of 2,with dramatic increase of amplitude. This may be explained by the difference map of G500 (fig.3k). Higher heights over the Arctic ice cap and Antartica,and also near the Himalayas complex and around latitude 40S, together with a decrease of height over Siberia, Canada and the southern oceans, all contribute to the importance and high amplitude of the (6,0) harmonic. The effect of the continents on the longitudinal variations of G500 can be seen from the last four harmonics.Three of the harmonics, (6,2),(5,2) and (7,2), are of longitudinal wave number 2, and indicate relatively small scale or cellular structures by their high number of nodal parallels (n-m).

With the presence of elevated heat and cold sources, the (2,0) and (1,0) harmonics of T10-6 in run 3 still remain as the first two leading components,with little higher amplitude than in 2 . Furthermore, the (3,0) term,absent in 2, becomes the 3rd leading harmonic of run 3,its phase angle of 180 degrees reflecting colder temperatures in the northern polar region as well as warming in the Himalayas.However, the high temperature in this region is mainly due to the extrapolation from the surface temperature, as

discussed earlier. The influence of the colder elevated Siberian high is also seen in the increased magnitude of the (1,1) harmonic. The last 2 components of run 2,(3,3), and (3,1) , are now replaced in run 3 by (4,1) and (5,2). Finally, the 7th harmonic of run 2, (4,2) ,is replaced by a (5,4) harmonic, which indicates a more irregular or cellular temperature distribution in northern high latitudes.

Although the sensible heat flux of run 3 (fig.3m) generally shows a similar pattern to that of run 2 , the difference and significance maps (fig. 3n) do reflect the differences discussed in the context of the SAT. For example, the northward movement of the cold Siberian high results in more sensible heat flux over northern Japan, while a dramatic and significant reduction takes place in the Bering Sea and Alaska, where relatively warm southerly flow now comes from the Aleutian low. For the same reason , the relatively warm onshore advection from the Pacific ocean has also reduced the sensible heat transfer over eastern China and north of India.

In the western hemisphere, a slight but significant increase of heat flux can be found on the New England coast and northeast of Hudsons Bay. Surrounding Iceland , a highly significant drop of sensible heat transfer is seen. This can best be explained by comparing the surface winds of both runs (fig. 3f) in the region around latitude 60N. Briefly,a generally southerly warm air flow is found south of Iceland in run 3 compared with the mainly zonal westerlies and weak northerly flow of cold air from Greenland in run 2.

A significant increase of the sensible heat flux in the low layers is also seen over the region of the White Sea in northwestern USSR .The cold low south of the Gulf of Alaska discussed earlier also shows a significant increase of appreciable amount from the oceanic region. A generally insignificant increase of sensible heat in the northern part of South America and a decrease in the central

part are found .This is related to the southward shift of the rainbelt in South America resulting from topography ,which will be discussed later.

Relatively small but significant increases of sensible heat flux are found in the oceans west of Chile and South Africa, and are also seen in the zonal profile (fig. 1h).This appears to be due to the flow of cold air around the subtropical highs ,which is now diverted toward the ocean by the Andes and the highlands of southern Africa. Finally, a significant increase of sensible heat flux can also be found over the elevated Antarctic continent.

Figure 3m shows the map of mean daily evaporation of run 3,while the mean meridional profile is seen in figure 1h. As in the profile of run 2 (in the same figure),high evaporation is found in run 3 between latitudes 35N and S, while the high northern latitudes show stronger evaporation than the corresponding latitudes in the Southern Hemisphere mainly due to the vigorous transport of cold dry air from the continents to the adjacent oceans.

The difference and significance maps of evaporation (fig. 3o) reflect many of the features discussed earlier. Increased evaporation is found to the west of the southern continents and farther extended into the oceans along about latitude 25S. This increase can be explained by the surface winds of run 3 (fig.3f) in which stronger wind can be found over the region of increased evaporation. This is particularly evident off the coast of Chile.

The Himalayas complex also creates an irregular evaporation pattern, as can be seen from the significant positive and negative differences in the northern Indian ocean. A careful

examination of the SLP map of run 3 in the region shows a small high pressure area in the Arabian Sea. Surface winds are onshore in western India in run 3,which is certainly unrealistic compared to run 2 where the flow is offshore. On the other hand, the increase of evaporation north of Japan and the decrease to its south are expected results of the northward shift of the Siberian high. In addition, there are many local regions where the evaporation differences are significant: for example, in the cold low south of the Gulf of Alaska, and with smaller magnitude, in the Gulf of Mexico as well as southwest of the Canary Islands. Finally, decreased evaporation south of Iceland and also in the Bering Sea are due ,more or less, to the same cause as discussed with respect to the sensible heat flux difference.

In figure 3p,it appears that high elevation of Antarctica has induced more low cloud cover in run 3. The difference and significance maps (fig. 3q) also reflect more than a 20 percent increase of low clouds there.Furthermore,they reveal many large and small scale regional differences. The increase of evaporation in the South Pacific and Indian Oceans between 10S and 30S noted above also results in a significant increase of low cloud cover. Somewhat less significance is associated with the low clouds in the South Atlantic.

Highly significant increases of cloud cover can be seen over the ocean west of Mexico and in the Arabian Sea, with increases of 30 percent or more. The positive differences over eastern China and significant negative difference of low cloud to the north once again demonstrate the influence of the Himalayas. Over Afghanistan, the incorporation of orography seems to suppress the formation of

low level clouds while significantly enhancing the middle and high clouds.

It is interesting to see a large area with slight increases of low cloud cover (5 percent or more) , but still highly significant, around northern mid-latitudes from the Mississippi valley across the Atlantic Ocean and through the Mediterranean Sea to the Caspian Sea. Similarly, another band can be seen extending from Japan across most of the Pacific along 40N.

The mean daily precipitation of run 3 is shown in figure 3p. In South America , the NW-SE oriented rainbelt of run 2 is now changed to a more longitudinal direction, and the northern part of the maximum rainfall region is now shifted south-westward over the Andes of Peru. This migration of heavy precipitation is best illustrated in the difference and significance maps (fig.3r) and also in the zonal precipitation profile (fig. 3i). Difference of more than 7mm daily rainfall due to the orographic effect can be found on both the west and east elevated regions. Apparently, the Andes Mountains have blocked the dry subsiding air from the subtropical high west of Chile from penetrating inland. This can be verified by comparing the surface winds of run 3 and 2 in figure 3f .

Increased daily precipitation is also found along the African highlands and a slight but significant increase of rainfall can be seen extending to the South Atlantic Ocean. For much the same reason, the area of heavy rainfall has moved both westward and eastward to the higher elevations in Australia. In general, small but significant decreases of precipitation in run 3 are found over southern tropical oceans.

Over eastern China , a dramatic increase of precipitation is seen associated with the northward retreat of the Siberian high noted before. This area has experienced an onshore surface wind which advects warm moist air from the Pacific Ocean. A significant increase of total cloud cover is also found. Increased evaporation to the northeast of New Guinea and enhanced orographic uplift have increased the amount of precipitation in that area.

Other than the increase of precipitation over Iceland,where strong low level convergence occurred in run 3, there is no visible effect of topography on the computed precipitation over North America and Europe in the coarse-mesh model.

Meridional cross-sections

Figure 3s displays the temperature cross-section of run 3 which is qualitatively similar to that of run 2. In most of the troposphere outside of the high latitudes of the Northern Hemisphere the difference and significance cross-sections (fig.3t) show significant warming due to the elevated heat source. For example, over Antarctica , increases of more than 3 °C can be found in the troposophere and stratosphere. Furthermore, the thermal influence of the Andes and African highlands can be seen above 500mb in the southern tropics around 27S as well as at 4N, but with a far smaller contribution from the central African highland.The elevated cold sources of Siberia and Canada, as well as the northern ice cap,as discussed earlier, are also reflected in the colder zonal mean temperature of the lower troposphere.

In the subtropical latitude band of the Northern Hemi-

sphere, the effect of the Himalayas complex noted before is also seen , with temperatures more than 3 °C warmer at the surface in the difference cross-section . However, colder (negative) temperatures of 1.5 °C are found in the low stratosphere above.

An important role played by the mountains, as revealed in the temperature difference and significance cross-sections, is the generation of highly significant warming in the stratosphere, especially over the northern polar region where increases of 10 °C can be found. A strong ascending column ,which slants northward at higher alititudes into the stratosphere, is found at 65N near the surface in the vertical velocity cross-section of run 3 (which will be discussed later),associated with the Aleutian and Icelandic lows. A considerable amount of heat must have been transported upward to the polar stratosphere to cause the warming.

The cross-section of zonal wind for run 3 (fig. 3s) shows a pattern similar to that of run 2, except that the region of equatorial easterlies now extends southward to 23S. From the difference and significance cross-sections(fig.3u),the easterly circulation has weakened in the northern equatorial stratosphere,while strengthening significantly (by 6 m/sec) at 10S.

It may be helpful to compare the difference cross-sections of temperature and zonal wind through the thermal wind relationship. For instance, warming of the polar stratosphere in both hemispheres has significantly reduced the westerlies in those regions. The relative warming of the equatorial stratosphere together with cooling at 35N have strengthened the westerlies significantly by as much as 12 m/sec over 16N in the stratosphere. Similarly, the thermal influence of the southern continents results in a slight

increase of the westerlies (by 3 m/sec) over middle latitudes of the southern stratosphere.

The meridional wind cross-section of run 3 is displayed in figure 3v. As noted earlier, strong meridional flow patterns are found in middle and high northern latitudes in run 3. However, only a very small, or nearly zero, meridional component is seen in the cross-section due to the positive and negative cancellation. In the tropics, the trade winds at low levels and the divergence aloft are more consistent and well defined ,as illustrated in the cross-section. As compared to run 2, the Hadley cells of run 3 (especially the southern cell) show more intense circulation and also extend to higher stratospheric levels (see the vertically elongated pattern above 25S) including the strongest meridional wind regions of both cells. Furthermore, the ITCZ at higher levels has shifted a few degrees southward. All these features can be seen in the difference and significance cross-sections (fig. 3w).

In the lower stratosphere below 200mb at 39N, a positive difference of meridional circulation can be found ,while at the surface, run 3 shows a more northerly component. High SLP in the Arctic also creates a northerly component at the surface compared with the surface wind of run 2.

From the vertical velocity cross-section of run 3 (fig.3v), it appears that the Andes and African highlands have shifted the southern ascending branch from 12S in run 2 southward to 20S in run 3, with strongly enhanced rising motion. Consequently, strong subsidence is found to the south at 35S. In the northern counterpart, the ascending branch has weakened, but remains located

at 4N. Again, the difference and significance cross-sections (fig. 3x) reflect these features. Stronger rising motion is found at 4S above 300mb. This together with the stronger ascending motion in the southern Hadley cell may possibly be related to the warming of the tropical stratosphere (also see the meridional wind cross-section).

The thermal influence of the Himalayas complex has apparently separated the descending branch of the northern Hadley cell from a mid tropospheric sinking stream, associated with the cold high SLP to the north of the mountain complex.

Around latitude 67 in both hemispheres, relatively weak ascending motion can be found with corresponding subsidence at the poles, especially in the northern ascending branch, as mentioned earlier, is related to the polar stratosphere warming in run 3. Two regions of maximum rising motion can be found, one in the low level convergence and the other above 200mb farther north.

Summary and conclusions

From the results of the two water planet experiments, there is apparently no major large scale difference between the two runs. Furthermore, the model seems to be capable of generating a steady climatic state in only a few simulation months from an intial state of zero motion, as can be seen from the last three experiments. In the last run,with topography included,the dry initial state caused a radiative cooling effect in the polar region of the winter hemisphere in the first few months. However, in this run also , a quasi-steady climatic state is reached afterward. Therefore,the initial conditions seem to be a minor problem in a climate simulation.

As expected from the forcing by zonal symmetric surface boundary conditions,in the water planet run all mean variables show a predominantly zonal symmetric character, as confirmed by the leading terms of the spherical harmonic analysis. An ITCZ, with a band of maximum precipitation and strong upward vertical velocity is found over 4N where the SST is a maximum. This precipitation peak agrees very well with the most recent estimates of the observed precipitation over the Pacific Ocean. Furthermore, the water planet zonal mean profile of SLP is very close to the observed climatological profile in the tropics.

In run 2, through strong sensible heat flux, augmented by latent heat released, continents act as regional heat sources in the tropics and in the summer hemisphere. In contrast, high albedo snow extends southward to 30N over northern high latitude continents, which serve as large scale heat sinks. Dynamically, monsoonal mass exchange takes place between the cold (warm) cont-

inents and the warm (cold) adjacent oceans, accompanied by low cloud formation during the exchange process. However, the zonal mean sea level pressure profile of this flat dry continent model differs only slightly from that of the water planet. In addition, the 500 mb flow pattern of run 2 also shows a predominantly zonal circulation. Thus,the effects of the zero elevation dry continents seem to be confined to the lower troposphere.

In the flat continents run, the southern continents induce a second Hadley cell and ITCZ in the southern tropics, and cause strong easterly flow to appear in the equatorial region. Furthermore, the heated continents of the model have a desiccating effect on the precipitation. The band of maximum precipitation at 4N in the water planet is reduced sharply in run 2, and the heaviest rainfall is found over South America and the equatorial region of Africa.

In run 3, with orography included, the elevated terrain produces a colder surface air temperature in high latitudes of Eurasia and North America. Consequently, intense continental high sea-level pressure centers build up and move closer to their observed positions in the Northern Hemisphere, although in some cases these "corrections" are excessive. On the other hand, the elevated heat sources provided by the southern continents strengthen the Hadley circulation unrealistically in the Southern Hemisphere, and result in generally lower sea-level pressures than either observed or generated by the previous runs.

From the mean temperature difference cross-section, it is also apparent that the mountainous terrain exerts a considerable and significant effect on the model's stratosphere. The mid-tropospheric circulation generated with the mountainous model also generally shows a more meridional pattern and irregular, diffluent structures than that of the flat continent run.The presence of he Himalayas complex, the Andes, and the African highlands do have noticeable effects on the precipitation in these regions, but almost no effects are found over North America or Europe in the coarse-mesh model. Finally, none of the three runs generates the sub-Antarctic low found in nature.

Acknowledgements

This study was carried out at the Goddard Institute for Space studies (Robert Jastrow, Director) under Grant No.NGR 33-013-086 from the NASA Goddard Space Flight Center. The author gratefully acknowledges the support of James Hansen, head of the GISS climate research group, and his generous permission to use the GISS climate model , as well as the assistance of the GISS staff, especially David Rind for many discussions, and Reto Ruedy and Gary Russell for their guidance in computer programming and model operation.

Special thanks are due to Prof. Jerome Spar for his guidance and for his help in editing this paper into a more readable form. I also thank Charles Cohen for assisting with a portion of the computer work in this research.

Chervin, R.M., 1980a : Estimate of first- and second- moment climate statistics in GCM simulated climate ensembles. J. Atmos. Sci., 37, 1889-1902.

Chervin, R.M.,1980b: On the simulation of climate and climate change with general circulation models. J. Atmos. Sci.,37, 1903-1913.

Christidis,Z.D. and J. Spar, 1981: Spherical harmonic analysis of a model-generated climatology. Mon. Wea. Rev.,109,215-229.

Cohen, C.,1981: The effect of surface boundary conditions on the climate generated by a coarse-mesh general circulation model. Technical Report, Grant NGR 33-013-086, NASA Goddard Space Flight Center. The City College , N.Y., N.Y. 10031, June 1981. 40pp. + figs.

Dorman, C.E. and R.H. Bourke, 1979: Precipitation over the Pacific Ocean, 30S to 80N, Mon. Wea. Rev., 107, 896-910.

Hansen,J.,G. Russell, D. Rind, P. Stone, A Lacis, L. Travis, S. Lebedeff,and R. Ruedy,1980:An efficient three dimensional global model for climate studies. I. Model I. NASA,Goddard Institute for Space Studies. Goddard Space Flight Center, N.Y., N.Y.10025

Kasahara, A., 1980: Influence of orography on the atmospheric general circulation. GARP Publication Series No 23, World Meteorol Org, 4-49.

Kasahara, A., and W.M. Washington, 1971: General circulation experiments with a six-layer NCAR model,including orography, cloudiness and surface temperature calculations. J. Atmos. Sci., 28,657-701.

Kikuchi, Y.,1971: Influence of mountains and land-sea distribution on blocking action. J. Meteorol, Soc Jpn,49 Special Issue, 564-572.

Manabe, S. and T. B. Terpstra, 1974: The effects of mountains on the general circulation of the atmosphere as identified by numerical experiments. J.Atmos. Sci.,31,3-42.

Manabe, S.,Hahn,D.G. and Holloway, J.L.,Jr.,1974: The seasonal variation of the tropical circulation as simulated by a global model of the atmosphere. J. Atmos. Sci., 31,43-83.

Schlesinger, M.E. and W.L. Gates, 1979: Numerical simulation of the January and July global climate with the OSU two-level atmospheric general circulation model. Report No.9, Climatic Research Institute, Oregon State University, Corvallis, Oregon 97331.

Spar, J., 1961: Investigation of models for large - scale meteorological prediction experiments. Final report, Grant NGR 33-013-086, NASA Goddard Space Flight Center. The City College,New York,N.Y. 10031.

Figures

Fig.1a (Top) Mean sea-level pressure (SLP) for run 0 .
(Bottom) Mean SLP for run 1 .

Fig.1b SLP : (Top) Standard deviation of run 0 .
(Bottom) Standard deviation of run 1 .

Fig.1c (Top) Mean SLP difference of run 0 - run 1 .
Fig.1d (Bottom) Meridional SLP profiles for run 0 to 3 and observed.

Fig.1e (Top) 600mb height (G600) profiles for runs 0 to 3 .
(Bottom) Meridional surface air temperature (SAT) profiles for runs 0 to 3 and sea surface temperature (SST) profile.

Fig.1f (Top) Meridional profiles of layer temperature from 850-700mb (T8-7) for runs 0 to 3.
(Bottom) Mean T8-7 difference of run 0 - run 1 .

Fig.1g (Top) Mean G600 difference of run 0 - run 1 .
(Bottom) Mean SAT difference of run 0 - run 1 .

Fig.1h (Top) Meridional sensible heat flux profiles for runs 0 to 3.
(Bottom) Meridional evaporation profiles for runs 0 to 3.

Fig.1i (Top) Meridional precipitation profiles for run 0 to 3.
(Bottom) Mean winter rainfall depth by latitude over the Pacific Ocean (from C.E.Dorman and R.H.,Bourke).

Fig.1j Mean precipitation difference of run 0 - run 1.

Fig.1k (Top) Temperature cross-section of run 0 .
(Bottom) Temperature cross-section of run 1 .

Fig.1l (Top) Temperature difference cross-section for run 0 - run 1.
(Bottom) Time series of zonal mean temperature at 51S and 497mb. for runs 0 and 1.

Fig.1m (Top) Zonal wind cross-section for run 0 .
(Bottom) Zonal wind cross-section for run 1.

Fig.1n (Top) Zonal wind difference cross-section for run 0 - run 1.
(Bottom) Standard deviation of zonal wind cross-section for run 1 .

Fig.1o Time series of mean zonal wind on Equator at 82 mb level for runs 0 and 1.

Fig.1p (Top) Meridional wind cross-section for run 0 .
(Bottom) Meridional wind cross-section for run 1.

Fig.1q (Top) Meridional wind difference cross-section for run 0 - run 1 .
(Bottom) Vertical velocity defference cross-section for run 0 - run 1 .

Fig.1r (Top) Vertical velocity cross-section for run 0.
(Bottom) Vertical velocity cross-section for run 1.

Fig.2a (Top) Mean SAT for run 2 .
(Bottom) Mean T8-7 for run 2 .

Fig.2b SAT : (Top) Mean difference for run 2 - run 0 .
(Bottom) Significance level .

Fig.2c T8-7 : (Top) Mean difference for run 2 - run 0 .
(Bottom) Significance level .

Fig.2d (Top) Mean SLP for run 2 .
(Bottom) Mean G500 for run 2 .

Fig.2e SLP : (Top) Mean difference for run 2 - run 0 .
(Bottom) Significance level .

Fig.2f G500 : (Top) Mean difference for run 2 - run 0 .
(Bottom) Significance level .

Fig.2g (Top) Mean sensible heat flux for run 2 .
(Bottom) Mean evaporation for run 2 .

Fig.2h (Top) Mean low cloud cover for run 2 .
(Bottom) Mean precipitation for run 2 .

Fig.2i Evaporation : (Top) Mean difference for run 2 - run 0 .
(Bottom) Significance level .

Fig.2j Low cloud cover: (Top) Mean difference for run 2 - run 0 .
(Bottom) Significance level .

Fig.2k Precipitation : (Top) Mean difference for run 2 - run 0 .
(Bottom) Significance level .

Fig.2l (Top) Temperature cross-section of run 2 .
(Bottom) Zonal wind cross-section for run 2.

Fig.2m Temperature : (Top) Mean difference for run 2 - run 0 .
(Bottom) Significance level .

Fig.2n Zonal wind : (Top) Mean difference for run 2 - run 0.
(Bottom) Significance level .

Fig.2o (Top) Meridional wind cross-section of run 2 .
(Bottom) Vertical velocity cross-section for run 2 .

Fig.2p Meridional wind : (Top) Mean difference for run 2 - run 0.
(Bottom) Significance level .

Fig.2q Vertical velocity : (Top) Mean difference for run 2 - run 0.
(Bottom) Significance level .

Fig.3a (Top) Topography of the model .
(Bottom) Mean SAT for run 3 .

Fig.3b (Top) Mean Layer temperature from 1000-850 mb (T10-8)
for run 3 .
(Botom) Mean T8-7 for run 3 .

Fig.3c SAT : (Top) Mean difference for run 3 - run 2 .
(Bottom) Significance level .

Fig.3d T10-8: (Top) Mean difference for run 3 - run 2 .
(Bottom) Significance level .

Fig.3e T8-7 : (Top) Mean difference for run 3 - run 2 .
(Bottom) Significance level .

Fig.3f (Top) Surface wind for run 3.
(Bottom) Surface wind for run 2.

Fig.3g Time series of T10-8 for runs 2 and 3 in region (i)
and region (ii).

Fig.3h Time series of T10-8 for runs 2 and 3 in region (iii).

Fig.3i (Top) Mean SLP for run 3 .
(Bottom) Mean G500 for run 3 .

Fig.3j SLP : (Top) Mean difference for run 3 - run 2 .
(Bottom) Significance level .

Fig.3k G500 : (Top) Mean difference for run 3 - run 2 .
(Bottom) Significance level .

Fig.3l Schematic representation of the two types of blocking
situation, from Kasahara (1980).

Fig.3n (Top) Mean sensible heat flux for run 3 .
(Bottom) Mean evaporation for run 3 .

Fig.3n Sensible heat flux: (Top) Mean difference for run 3 - run 2.
(Bottom) Significance level .

Fig.3o Evaporation : (Top) Mean difference for run 3 - run 2 .
(Bottom) Significance level .

Fig.3p (Top) Mean low cloud cover for run 3 .
(Bottom) Mean precipitation for run 3 .

Fig.3q Low cloud cover: (Top) Mean difference for run 3 - run 2 .
(Bottom) Significance level .

Fig.3r precipitation : (Top) Mean difference for run 3 - run 2 .
(Bottom) Significance level .

Fig.3s (Top) Temperature cross-section for run 3 .
(Bottom) Zonal wind cross-section for run 3.

Fig.3t Temperature : (Top) Mean difference for run 3 - run 2 .
(Bottom) Significance level .

Fig.3u Zonal wind : (Top) Mean difference for run 3 - run 2
(Bottom) Significance level .

Fig.3v (Top) Meridional wind cross-section of run 3 .
(Bottom) Vertical velocity cross-section for run 3 .

Fig.3w Meridional wind : (Top) Mean difference for run 3 - run 2.
(Bottom) Significance level .

Fig.3x Vertical velocity : (Top) Mean difference for run 3 - run 2.
(Bottom) Significance level .

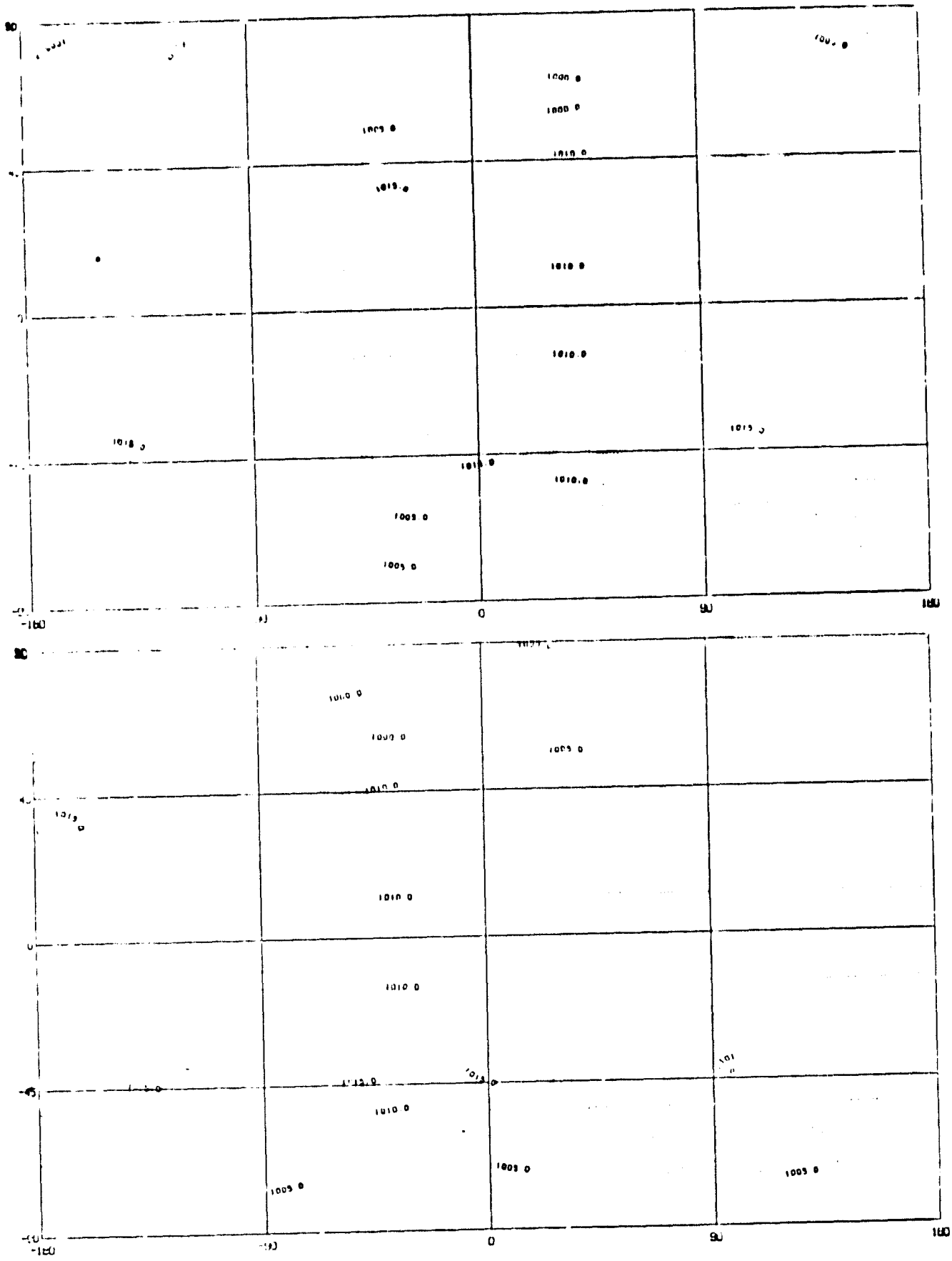

Fig. 1a (Top) Mean sea-level pressure (SLP) for run 0 (mb). (Bottom) Mean SLP for run 1 (mb).

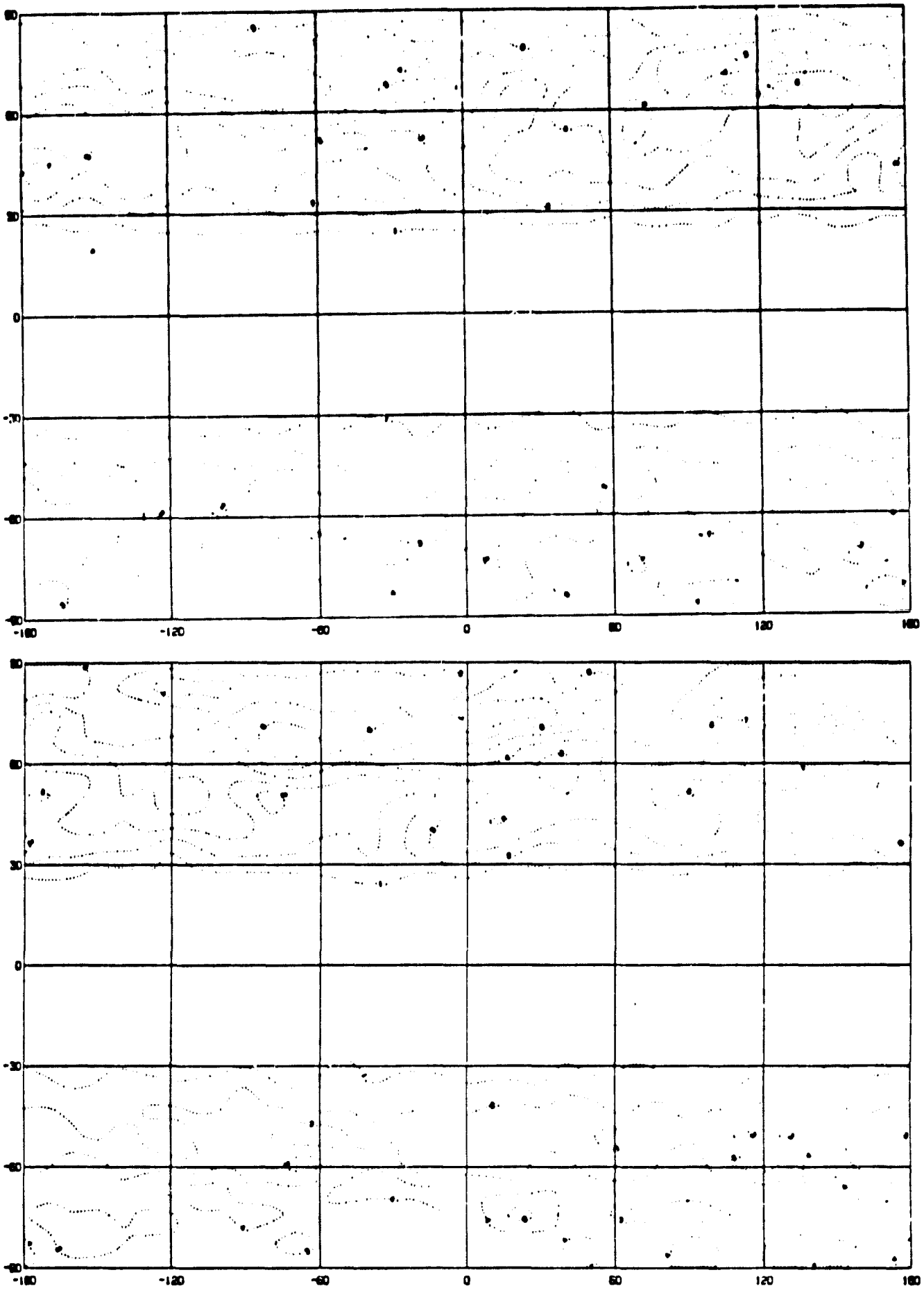

Fig. 1b *SLP : (Top) Standard deviation of run 0 (mb).*
(Bottom) Standard deviation of run 1 (mb).

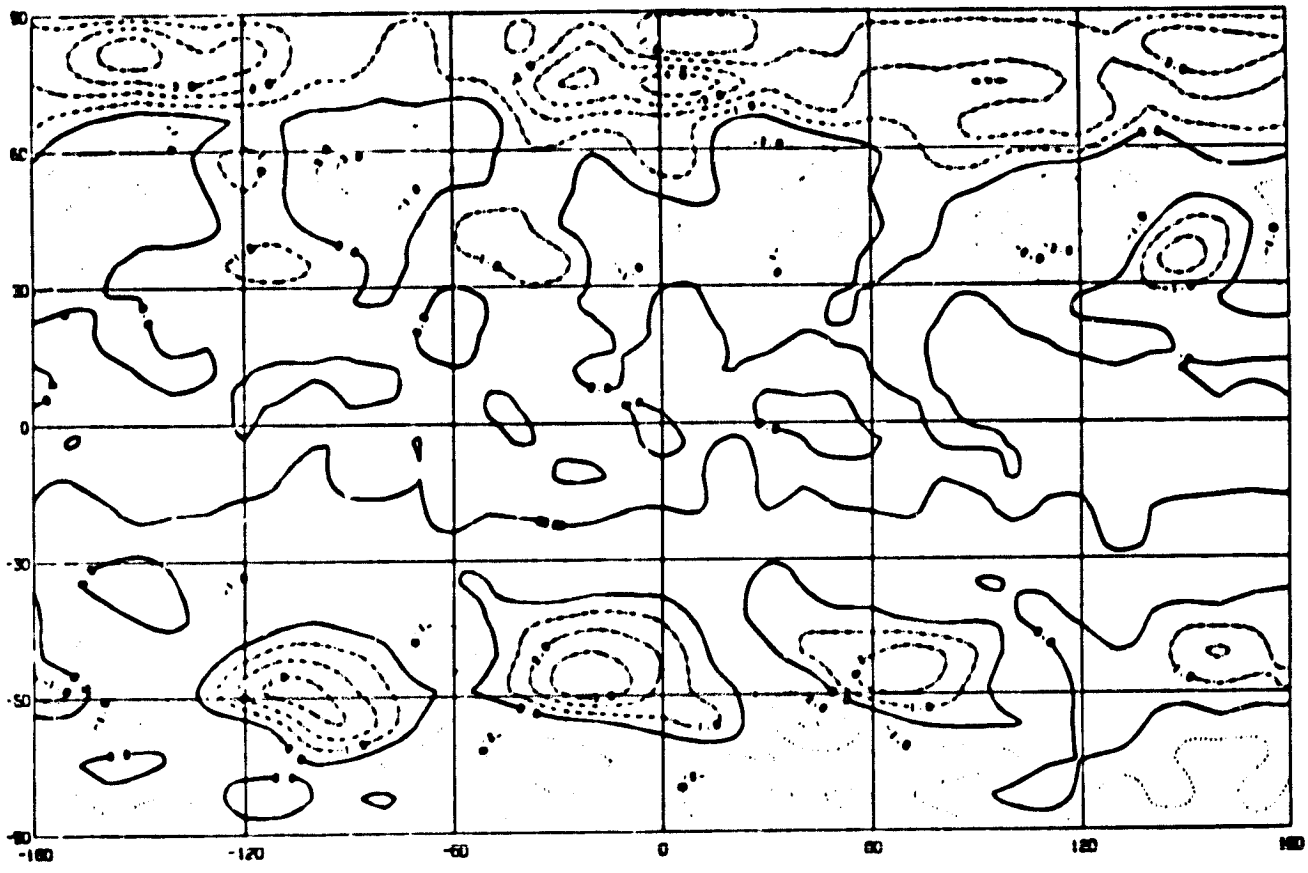

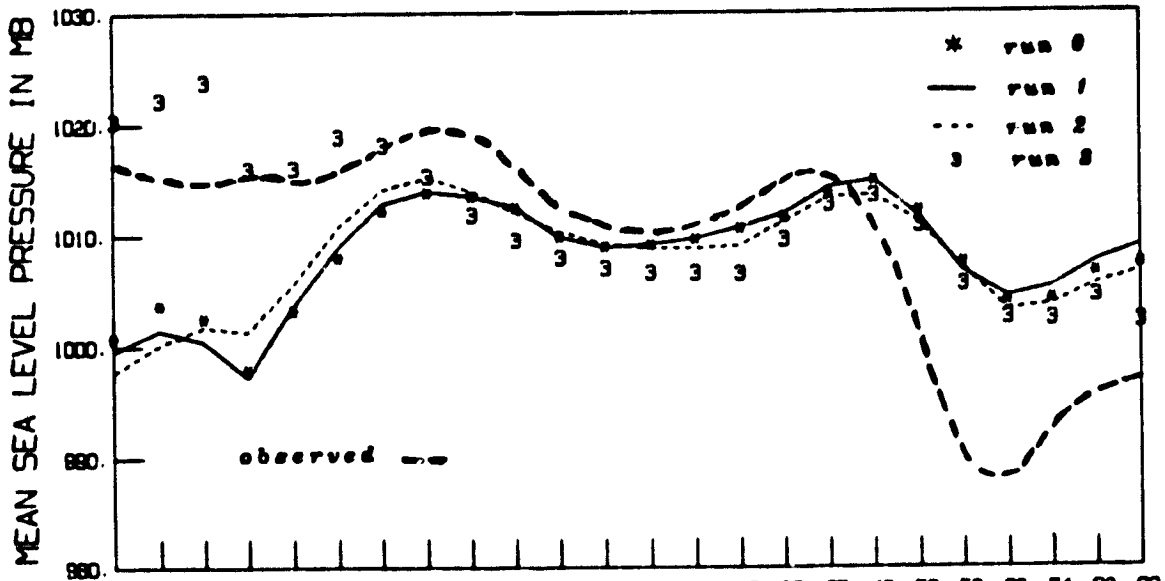

Fig.1c *(Top) Mean SLP difference of run 0 - run 1 (mb).*
Fig.1d *(Bottom) Meridional SLP profiles for runs 0, 1, 2, 3 and observed (mb). The observed profile is taken from Schlesinger and Gates (1979).*

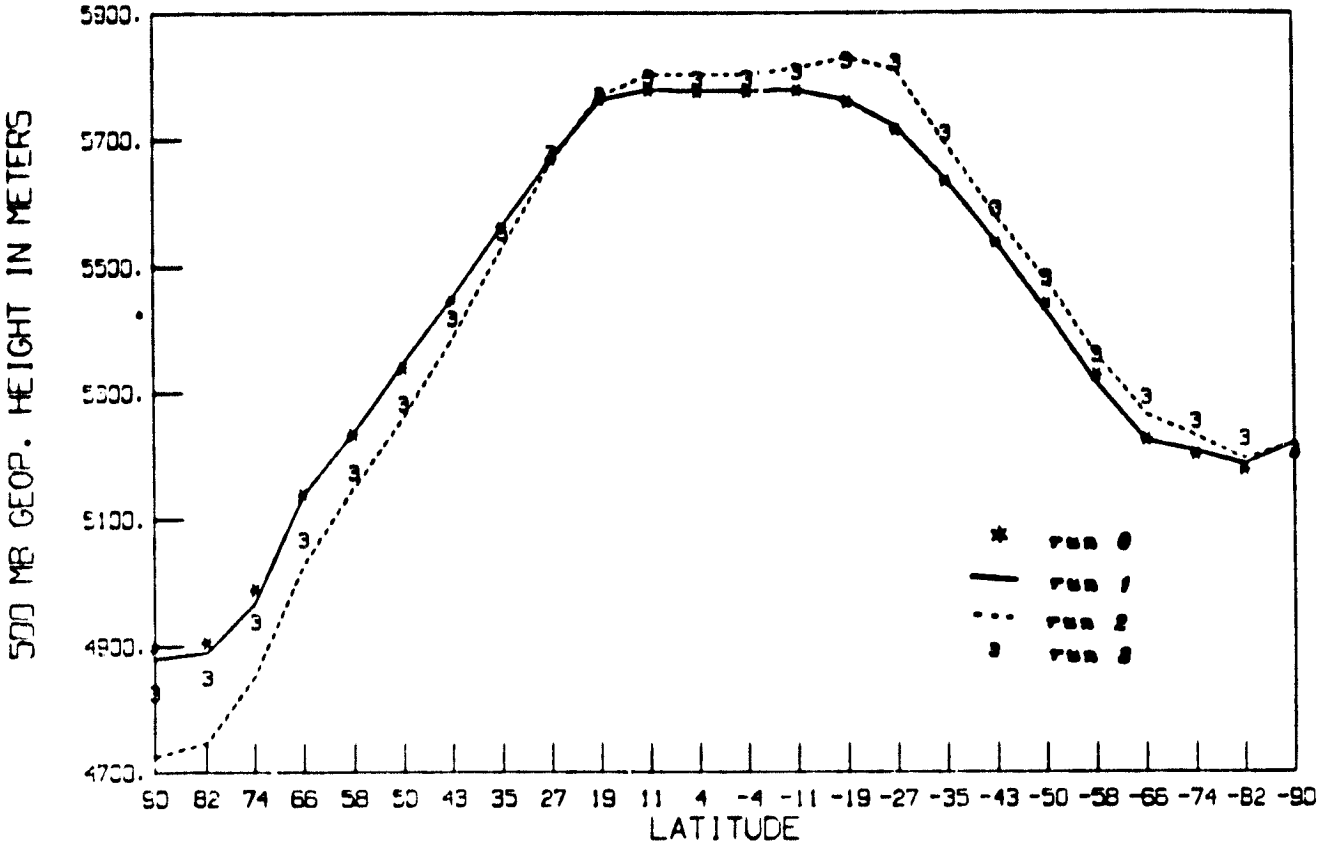

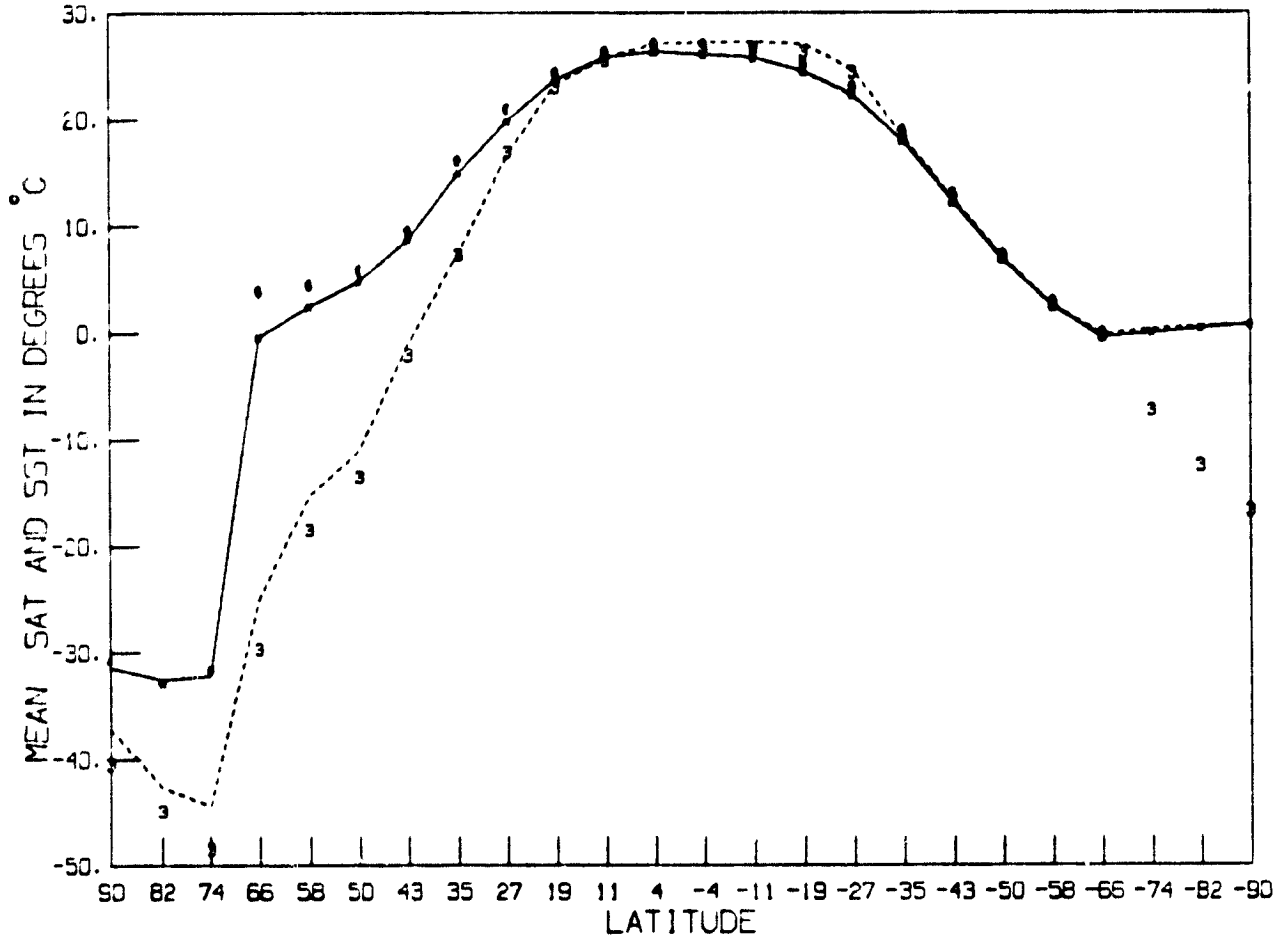

Fig. 1e *(Top) 500mb height (G500) profiles for runs 0 to 3 (m). (Bottom) Meridional surface air temperature (SAT) profiles for runs 0 to 3, and sea surface temperature (SST) profile (°C).*

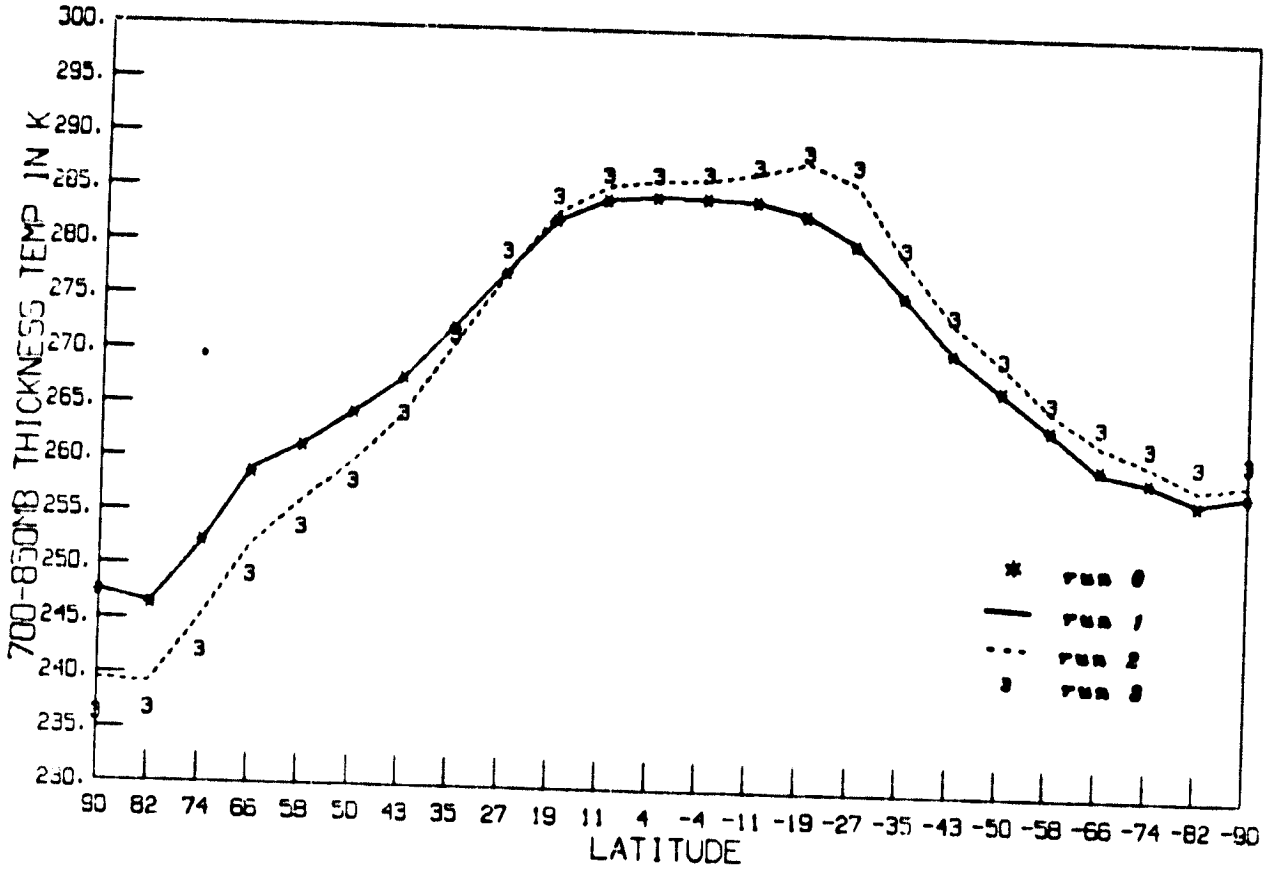

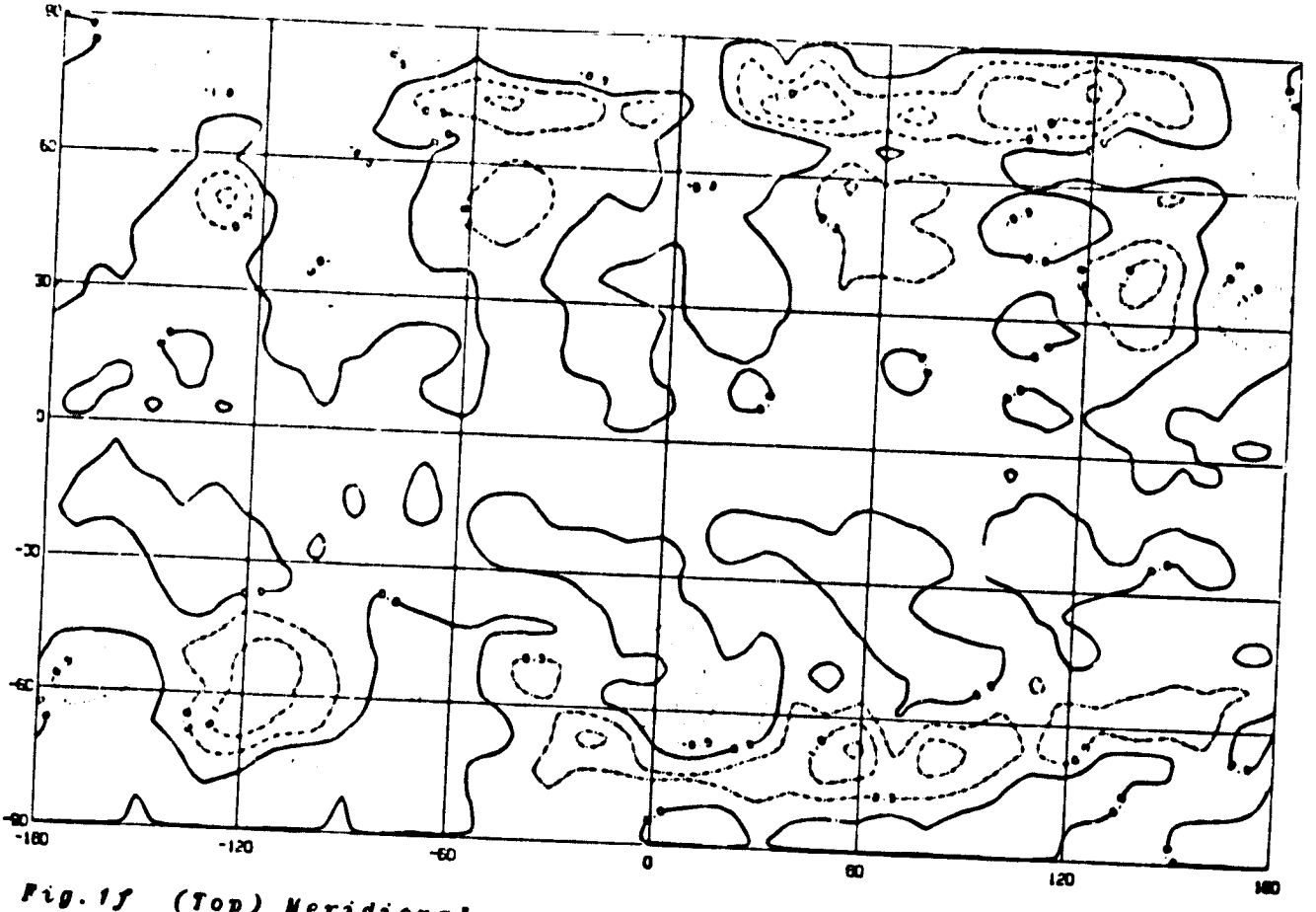

Fig. 1f (Top) Meridional profiles of layer temperature from 850-700mb (T8-7) for runs 0 to 3 (K). (Bottom) Mean T8-7 difference of run 0 - run 1 (K).

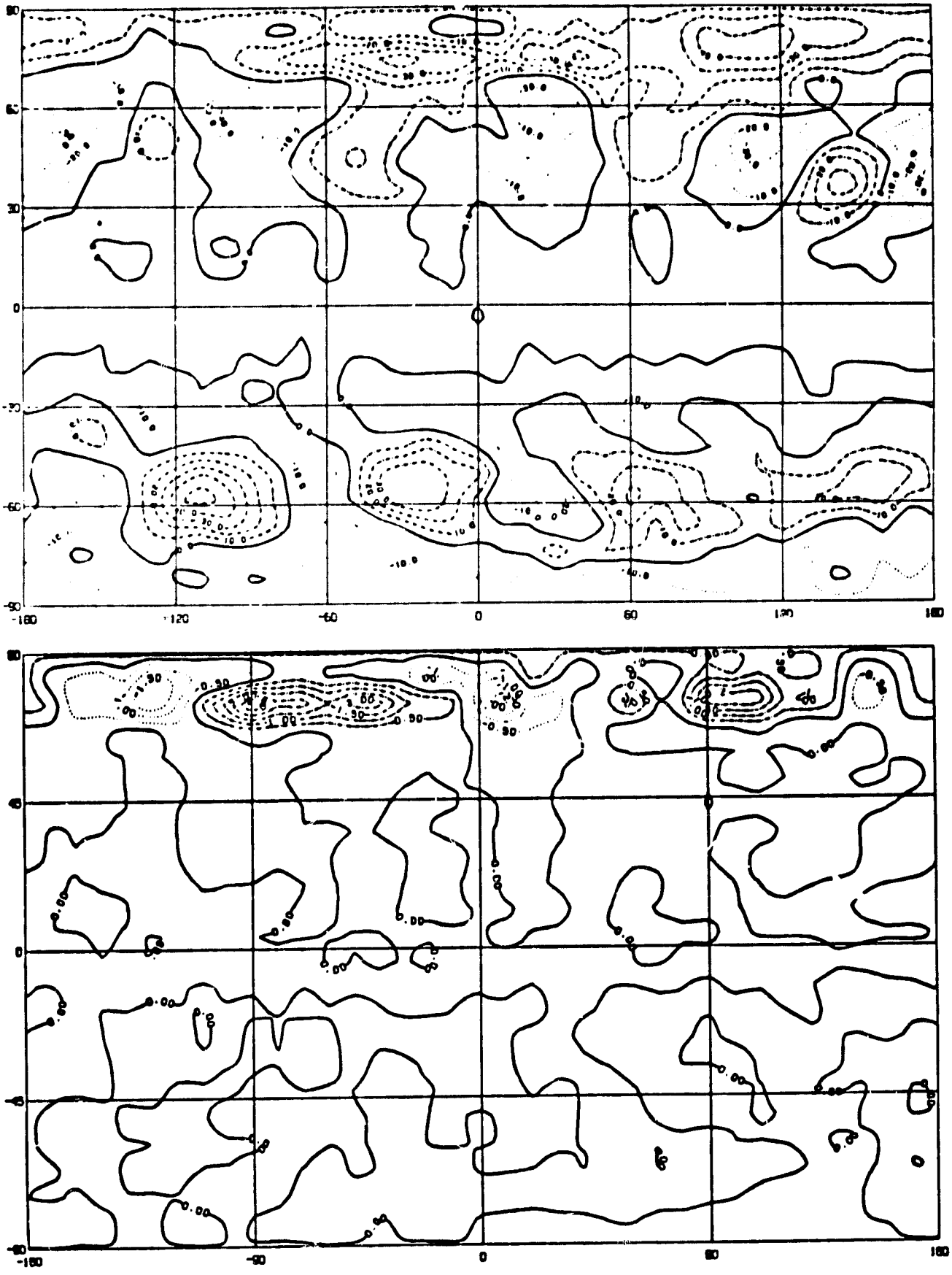

Fig. 1g (Top) Mean G500 difference of run 0 - run 1 (m).
(Bottom) Mean SAT difference of run 0 - run 1 (°C).

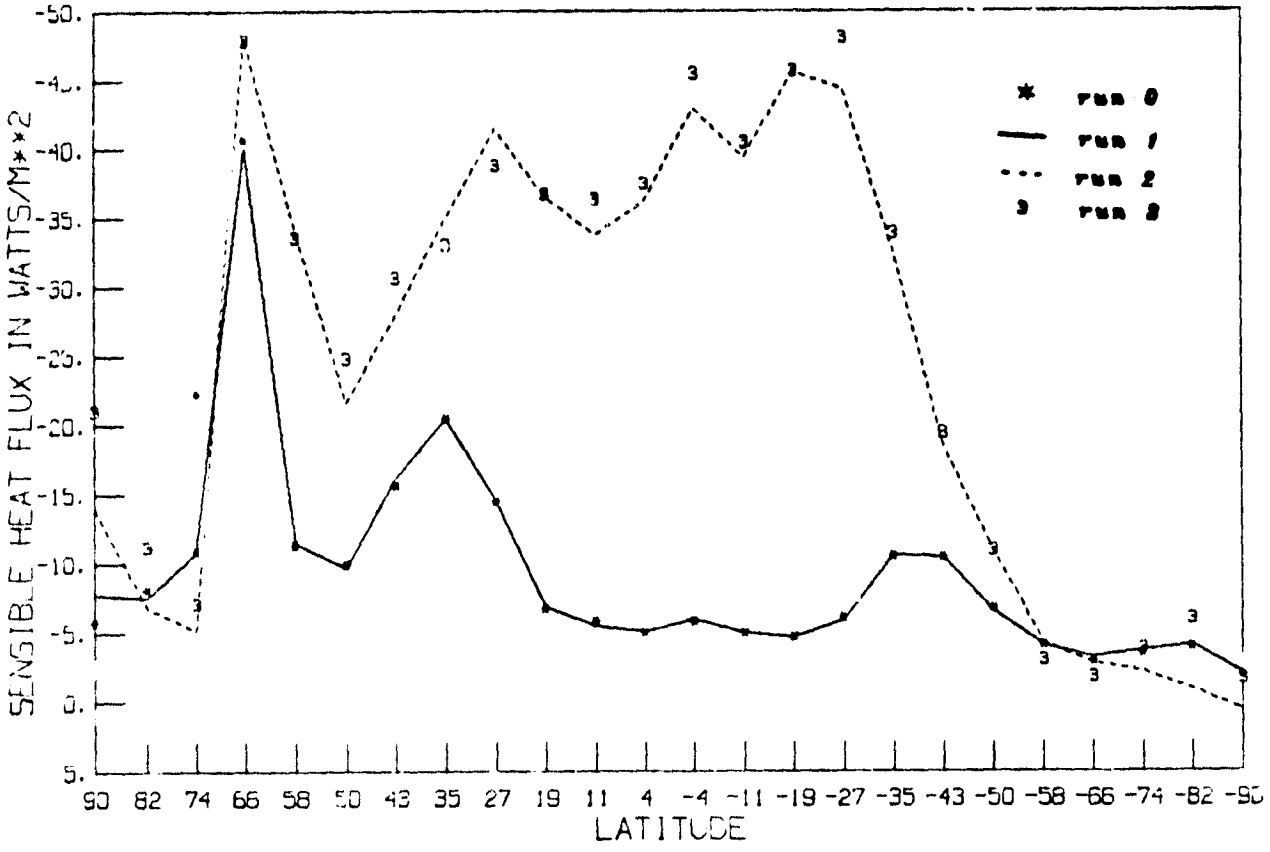

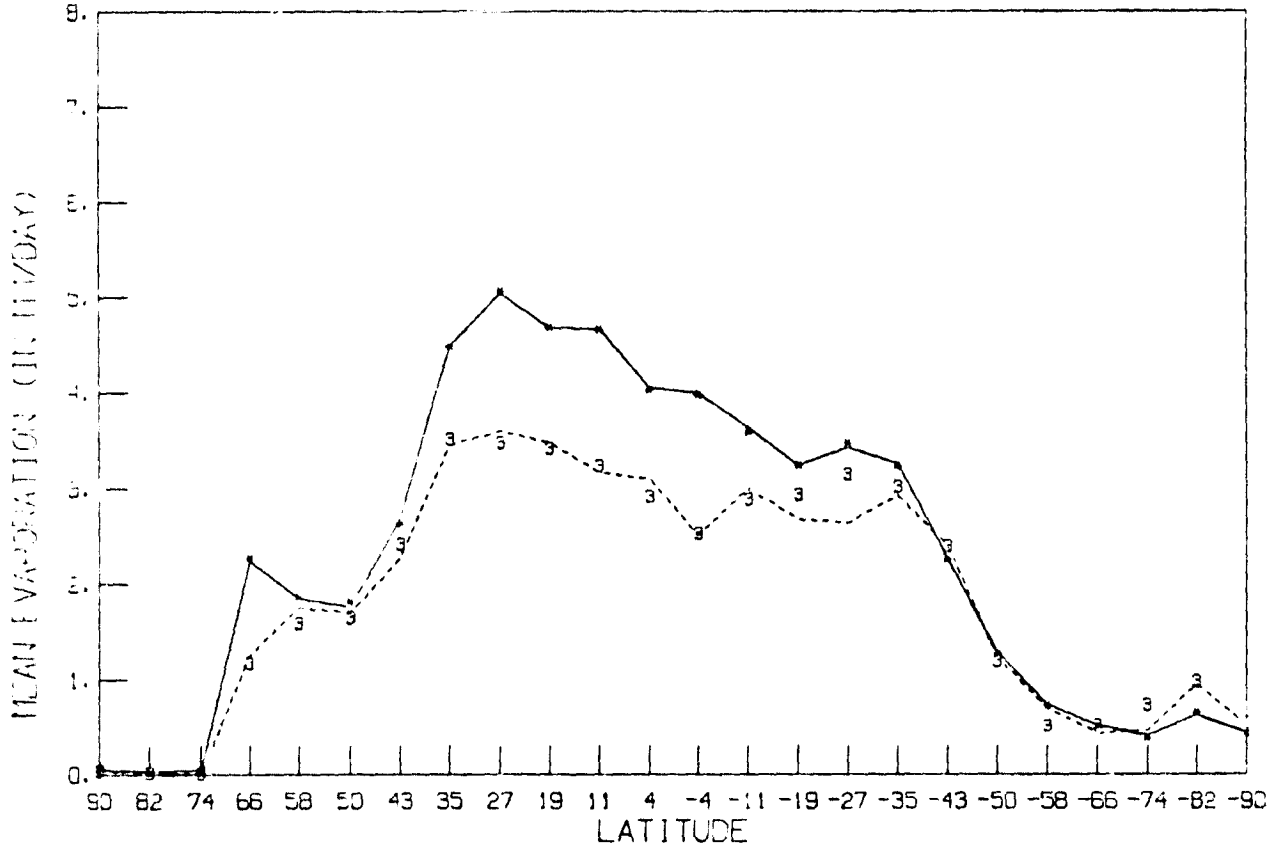

*Fig. 1h (Top) Meridional sensible heat flux profiles for runs 0 to 3 (watts/m**2).*
(Bottom) Meridional evaporation profiles for runs 0 to 3 (mm/day).

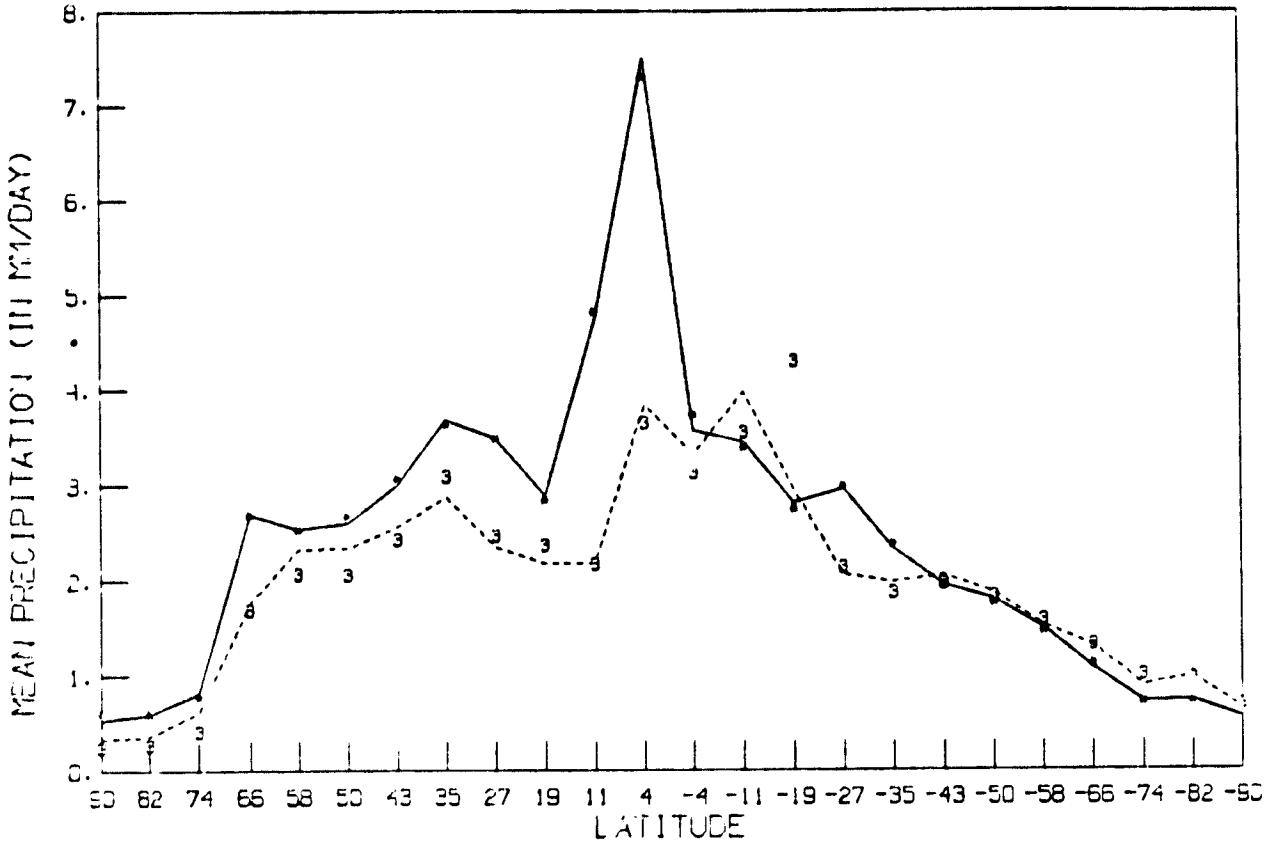

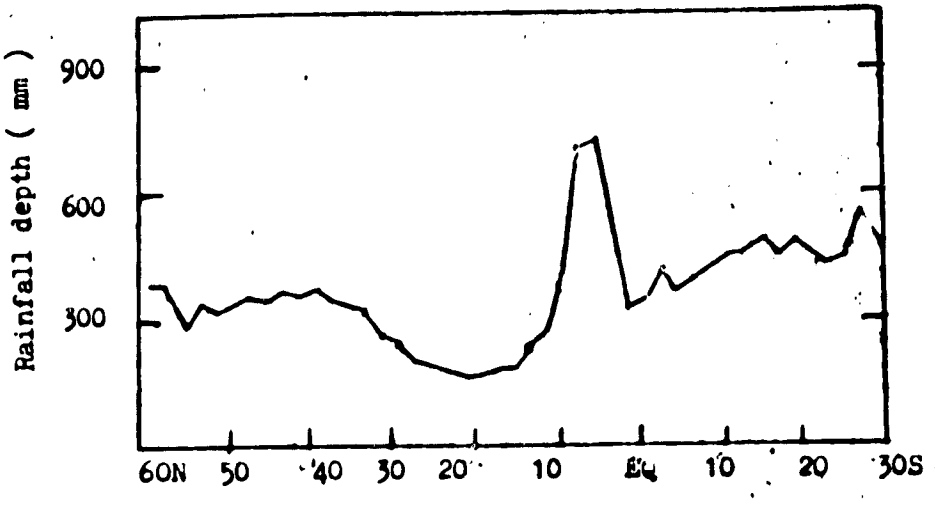

Fig. 1i (Top) Meridional precipitation profile for run 0 to 3 (mm/day).

(Bottom) Mean winter rainfall (mm) by latitude over the Pacific Ocean (from C.E.Dorman and R.H.,Bourke).

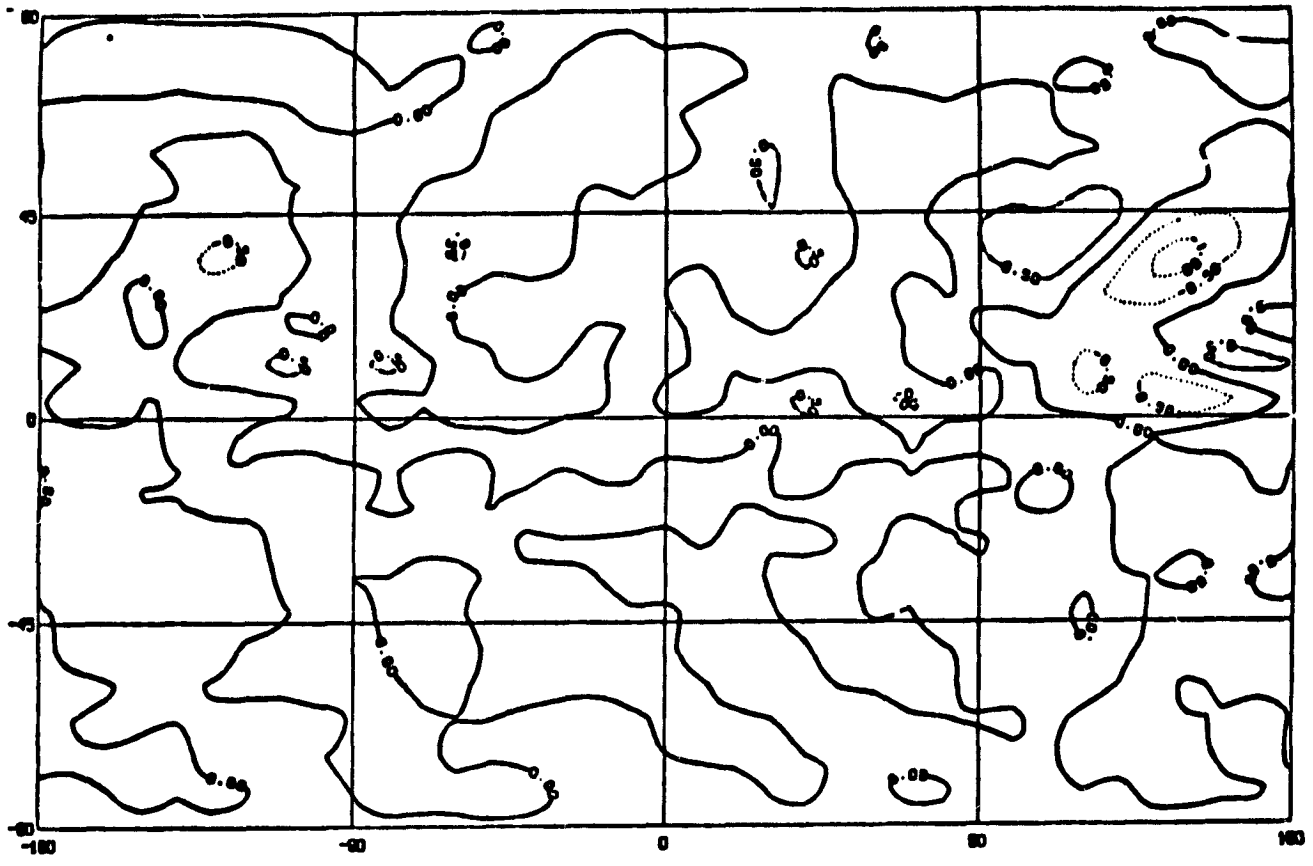

Fig. 1j (Top) Mean precipitation difference of run 0 - run 1 (mm/day).

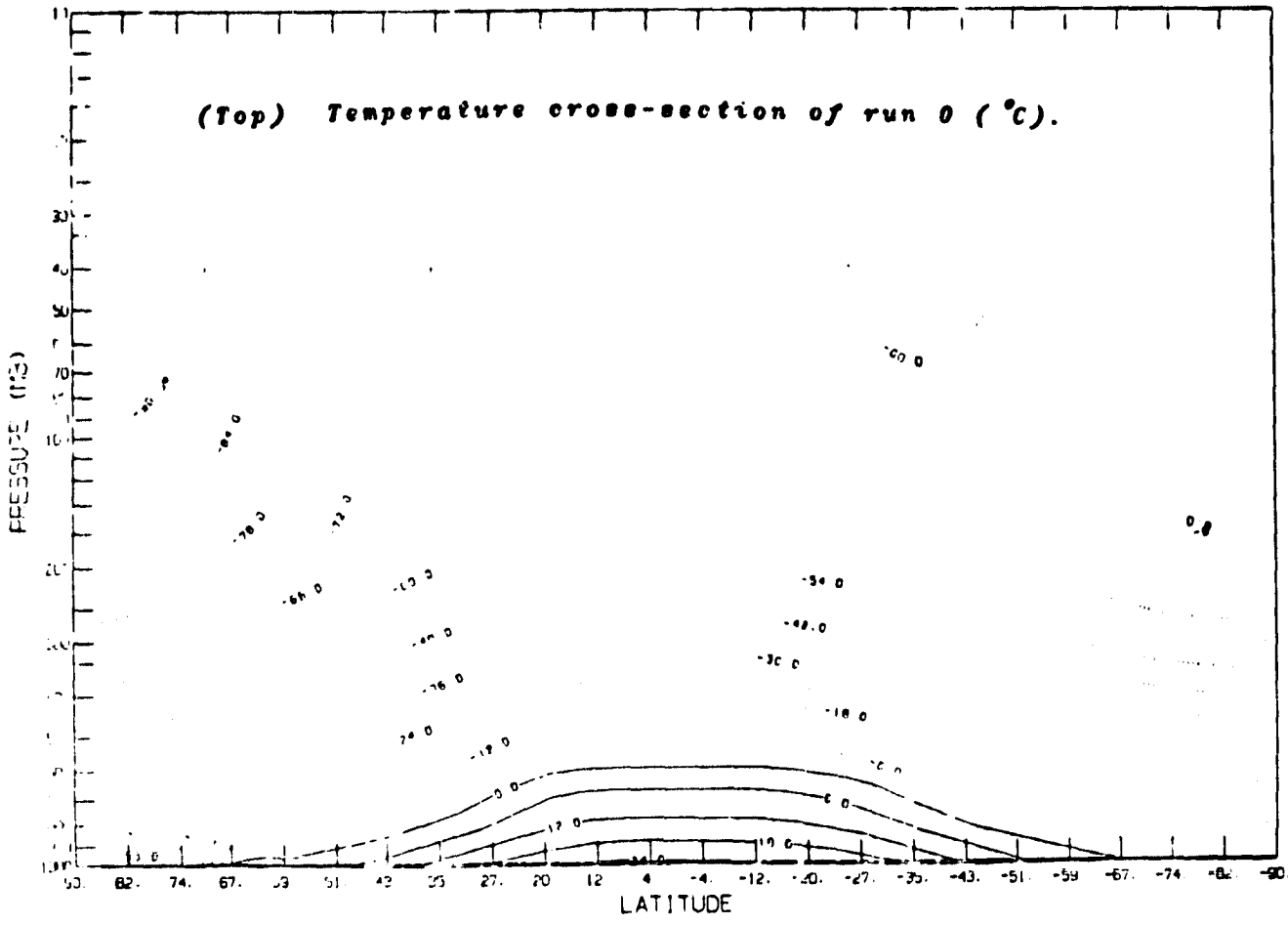

(Top) Temperature cross-section of run 0 (°C).

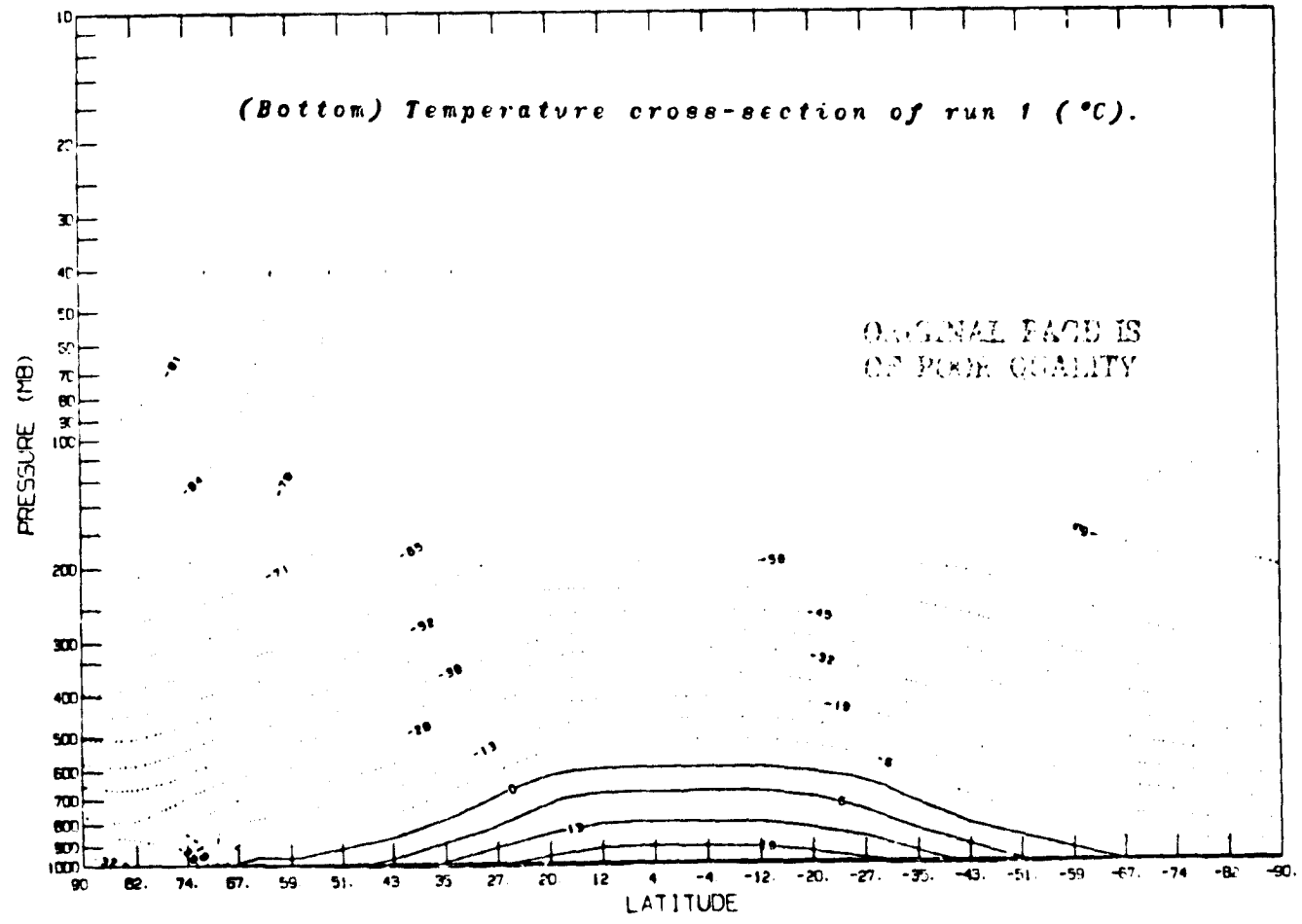

(Bottom) Temperature cross-section of run 1 (°C).

Fig. 1k

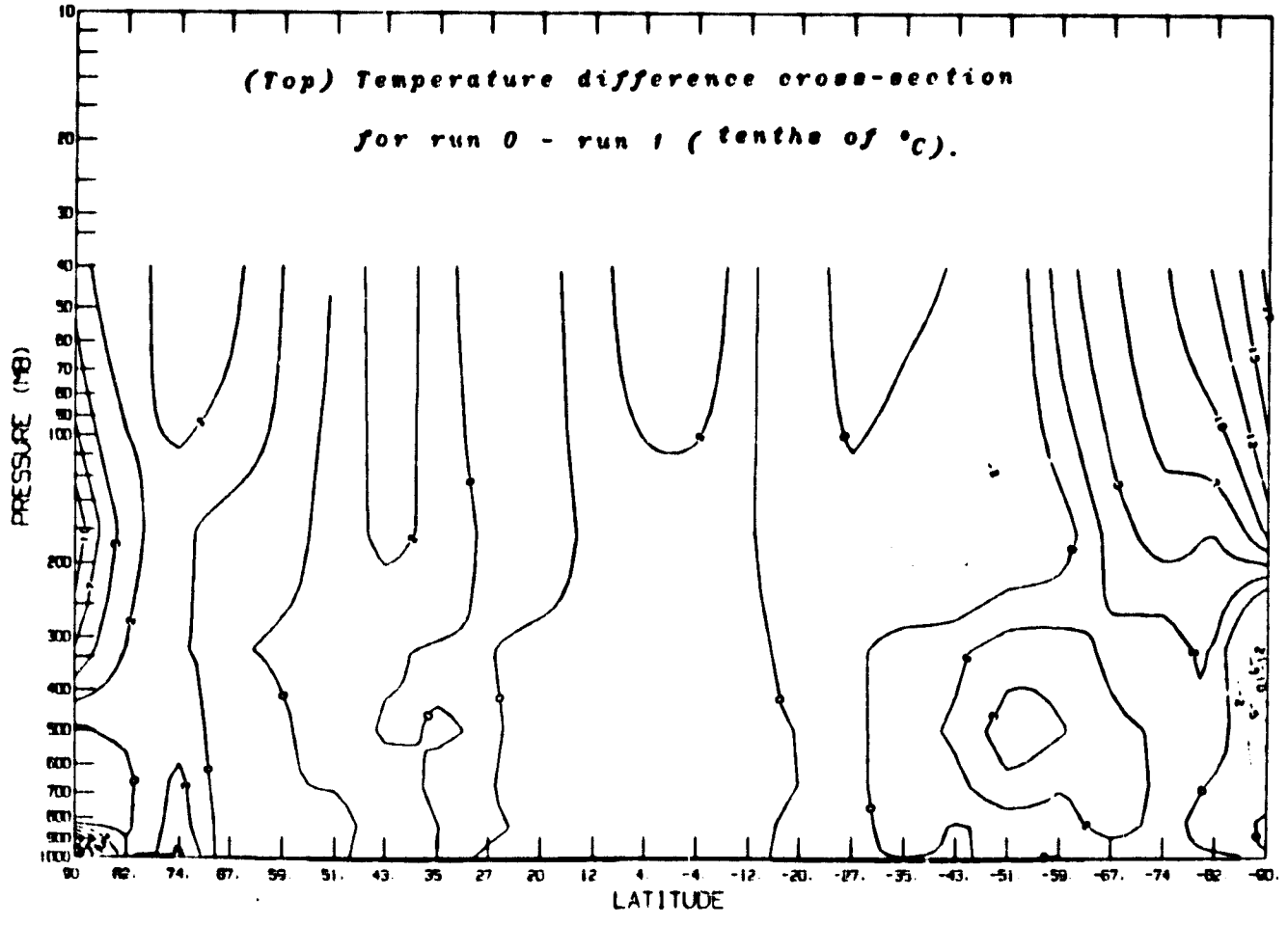

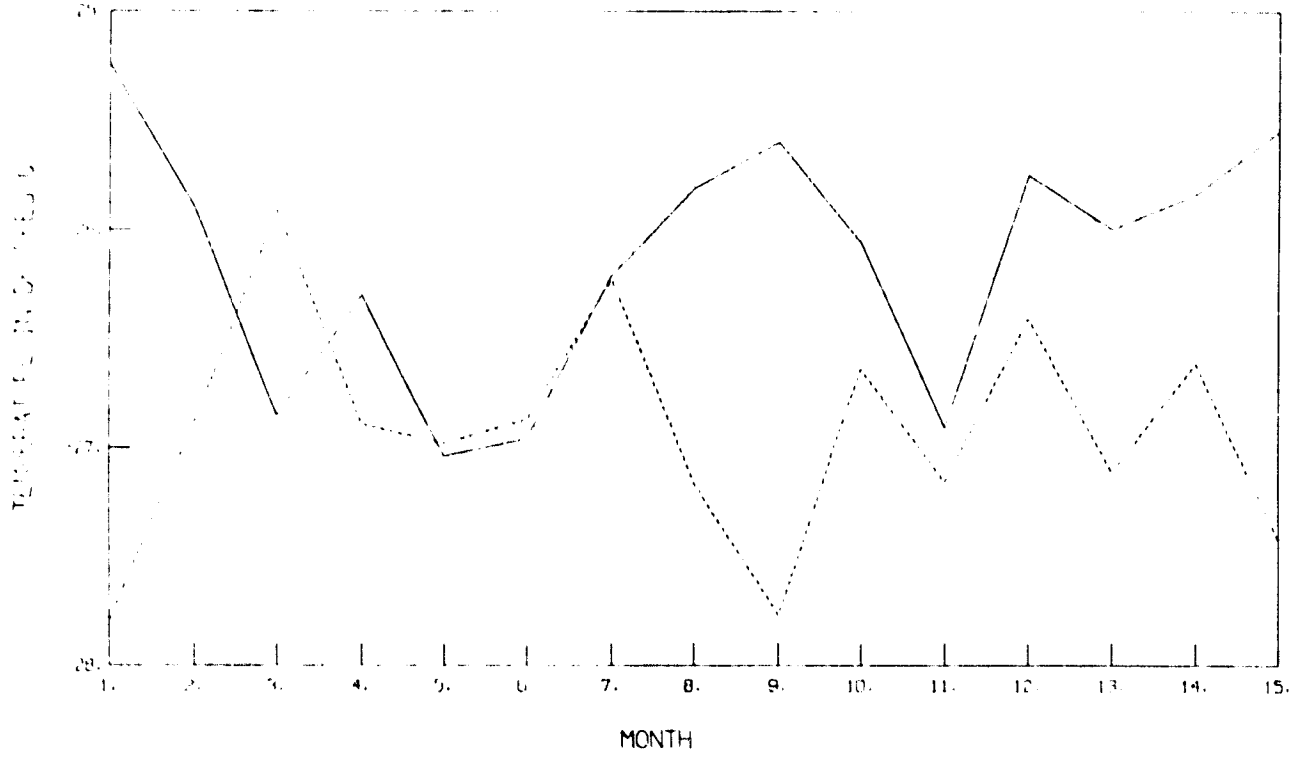

Fig. 11 (Bottom) Time series of sonal mean temperature at 51S and 497mb. for runs 0 and 1.

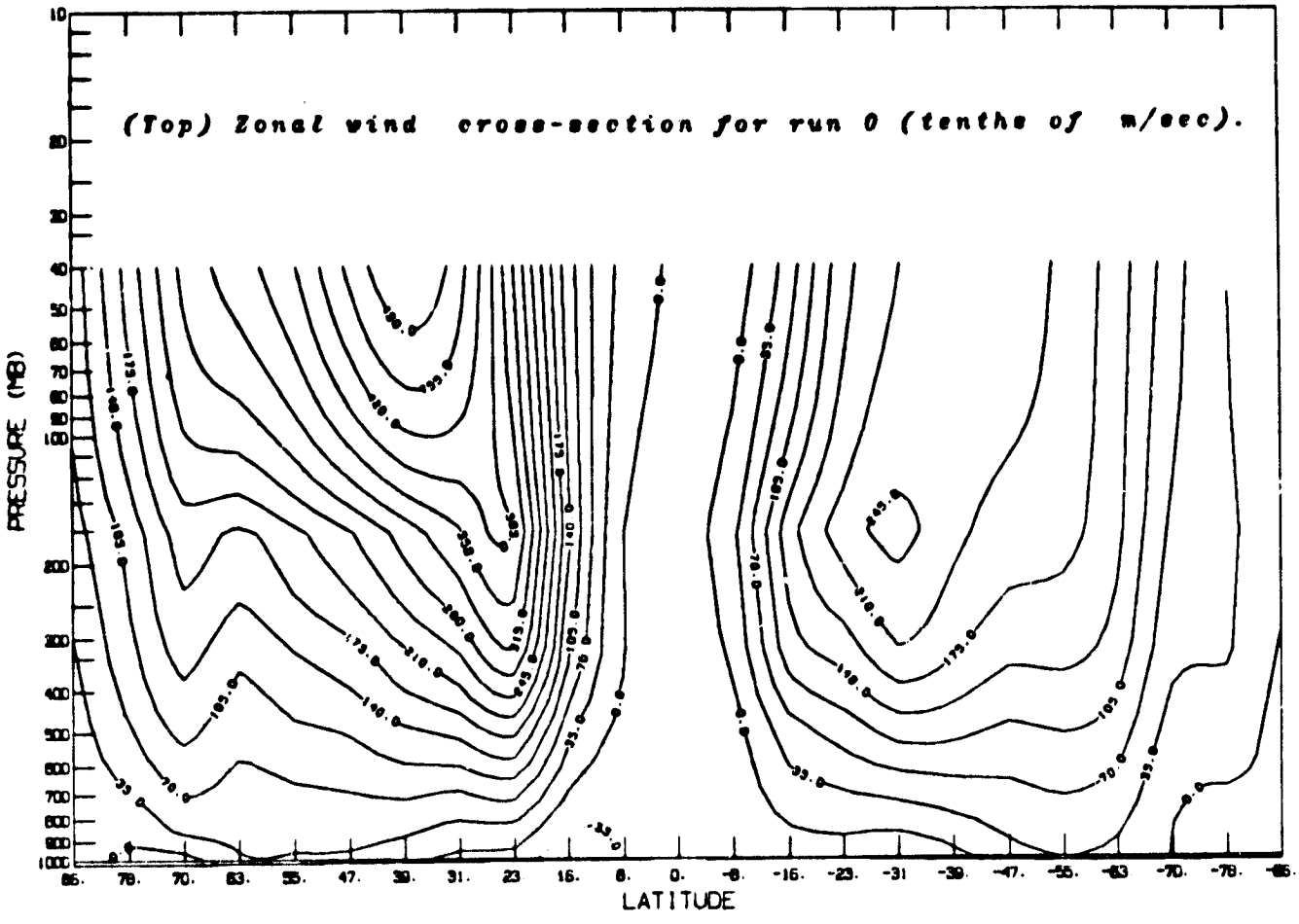
(Top) Zonal wind cross-section for run 0 (tenths of m/sec).
PRESSURE (MB)
LATITUDE
85. 78. 70. 63. 55. 47. 39. 31. 23. 16. 8. 0. -8. -16. -23. -31. -39. -47. -55. -63. -70. -78. -85.

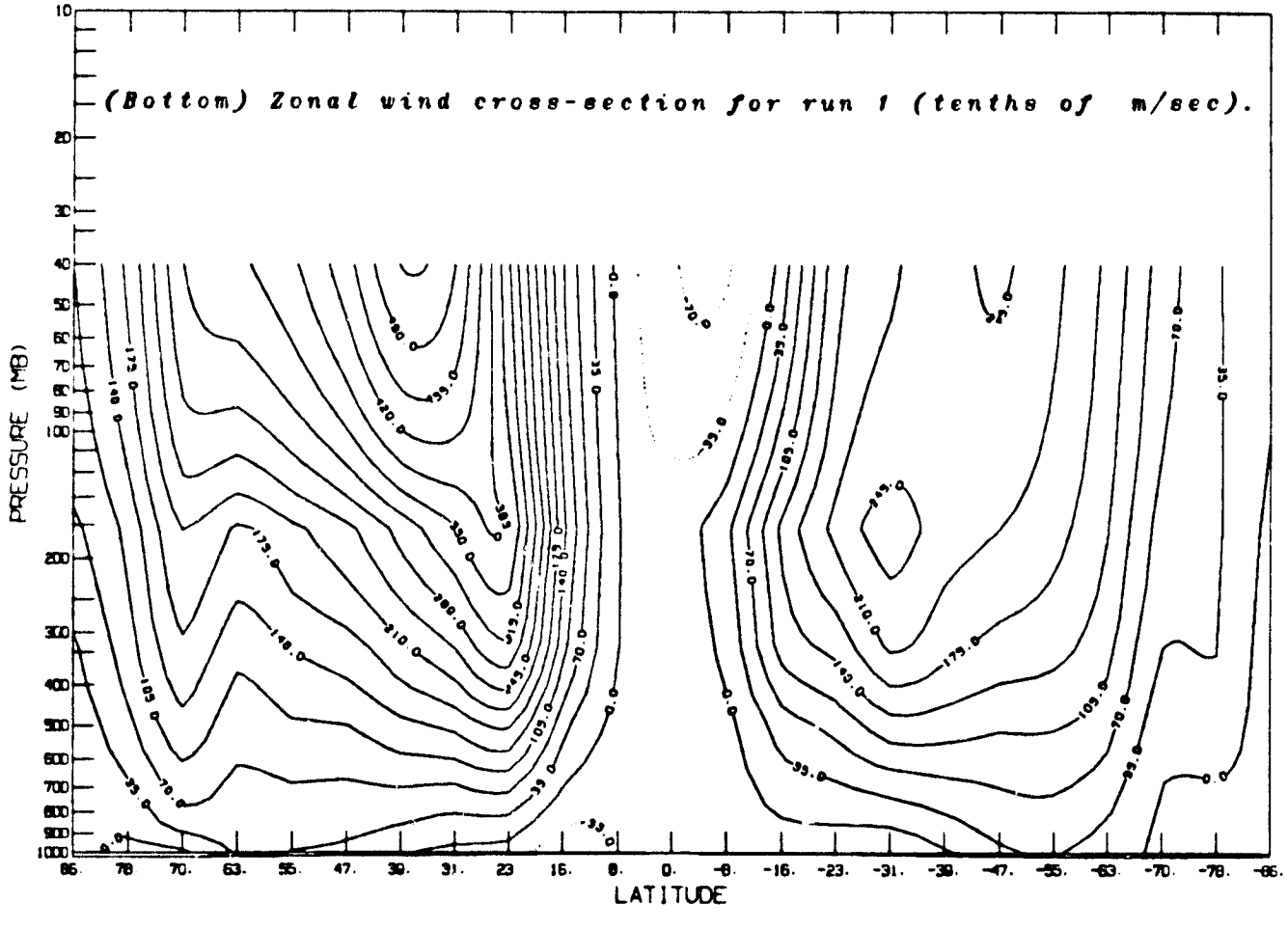
(Bottom) Zonal wind cross-section for run 1 (tenths of m/sec).
PRESSURE (MB)
LATITUDE
85. 78. 70. 63. 55. 47. 39. 31. 23. 16. 8. 0. -8. -16. -23. -31. -39. -47. -55. -63. -70. -78. -85.

Fig. 1m

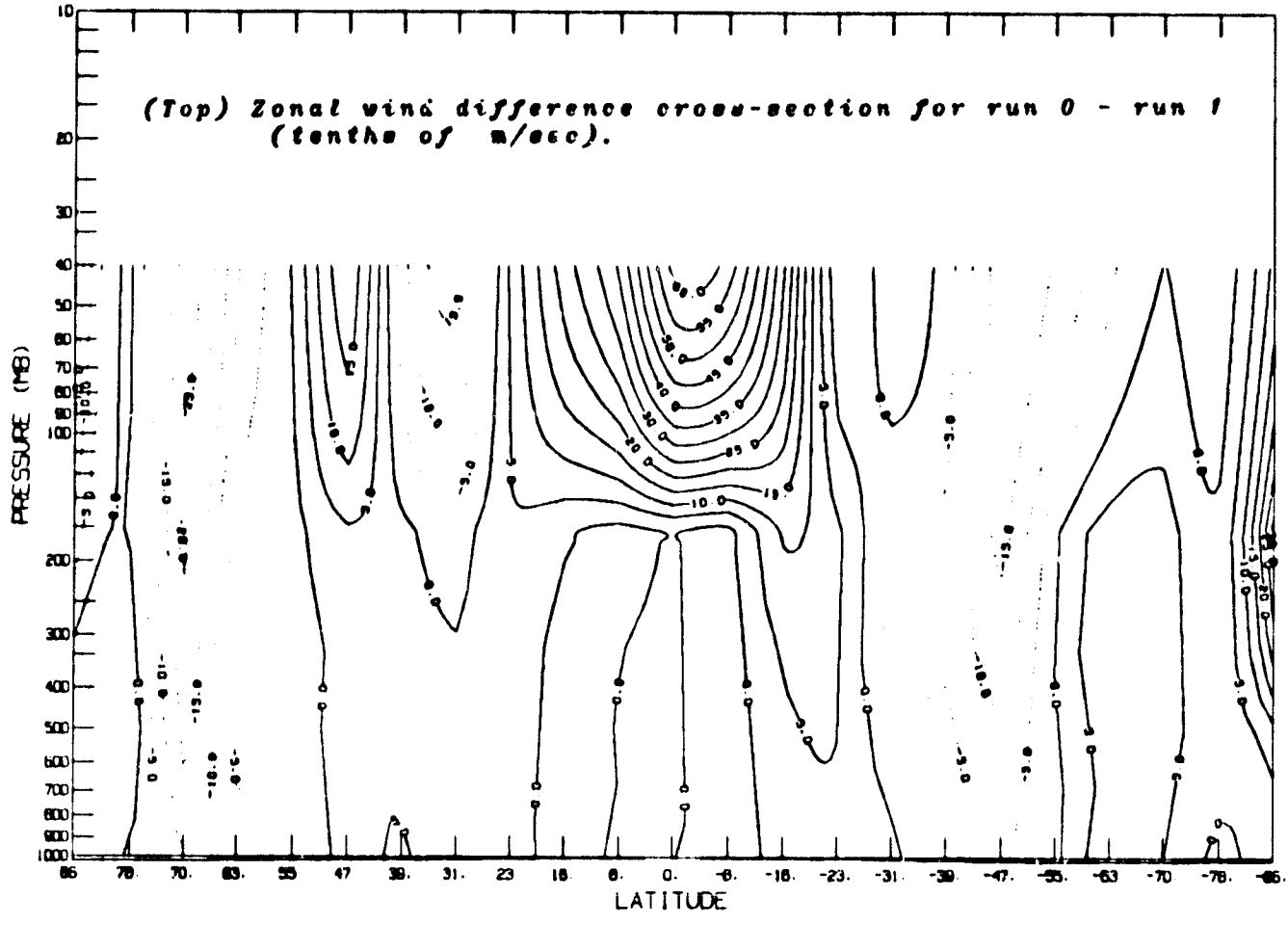
(Top) Zonal wind difference cross-section for run 0 - run 1
(tenths of m/sec).
PRESSURE (MB)
LATITUDE

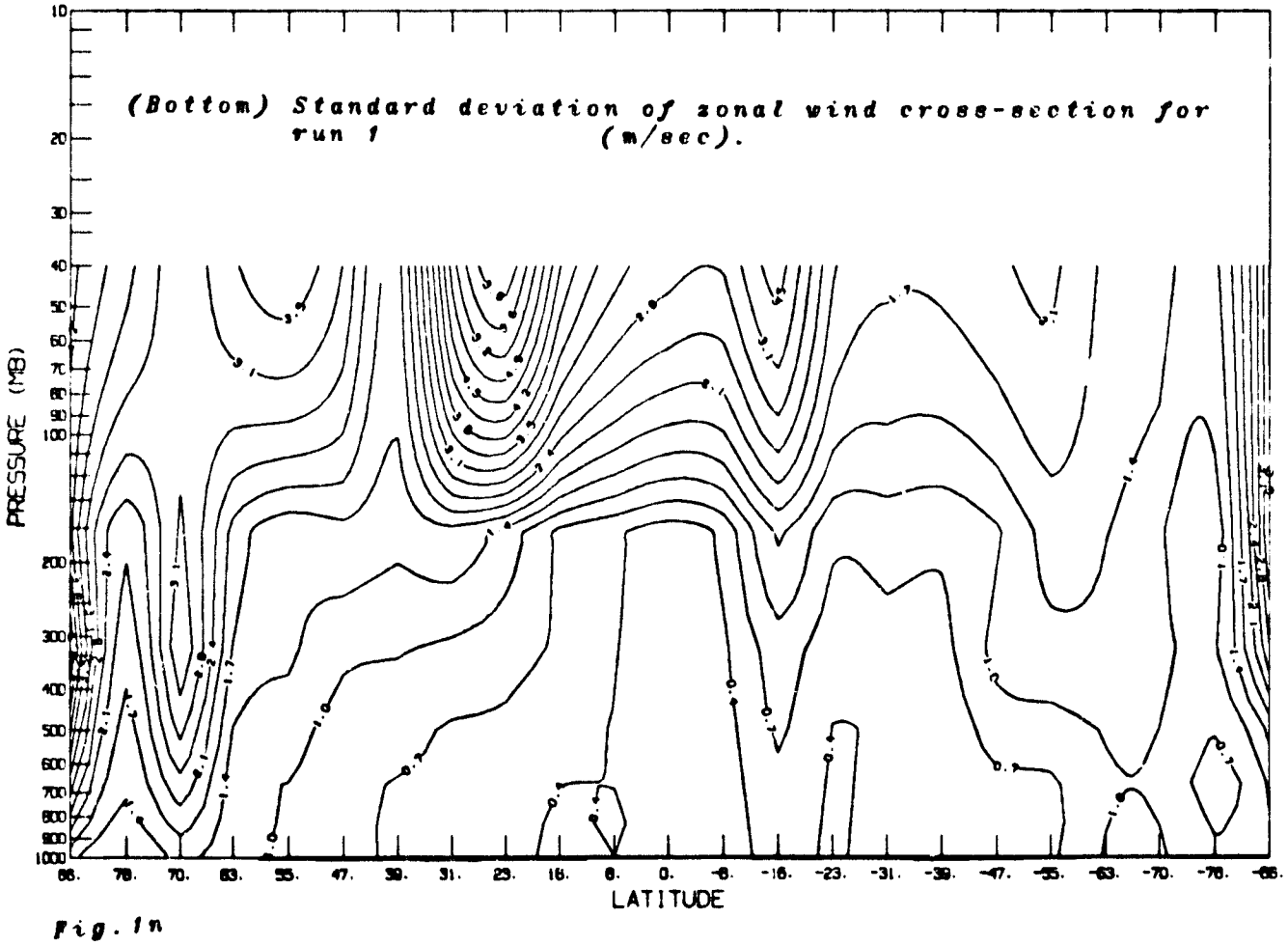
(Bottom) Standard deviation of zonal wind cross-section for
run 1 (m/sec).
PRESSURE (MB)
LATITUDE

Fig. 1n

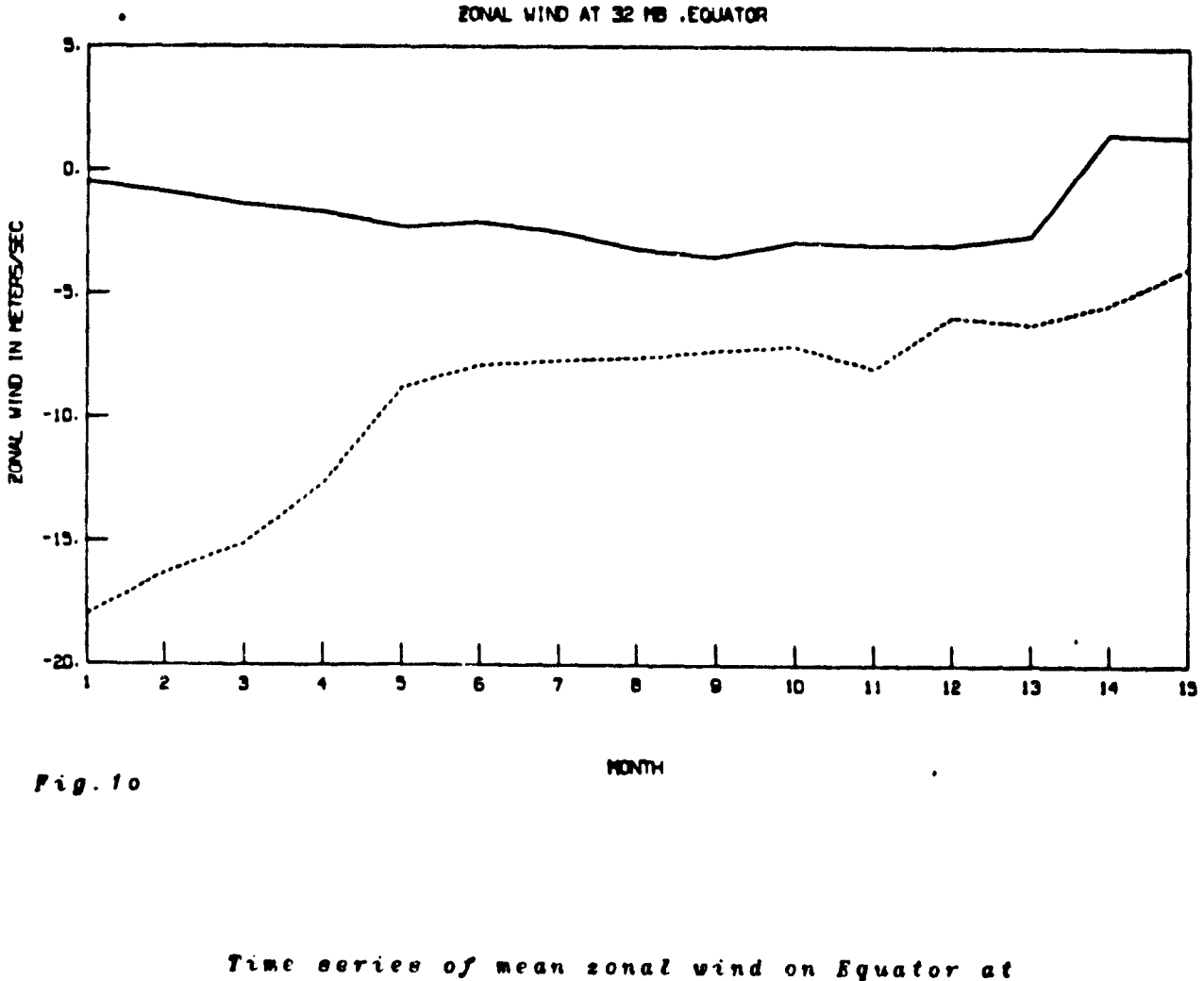

Fig. 1o

Time series of mean zonal wind on Equator at 32 mb level for runs 0 and 1 (m/sec).

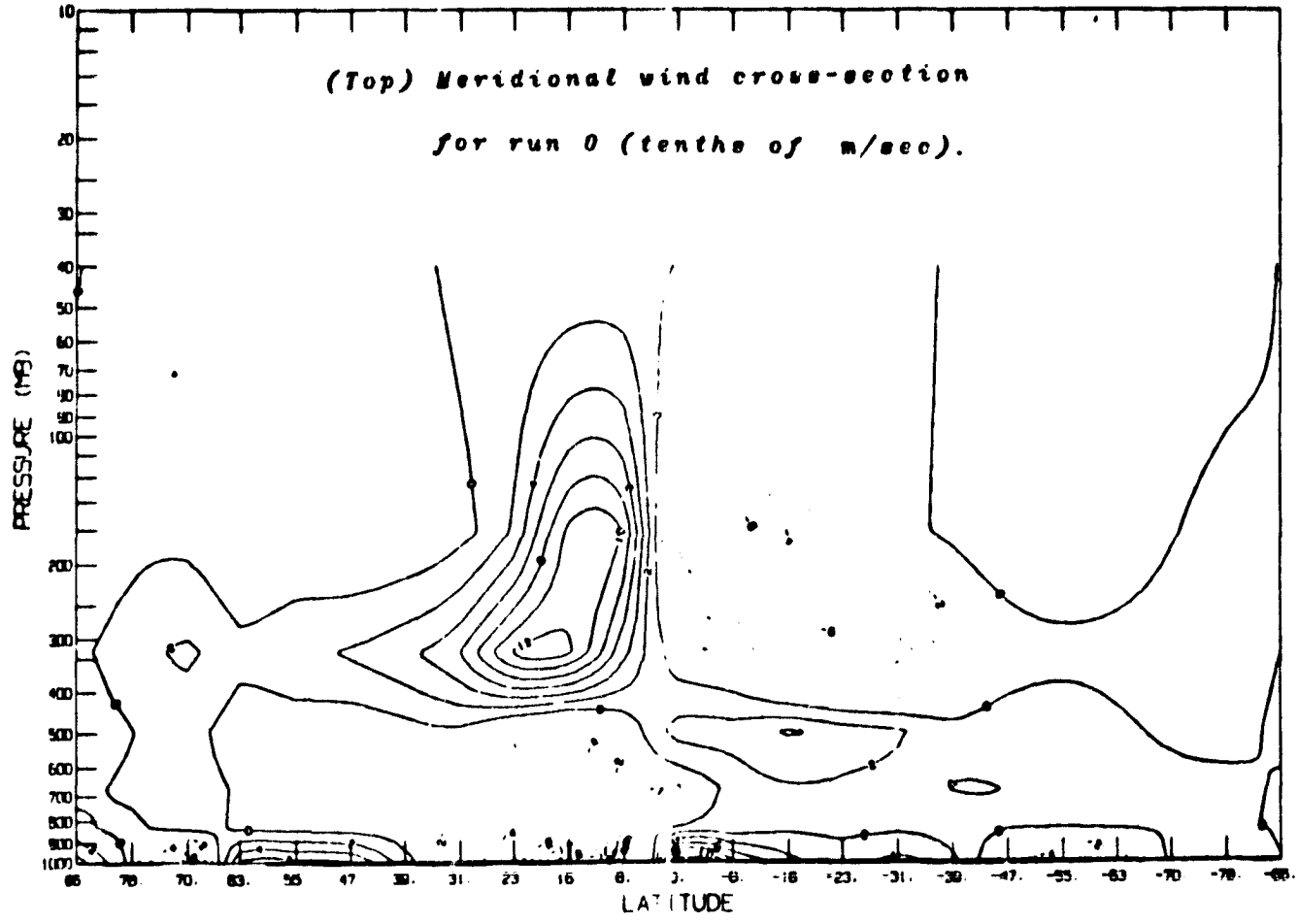
(Top) Meridional wind cross-section
for run 0 (tenths of m/sec).
PRESSURE (MB)
LATITUDE

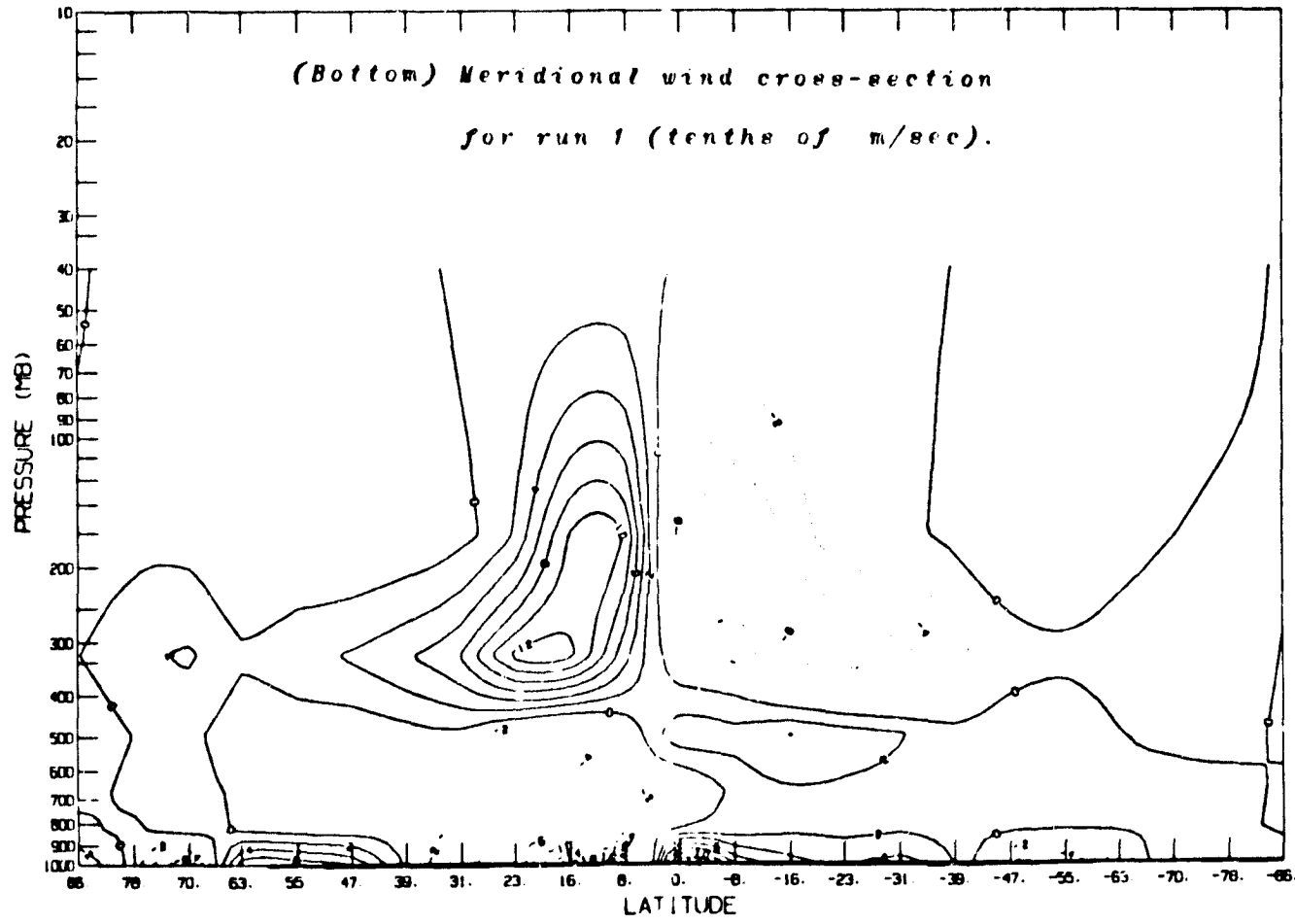
(Bottom) Meridional wind cross-section
for run 1 (tenths of m/sec).
PRESSURE (MB)
LATITUDE

Fig. 1p

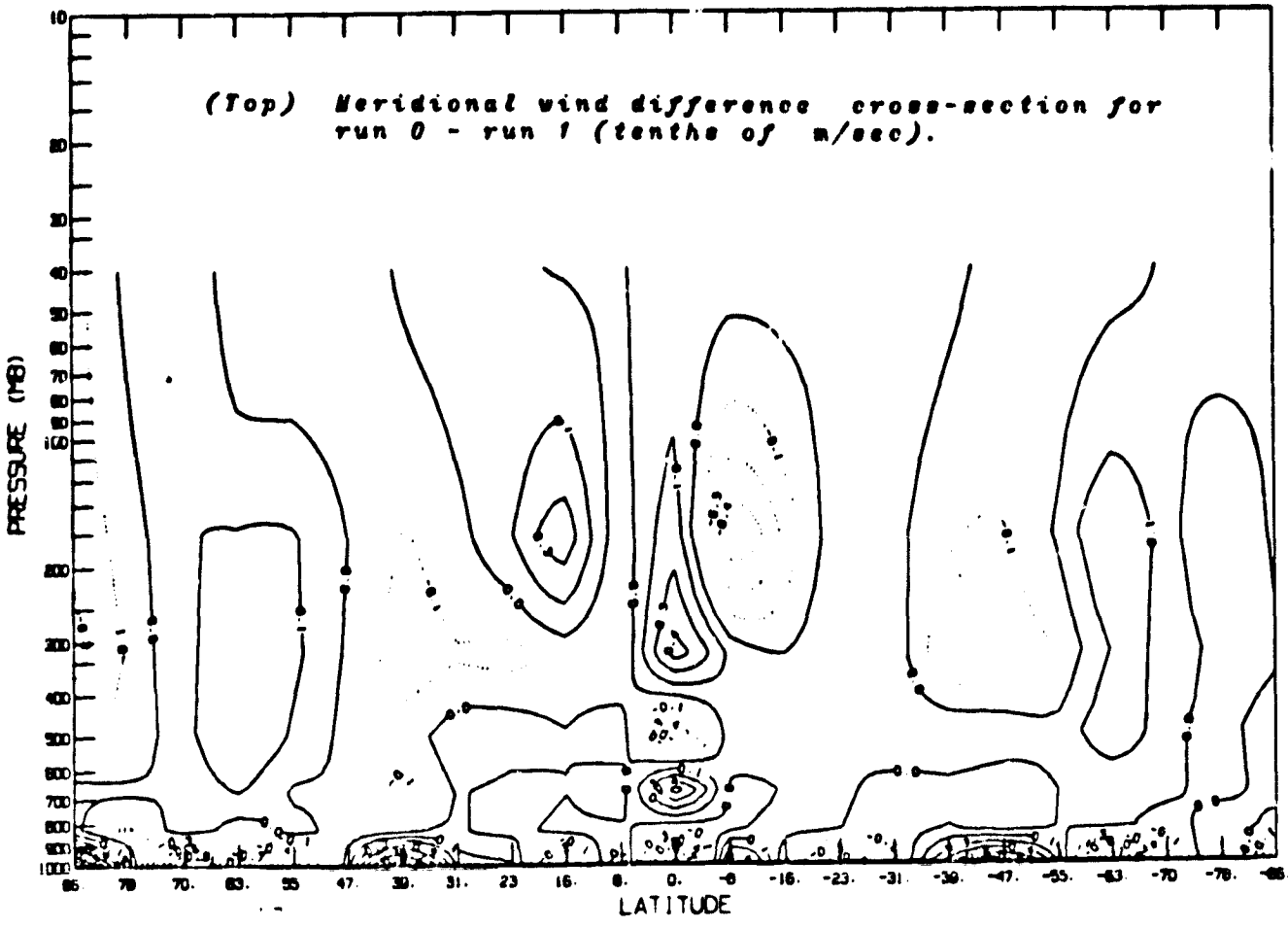
(Top) Meridional wind difference cross-section for run 0 - run 1 (tenths of m/sec).
PRESSURE (MB)
LATITUDE

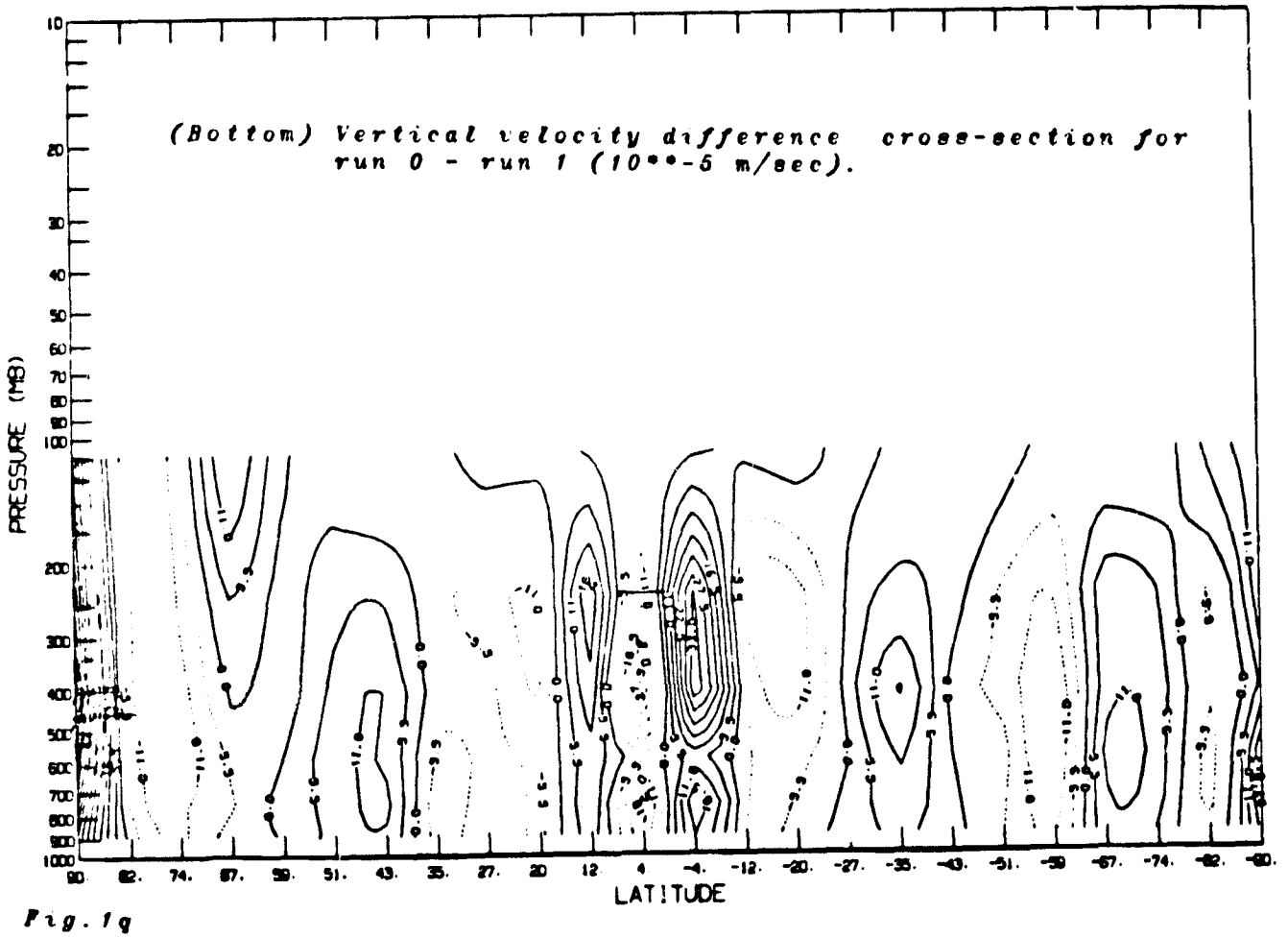
(Bottom) Vertical velocity difference cross-section for run 0 - run 1 (10**-5 m/sec).
PRESSURE (MB)
LATITUDE

Fig. 1q

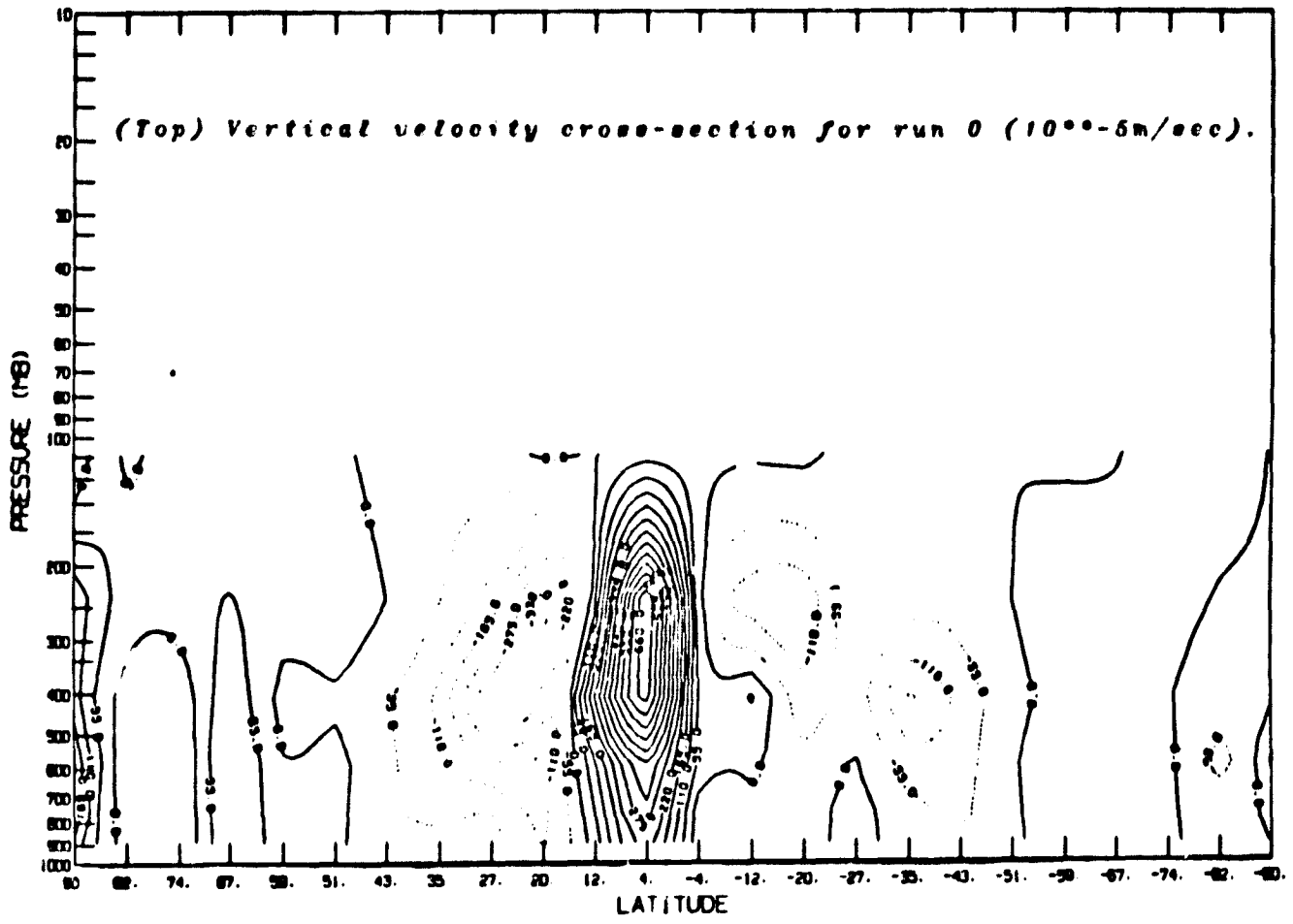
(Top) Vertical velocity cross-section for run 0 (10**-5m/sec).
PRESSURE (MB)
LATITUDE

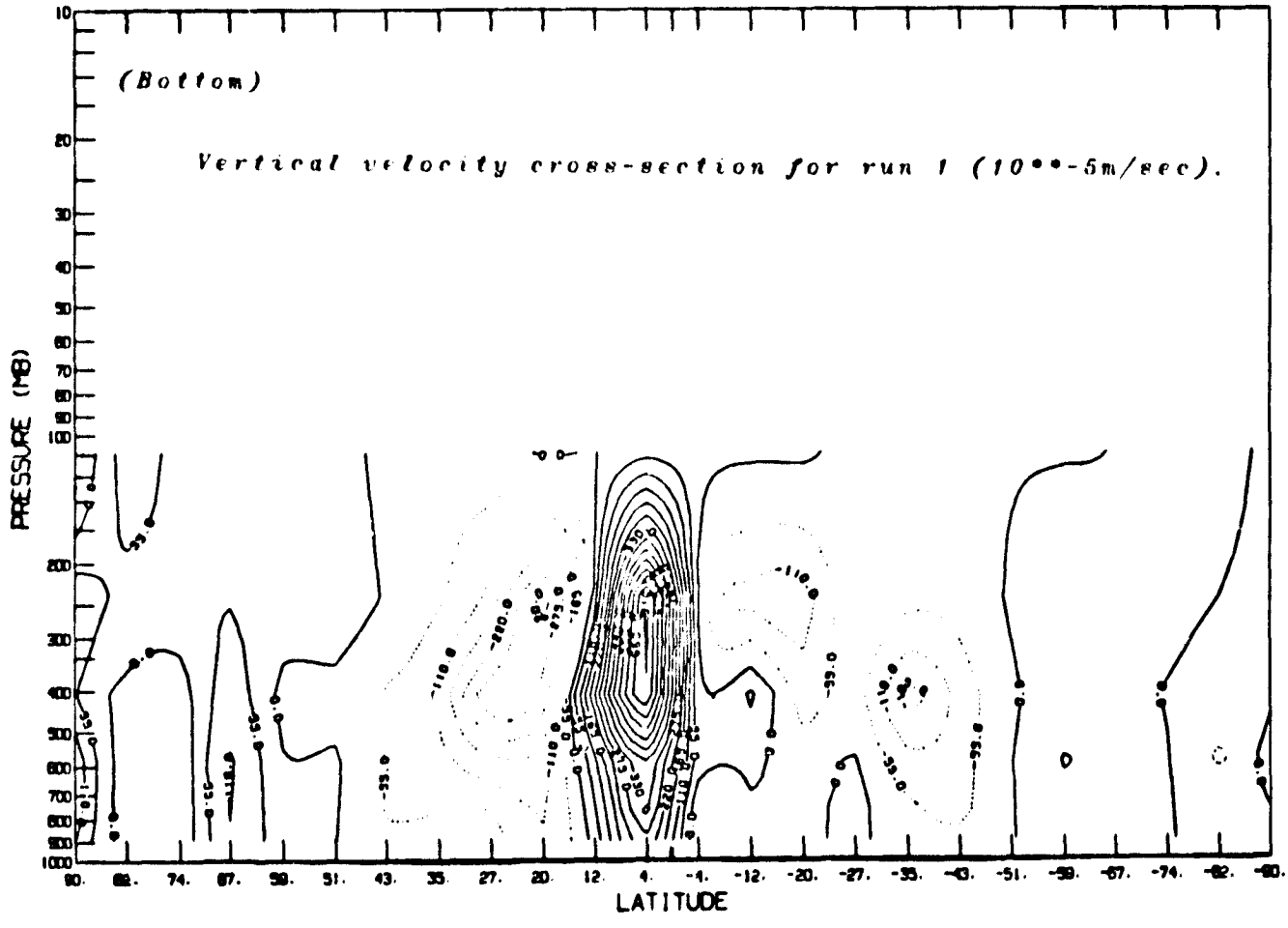
(Bottom)
Vertical velocity cross-section for run 1 (10**-5m/sec).
PRESSURE (MB)
LATITUDE

Fig. 1r

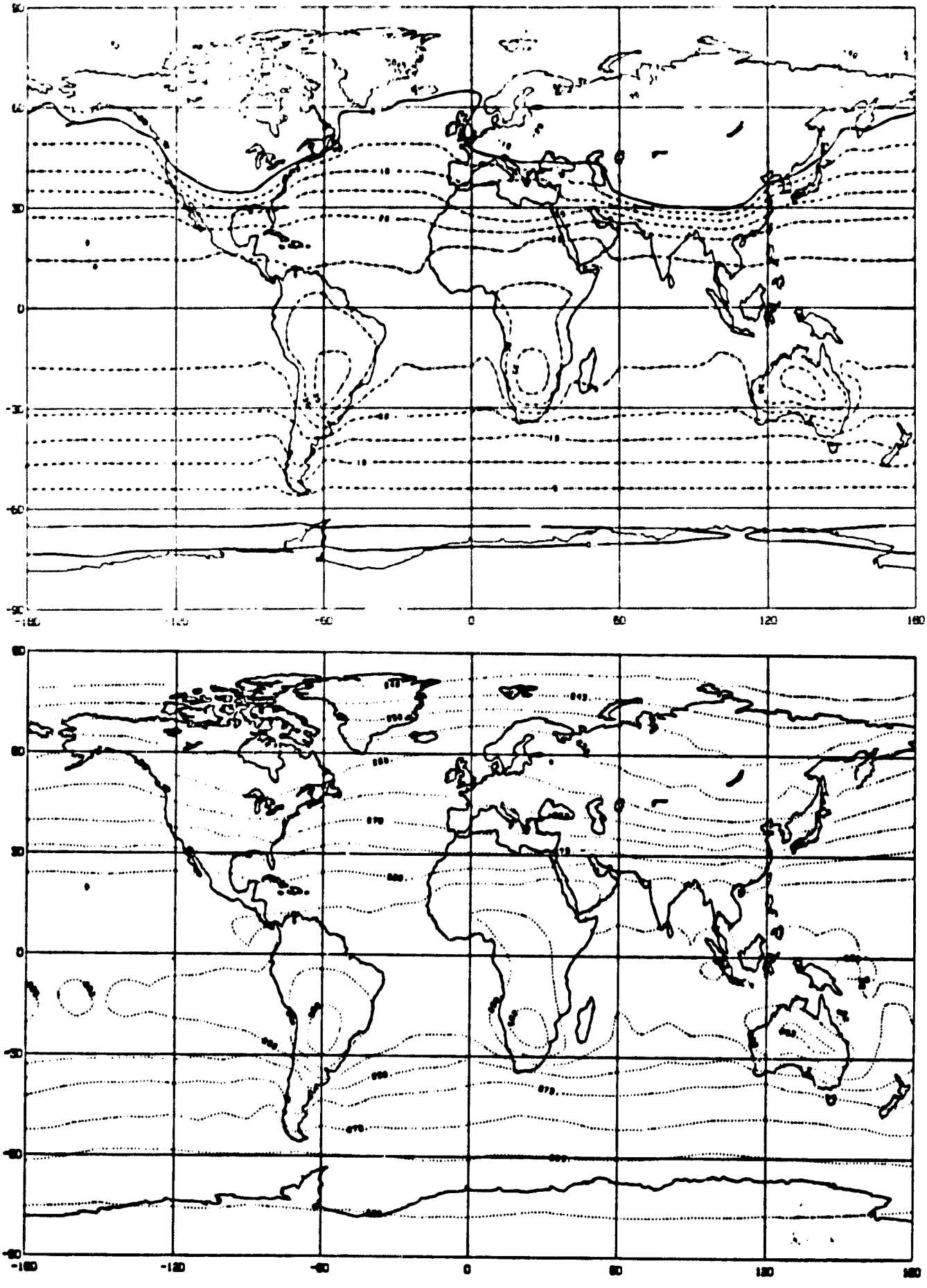

ORIGINAL PAGE IS
OF POOR QUALITY

Fig. 2a (Top) Mean SAT for run 2 (°C).
(Bottom) Mean TB-7 for run 2 (K).

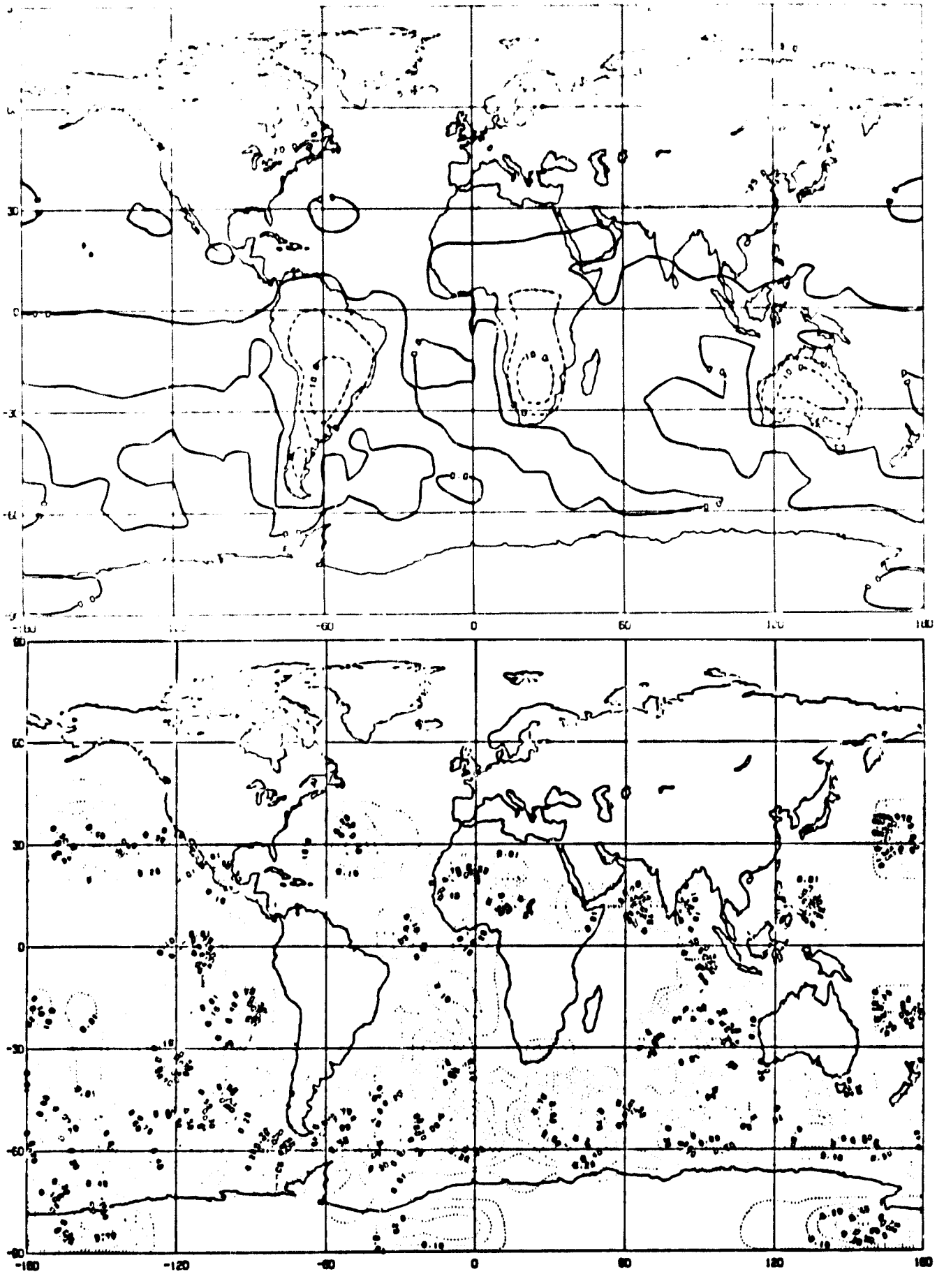

Fig. 2b SAT : (Top) Mean difference for run 2 - run 0 (°C). (Bottom) Significance level .

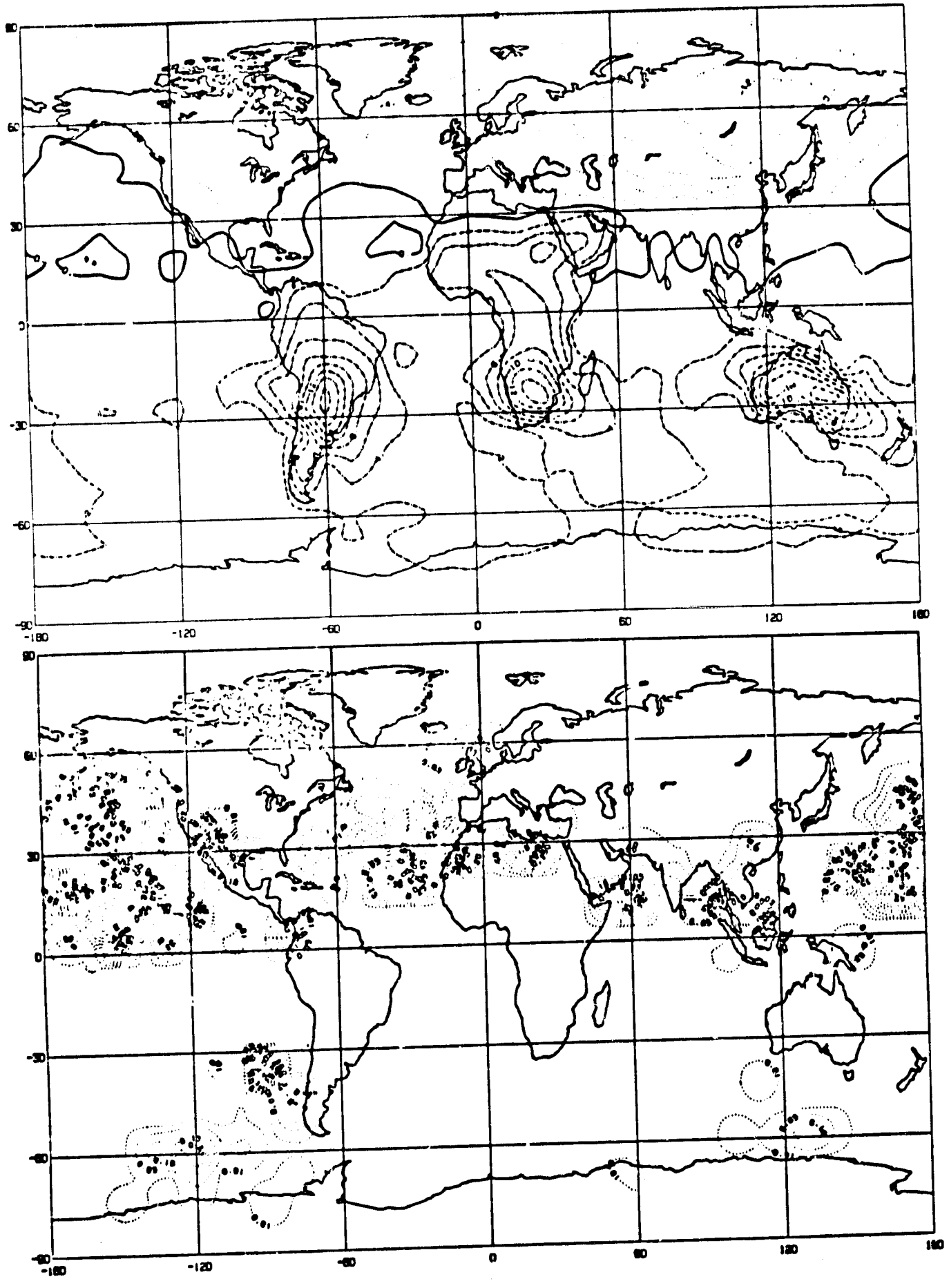

Fig. 2c T8-7 : (Top) Mean difference for run 2 - run 0 (K). (Bottom) Significance level .

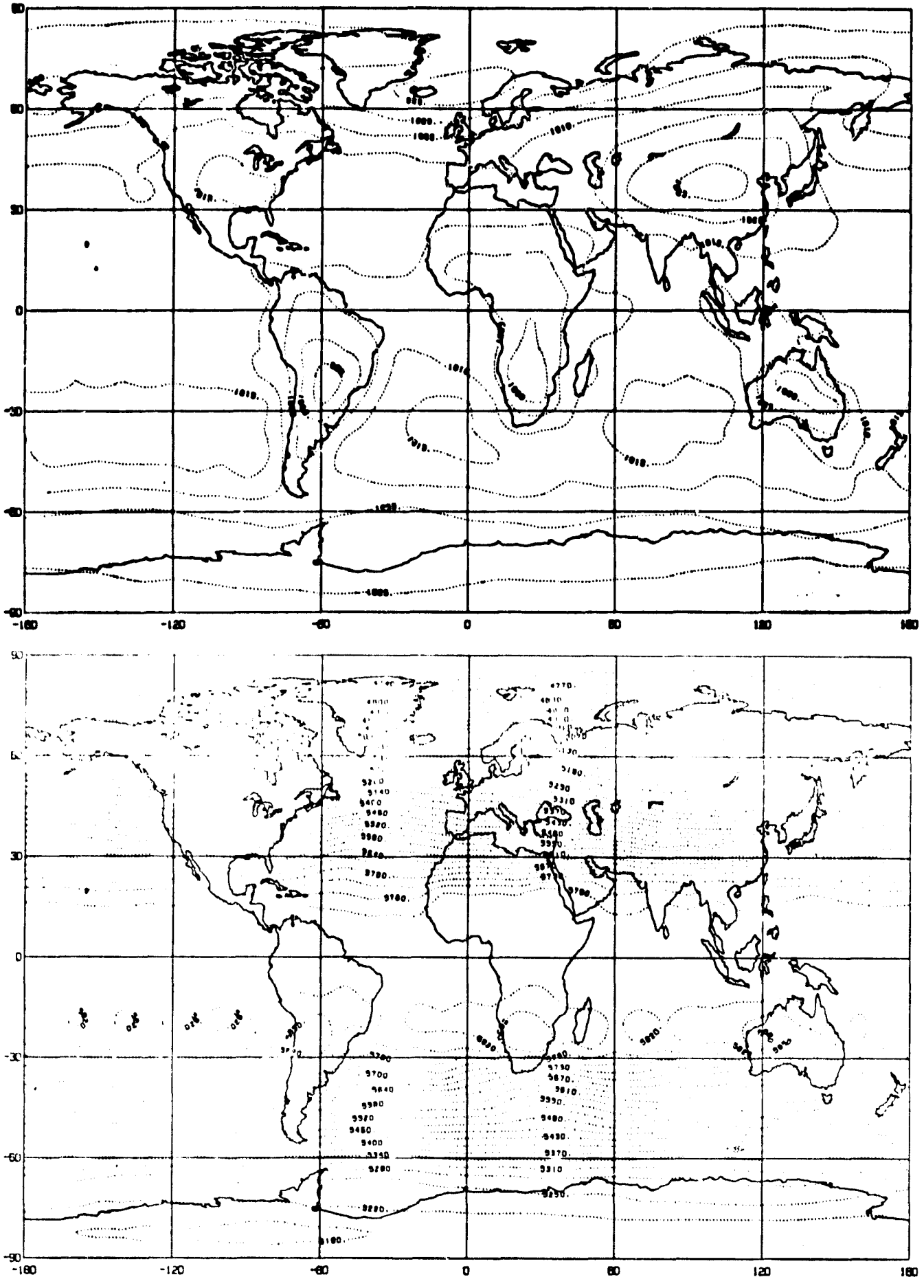

Fig. 2d (Top) Mean SLP for run 2 (mb).
(Bottom) Mean C500 for run 2 (m).

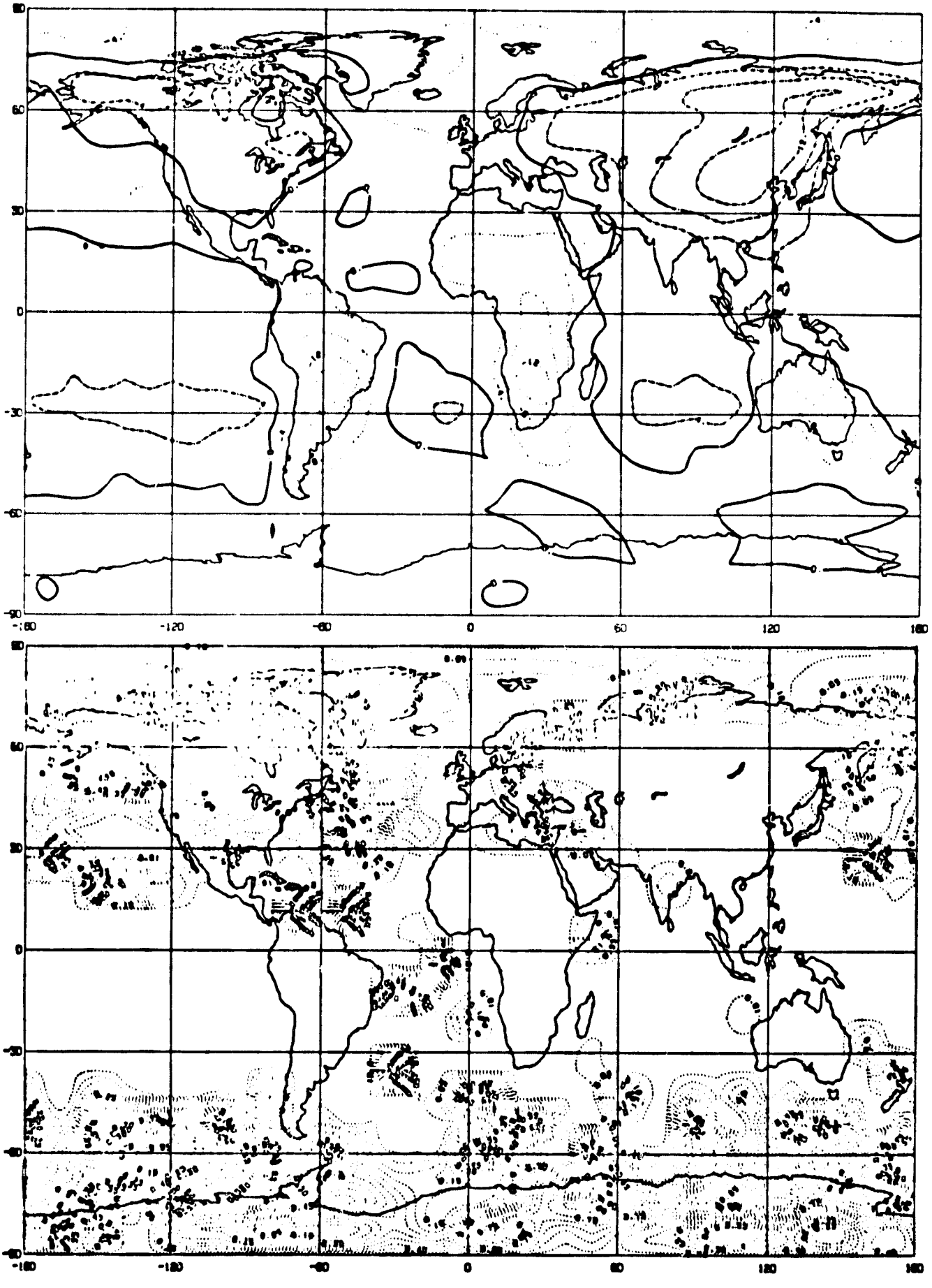

Fig. 2e SLP : (Top) Mean difference for run 2 - run 0 (mb). (Bottom) Significance level .

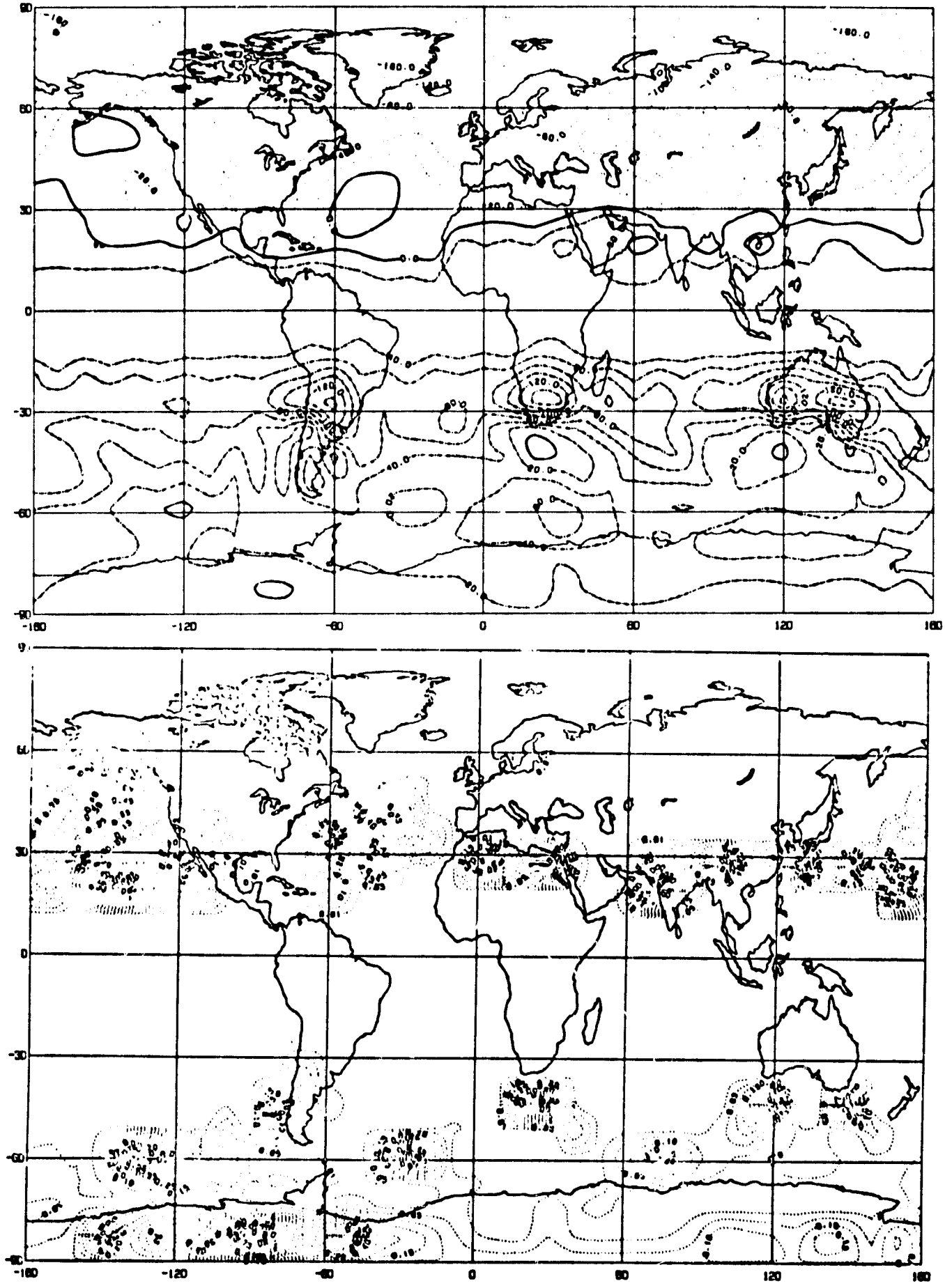

Fig.2f C500 : (Top) Mean difference for run 2 - run 0 (m). (Bottom) Significance level .

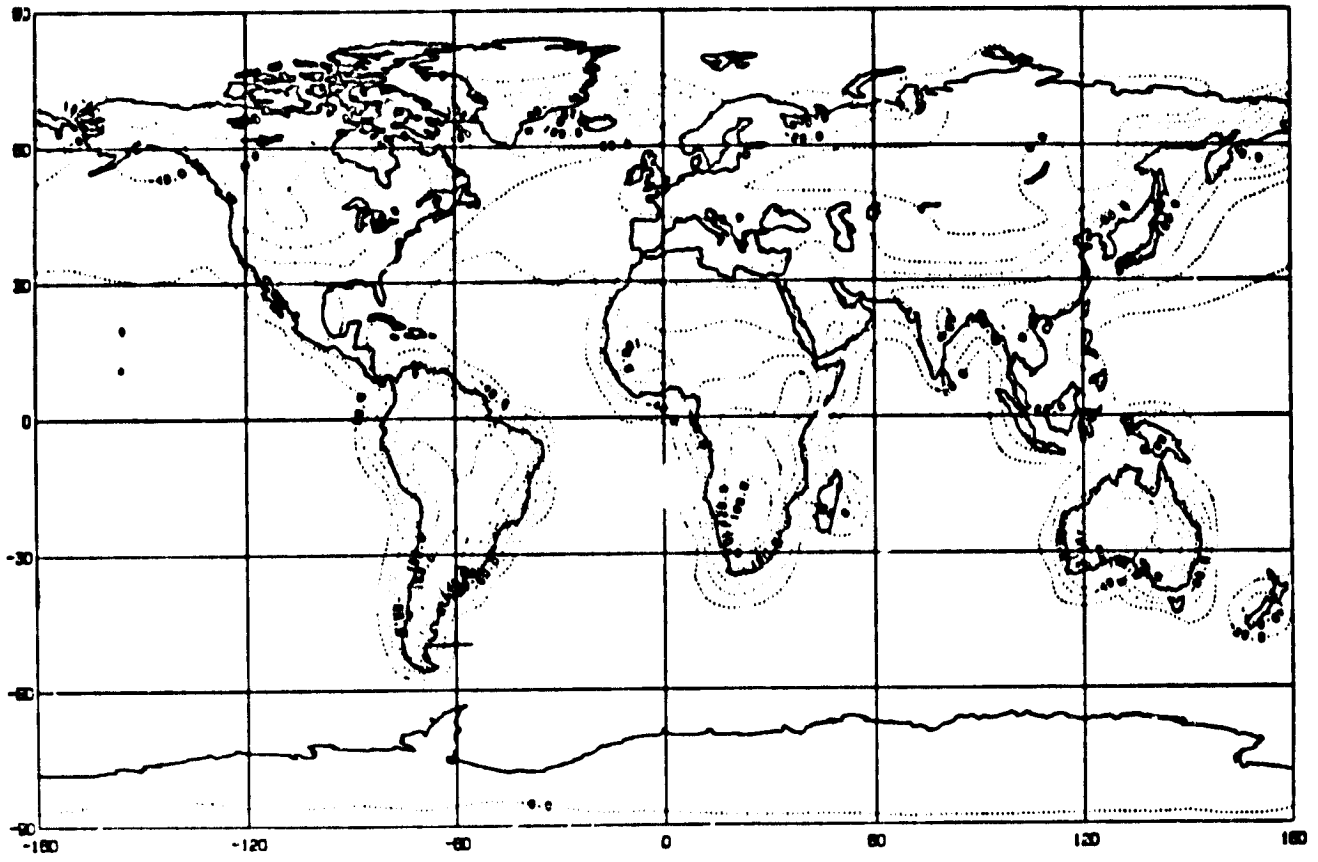

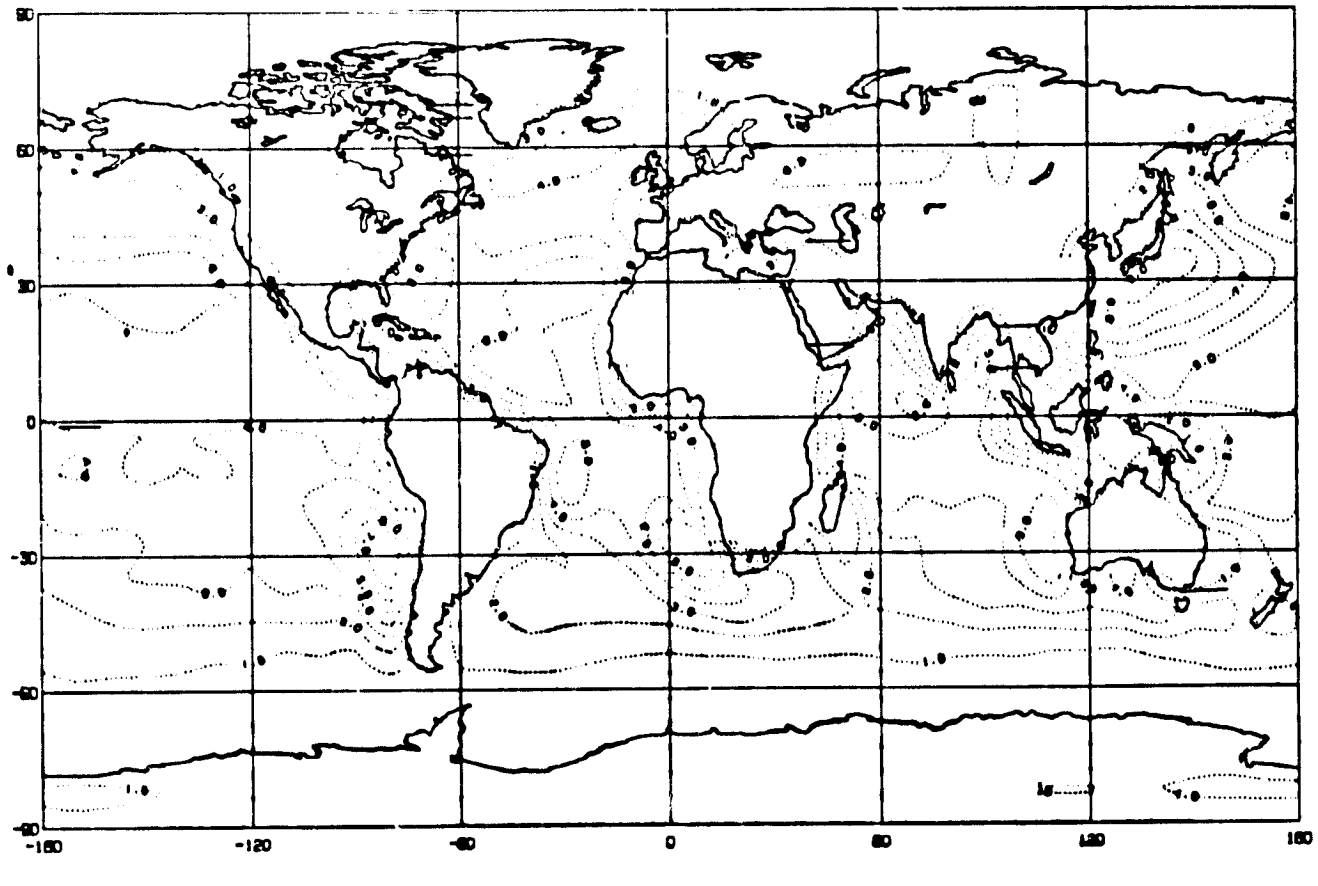

Fig. 2g *(Top) Mean sensible heat flux for run 2 (watts/m**2). (Bottom) Mean evaporation for run 2 (mm/day).*

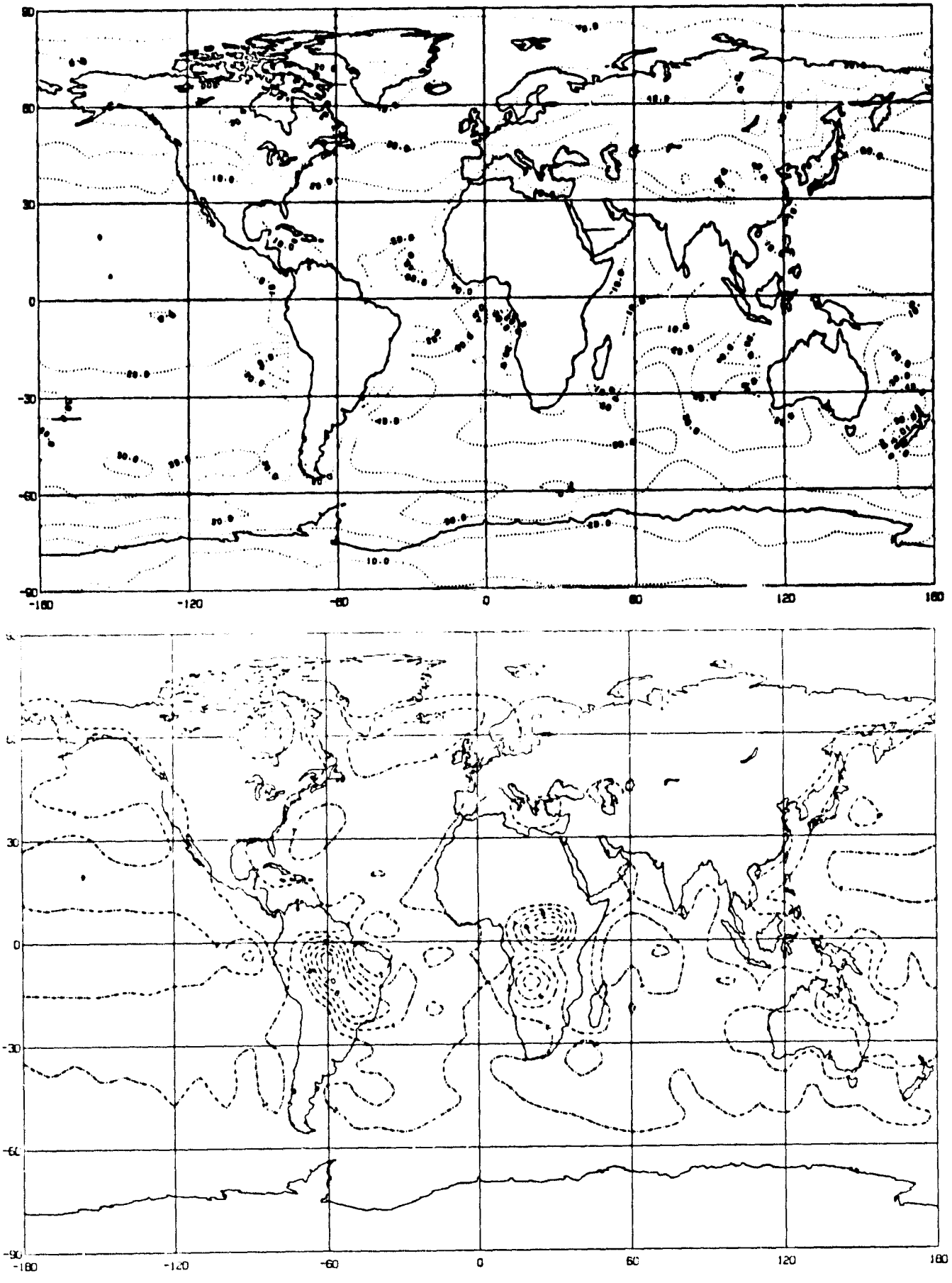

Fig. 2h (Top) Mean low cloud cover for run 2 (percent). (Bottom) Mean precipitation for run 2 (mm/day).

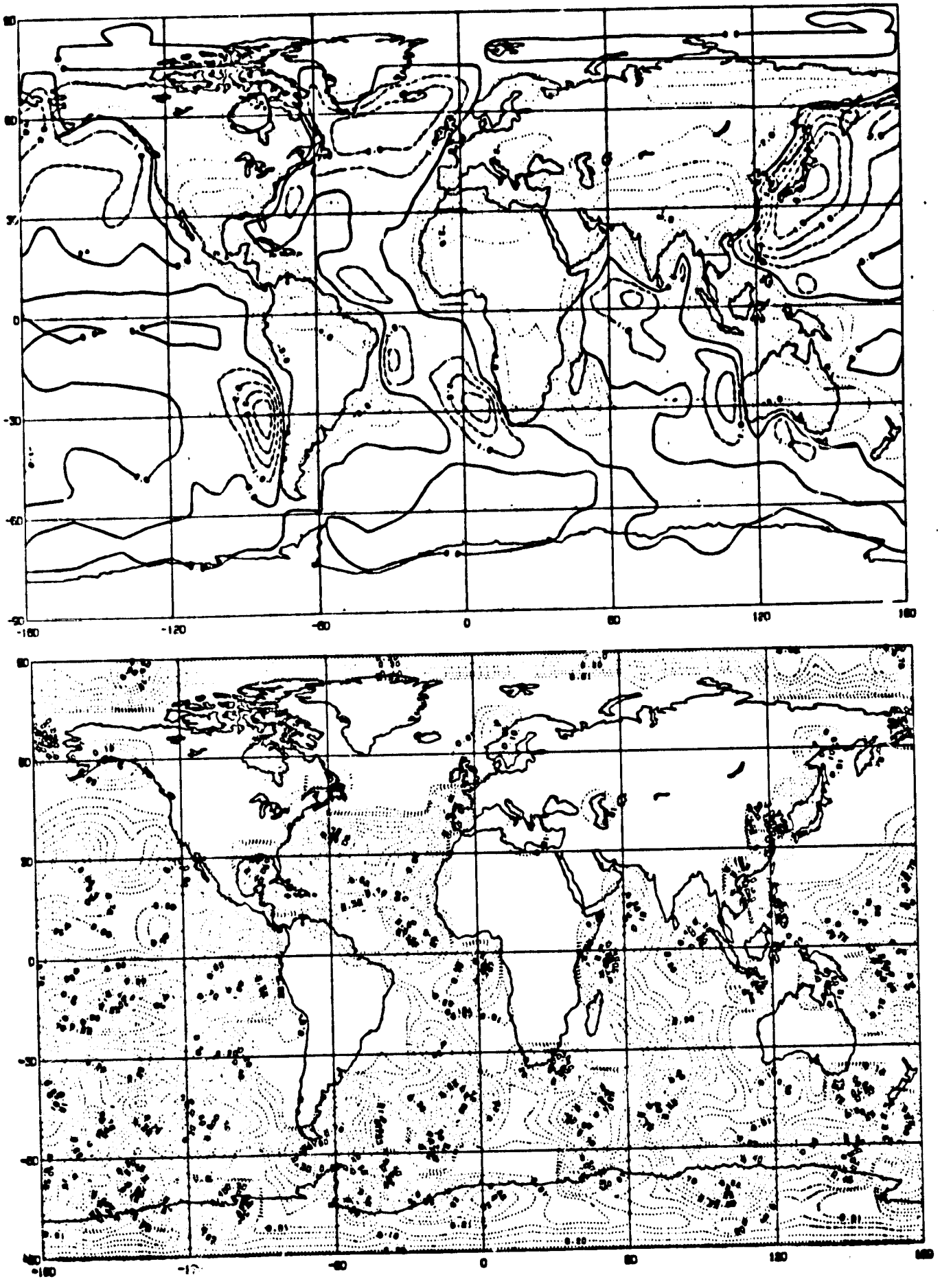

Fig. 2i Evaporati : (Top) Mean difference for run 2 - run 0 (mm/day). (Bottom) Significance level .

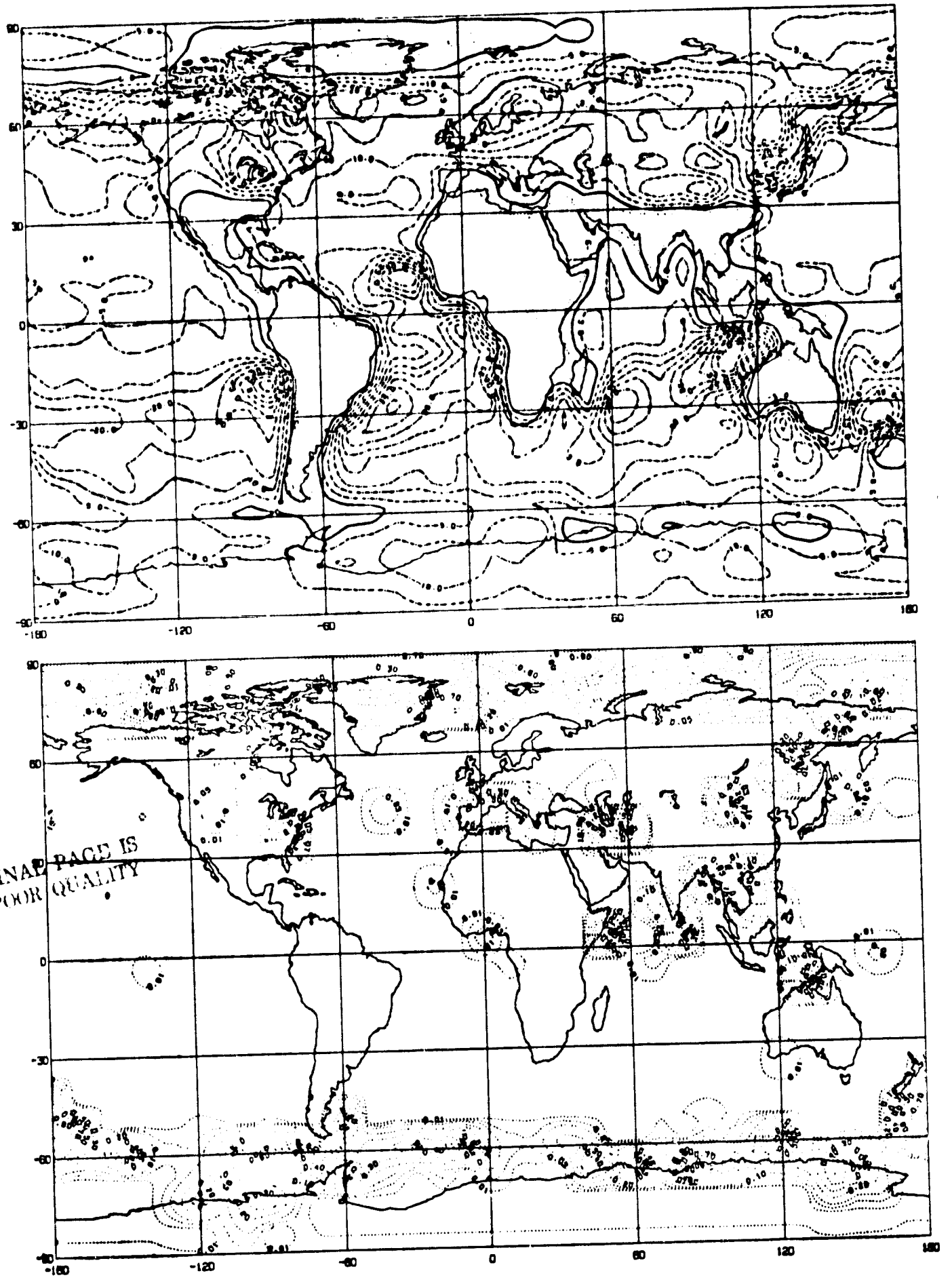

Fig. 2j Low cloud cover: (Top) Mean difference for run 2 - run 0 (percent). (Bottom) Significance level .

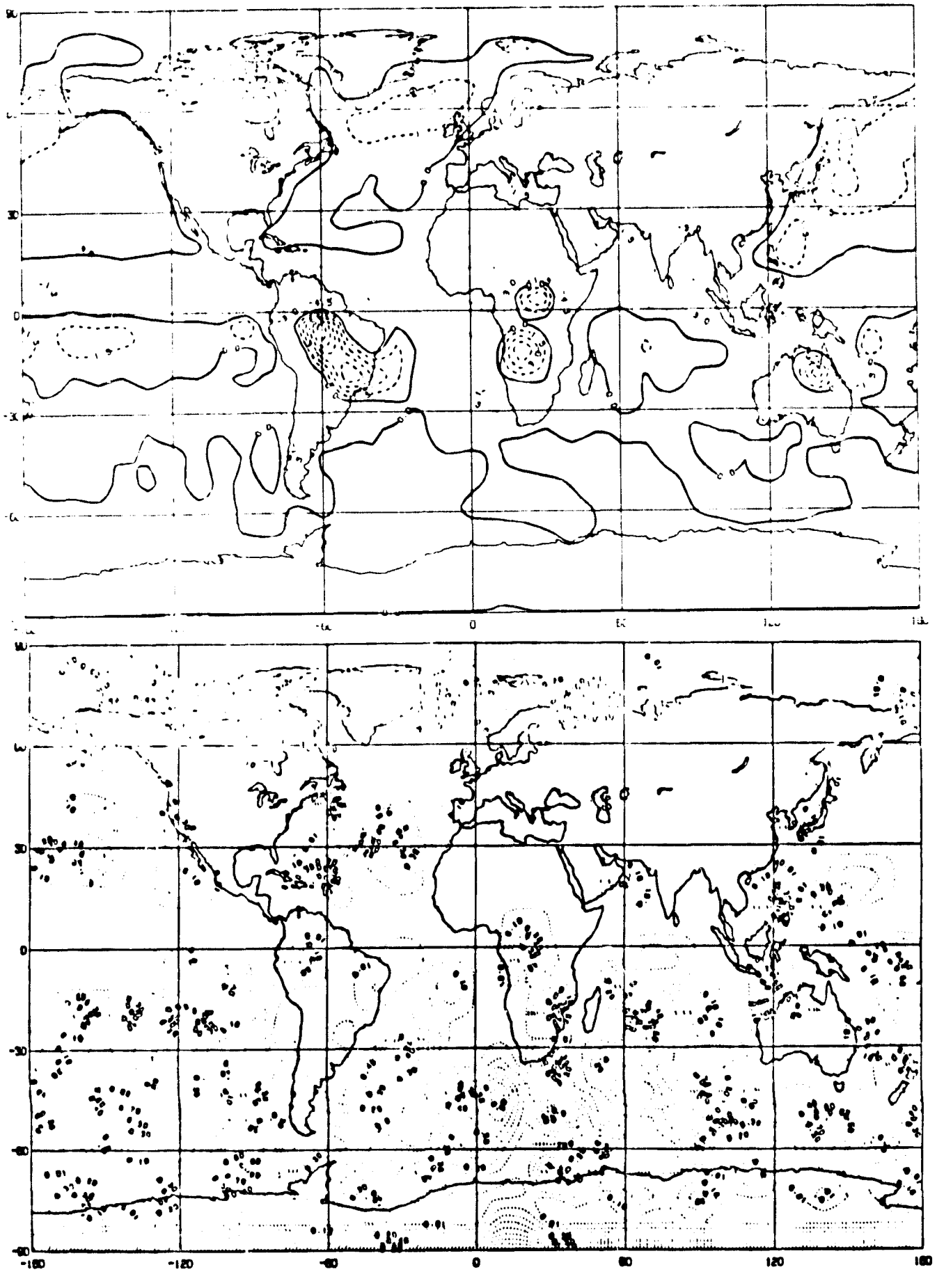

Fig. 2k Precipitation : (Top) Mean difference for run 2 - run 0 (mm/day). (Bottom) Significance level .

(Top) Temperature cross-section of run 2 (°C).

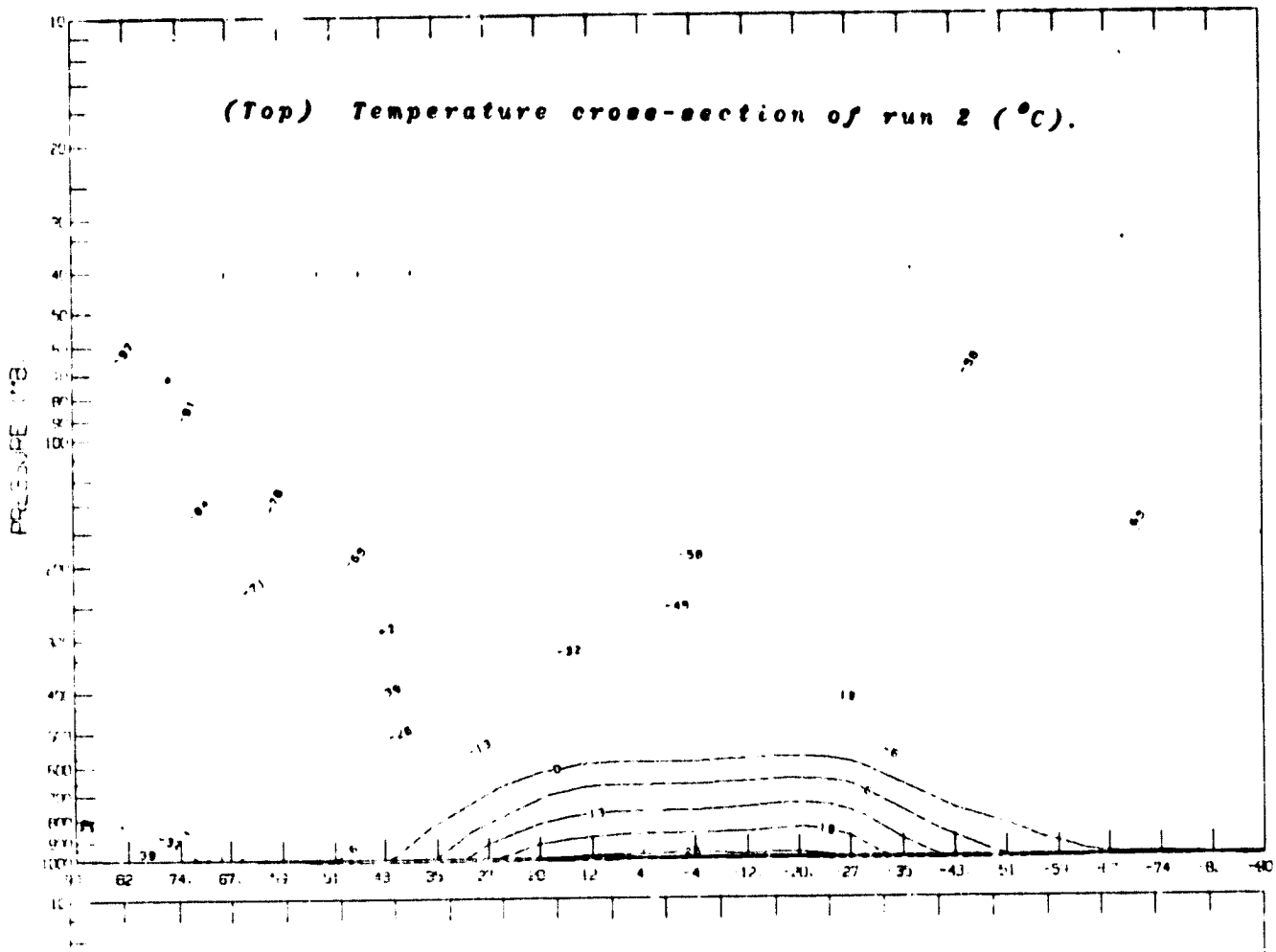

(Bottom) Zonal wind cross-section for run 2 (tenths of m/sec).

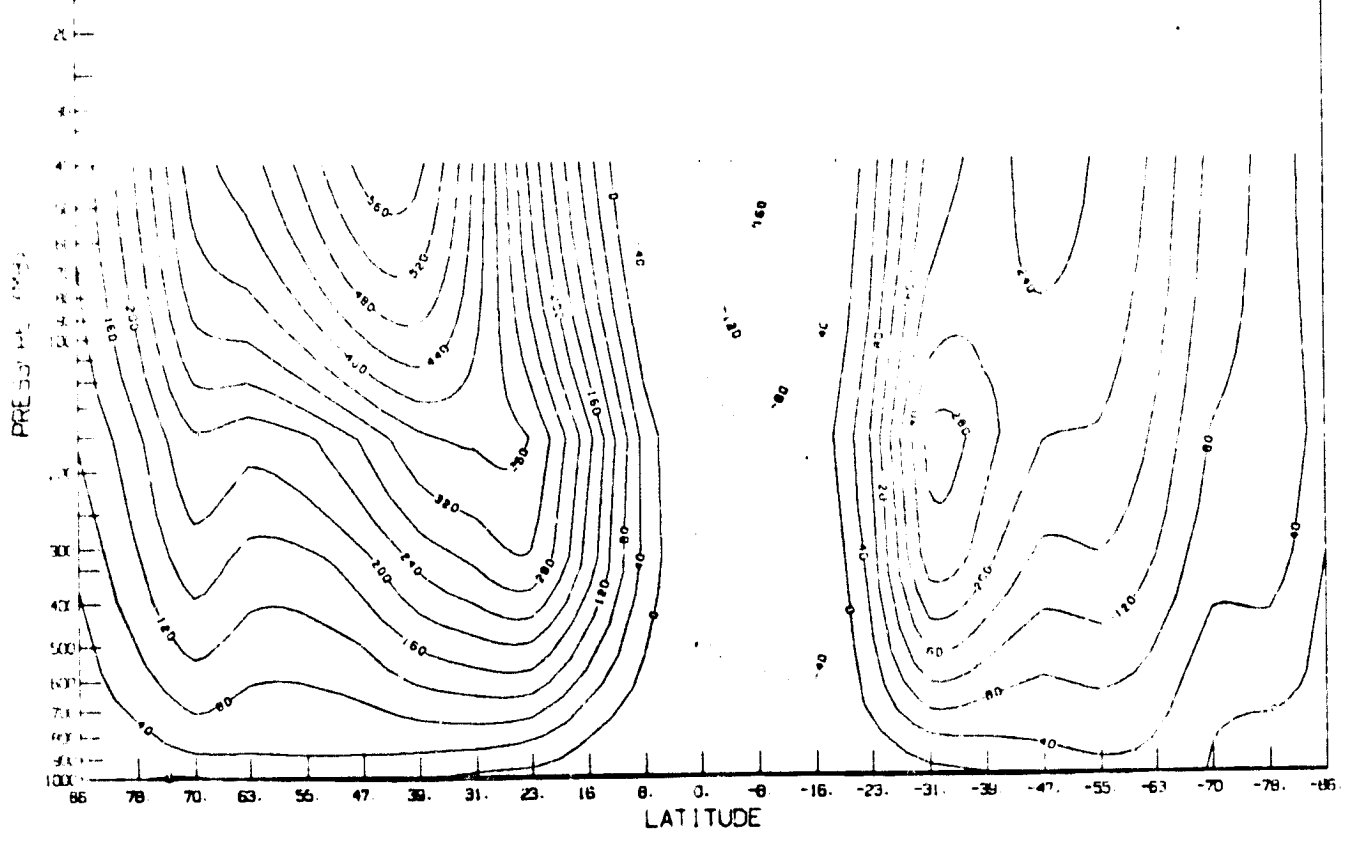

Fig. 2l

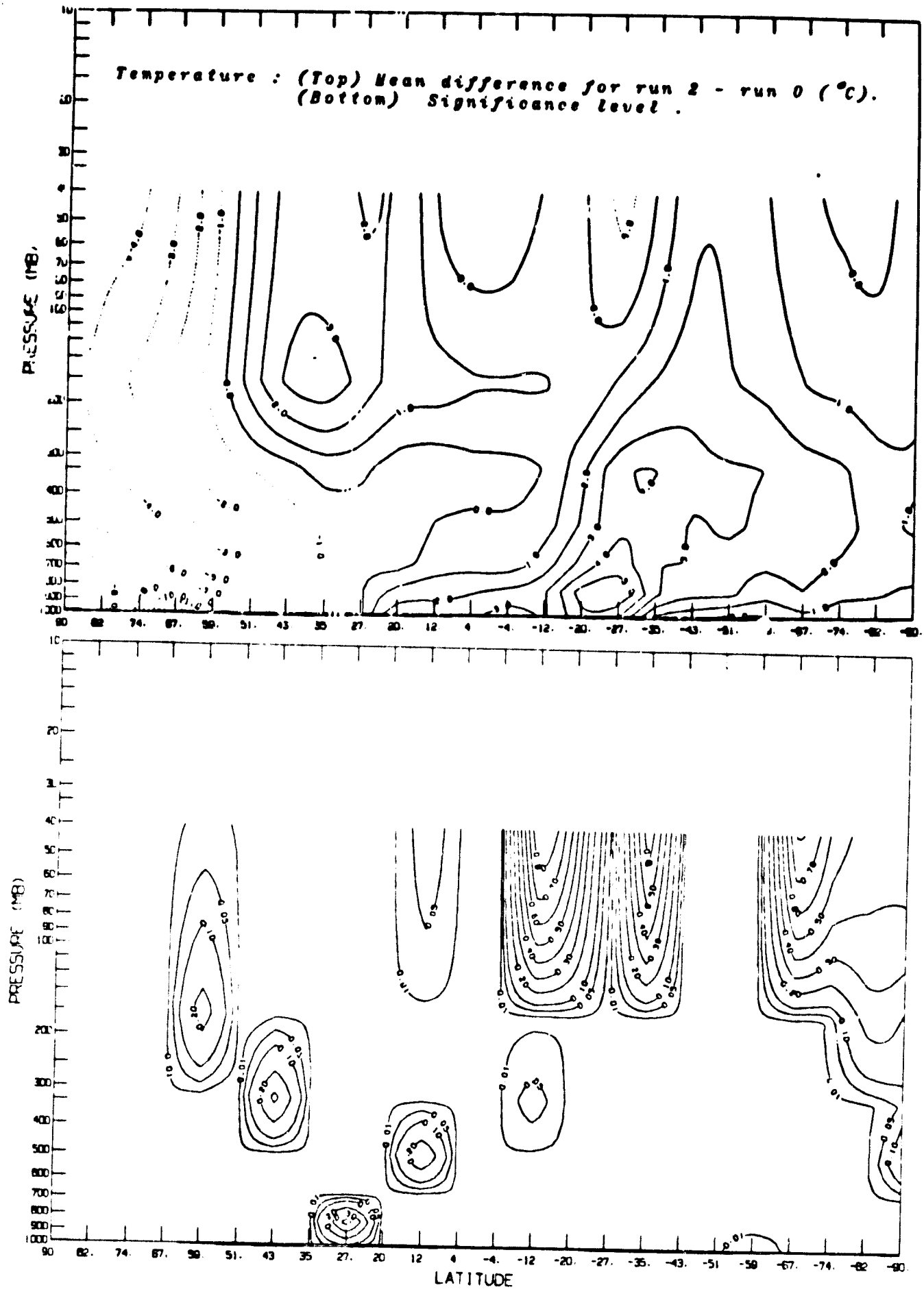
Temperature : (Top) Mean difference for run 2 - run 0 (°C).
(Bottom) Significance level .
PRESSURE (MB)
LATITUDE

Fig. 2m

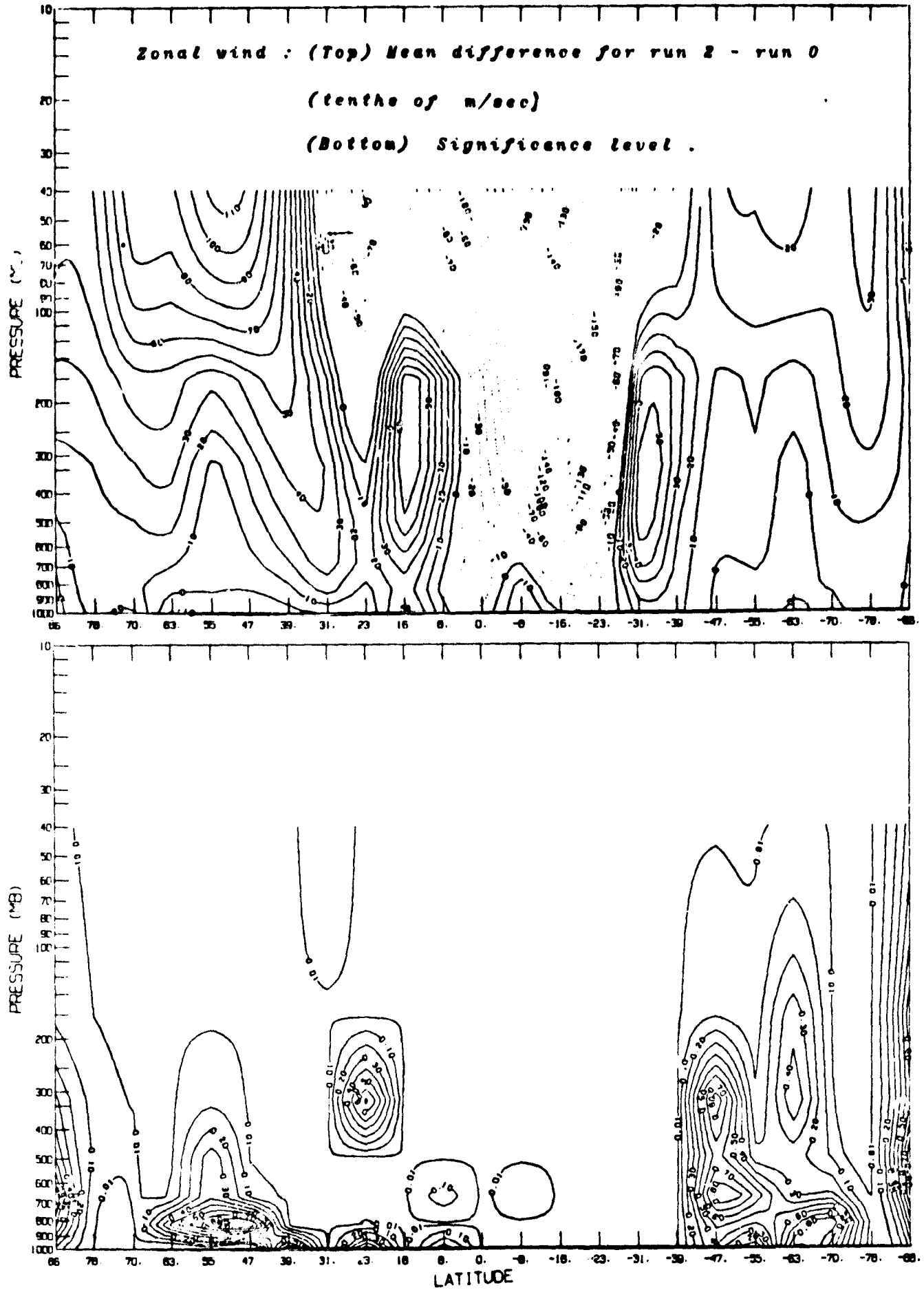
Zonal wind : (Top) Mean difference for run 2 - run 0
(tenths of m/sec)
(Bottom) Significance level .
PRESSURE (MB)
PRESSURE (MB)
LATITUDE

Fig. 2n

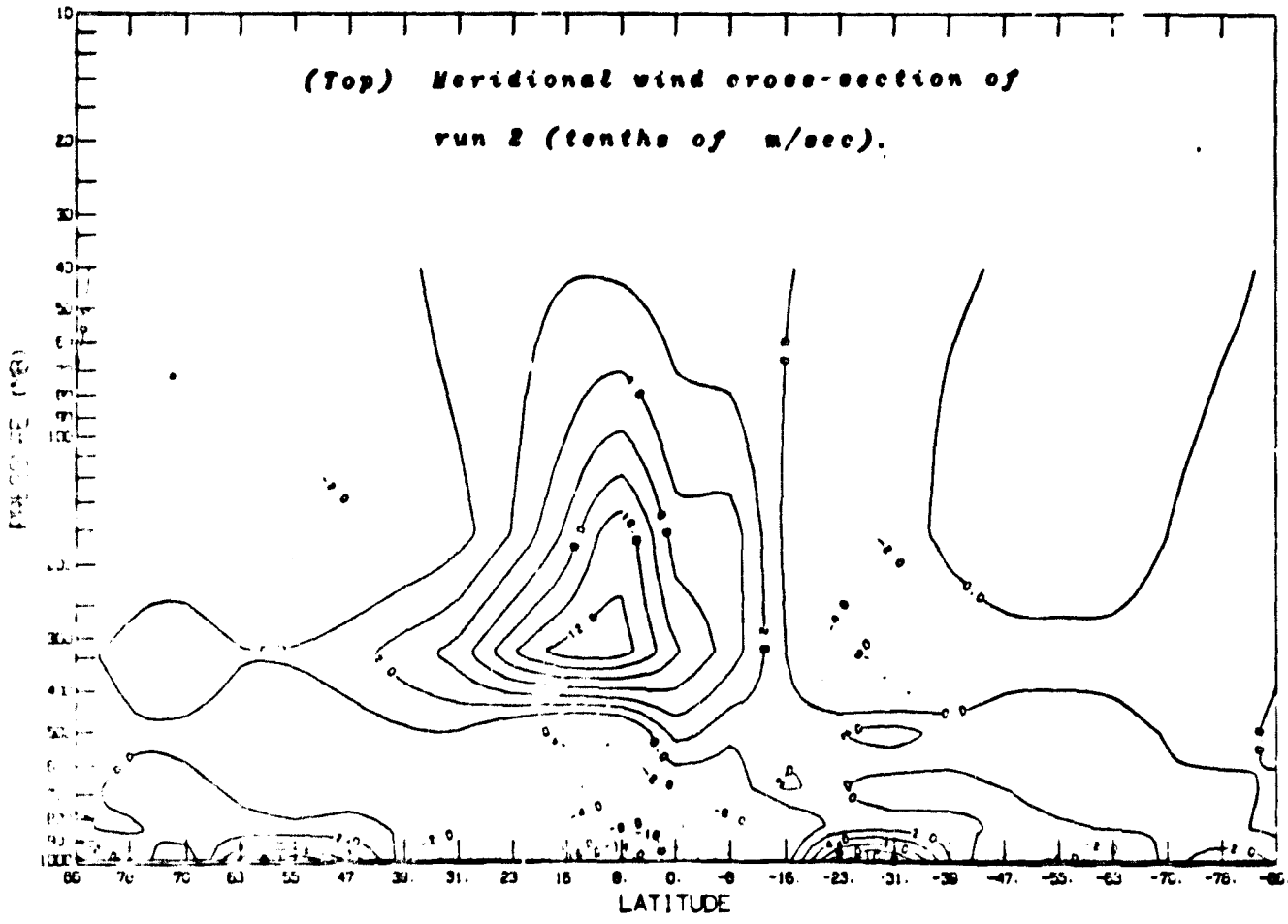
(Top) Meridional wind cross-section of
run 2 (tenths of m/sec).
LATITUDE

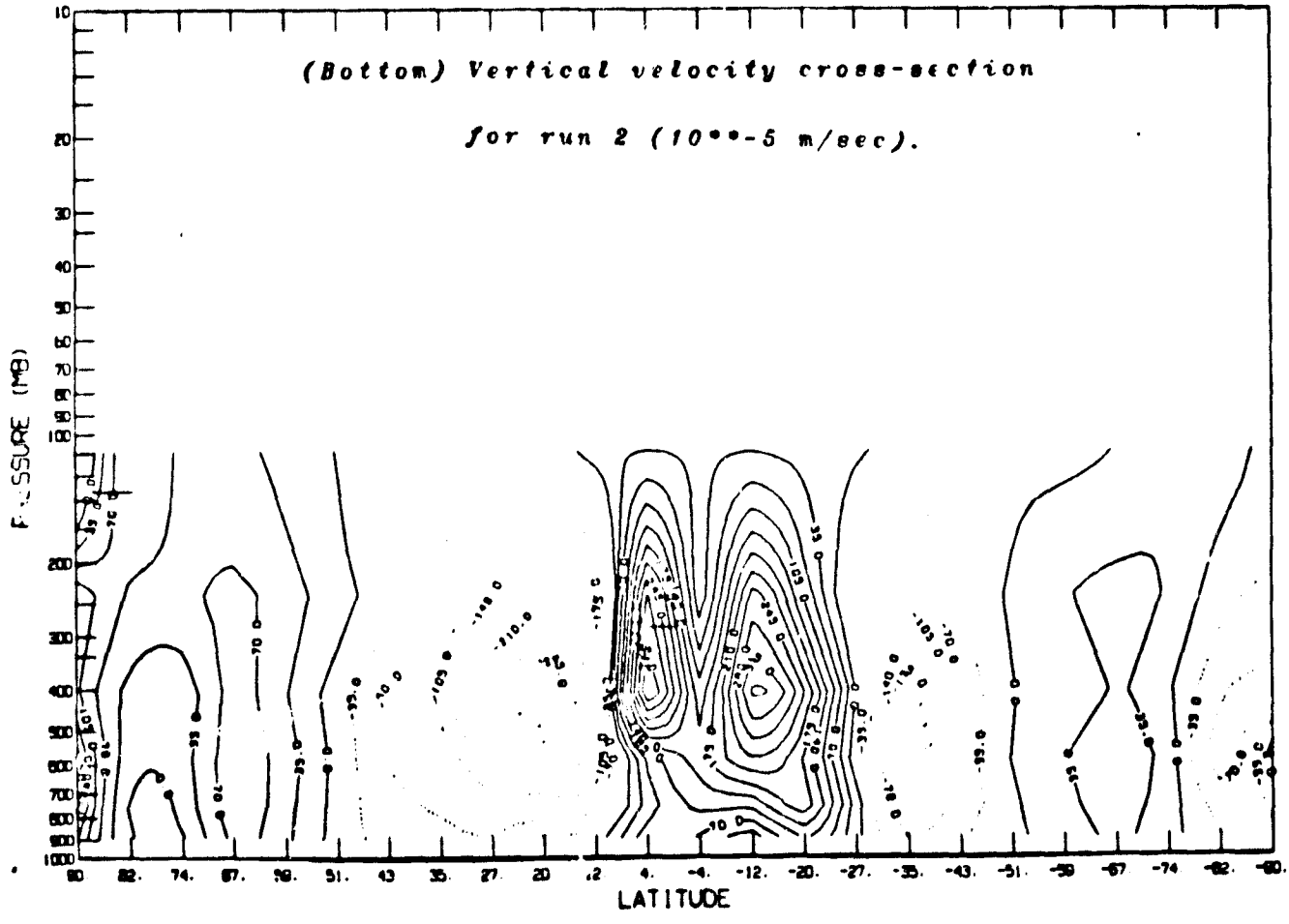
(Bottom) Vertical velocity cross-section
for run 2 (10**-5 m/sec).
PRESSURE (MB)
LATITUDE

Fig. 2o

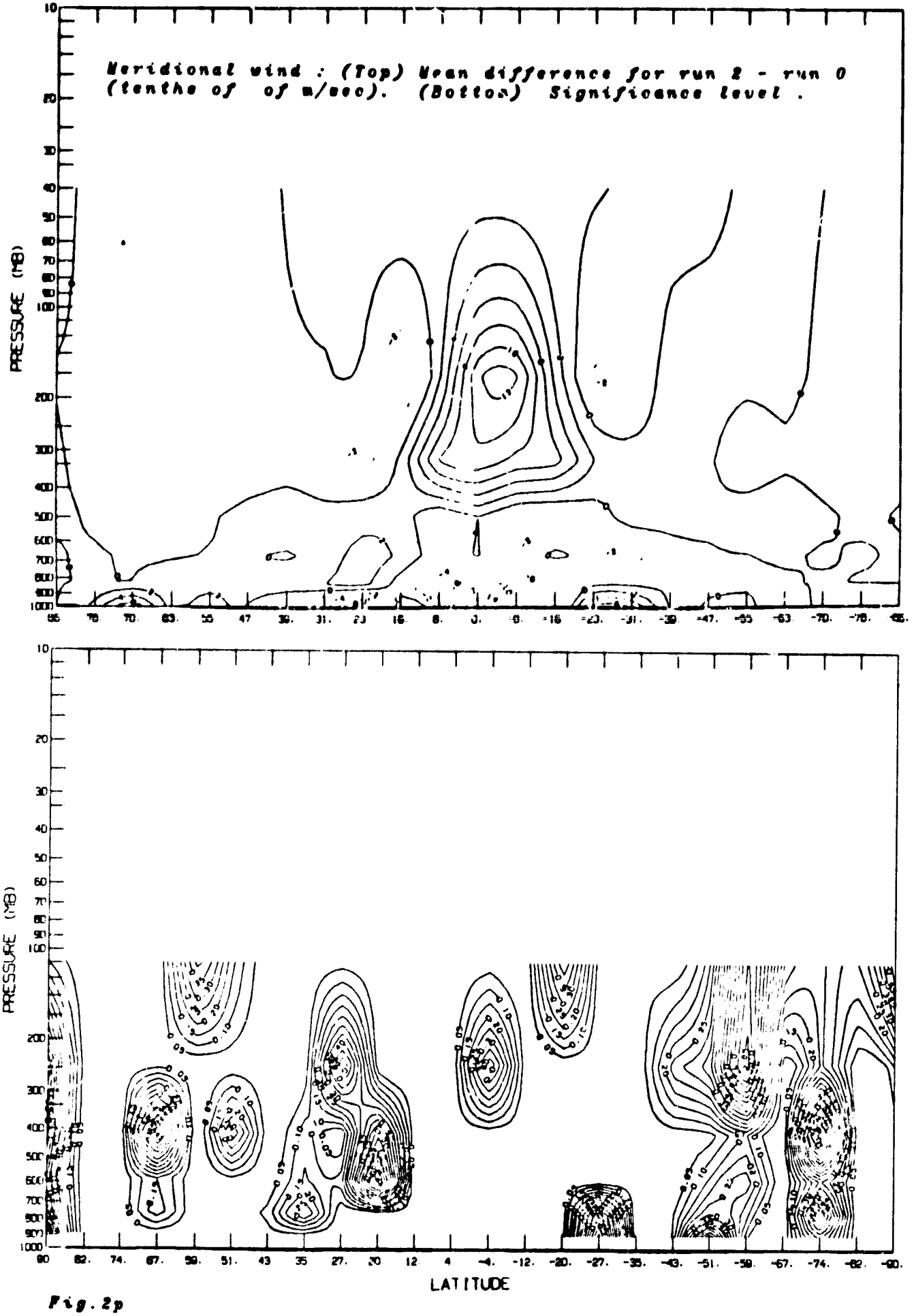
Meridional wind : (Top) Mean difference for run 2 - run 0 (tenths of of m/sec). (Bottom) Significance level .
PRESSURE (MB)
10
20
30
40
50
60
70
80
90
100
200
300
400
500
600
700
800
900
1000
90 82. 74. 67. 59. 51. 43 35 27. 20 12 4 -4. -12. -20. -27. -35. -43. -51. -59. -67. -74. -82. -90.
LATITUDE

Fig. 2p

Vertical velocity : (Top) Mean difference for run 2 - run 0 (10**-5 m/sec). (Bottom) Significance level .

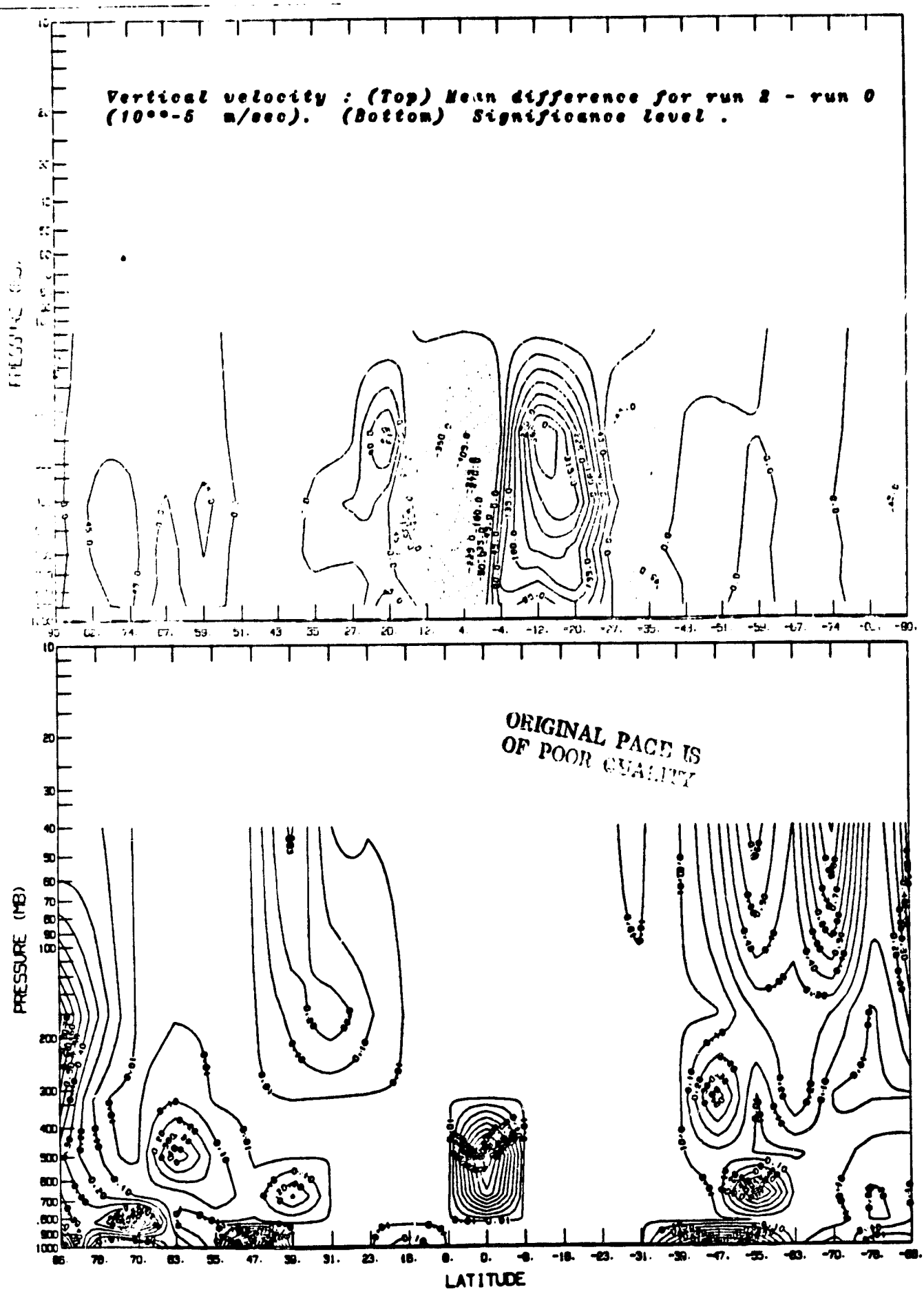

Fig. 29

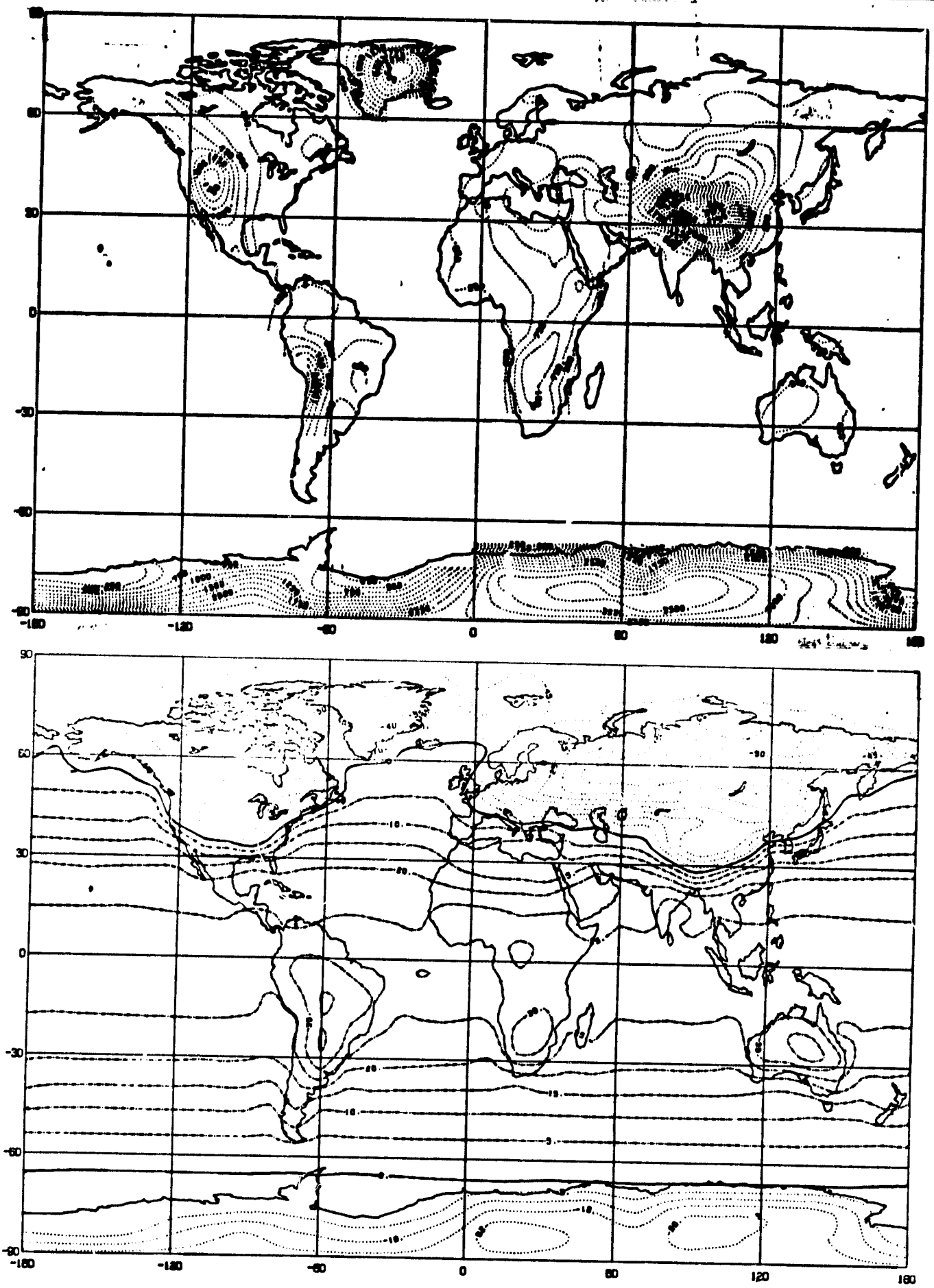

Fig. 8a *(Top) Topography of the model (m). (Bottom) Mean SAT for run 3 (°C).*

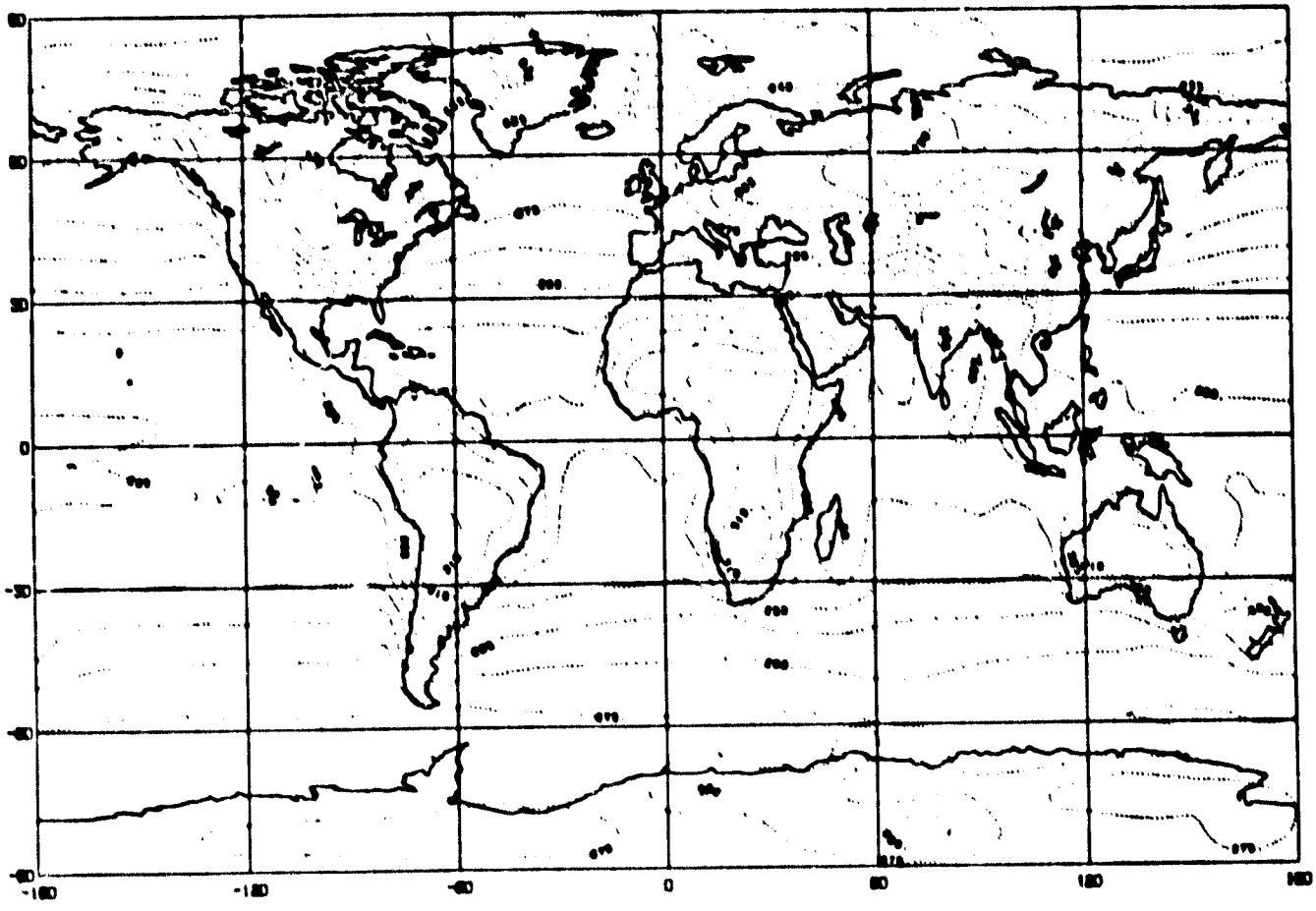

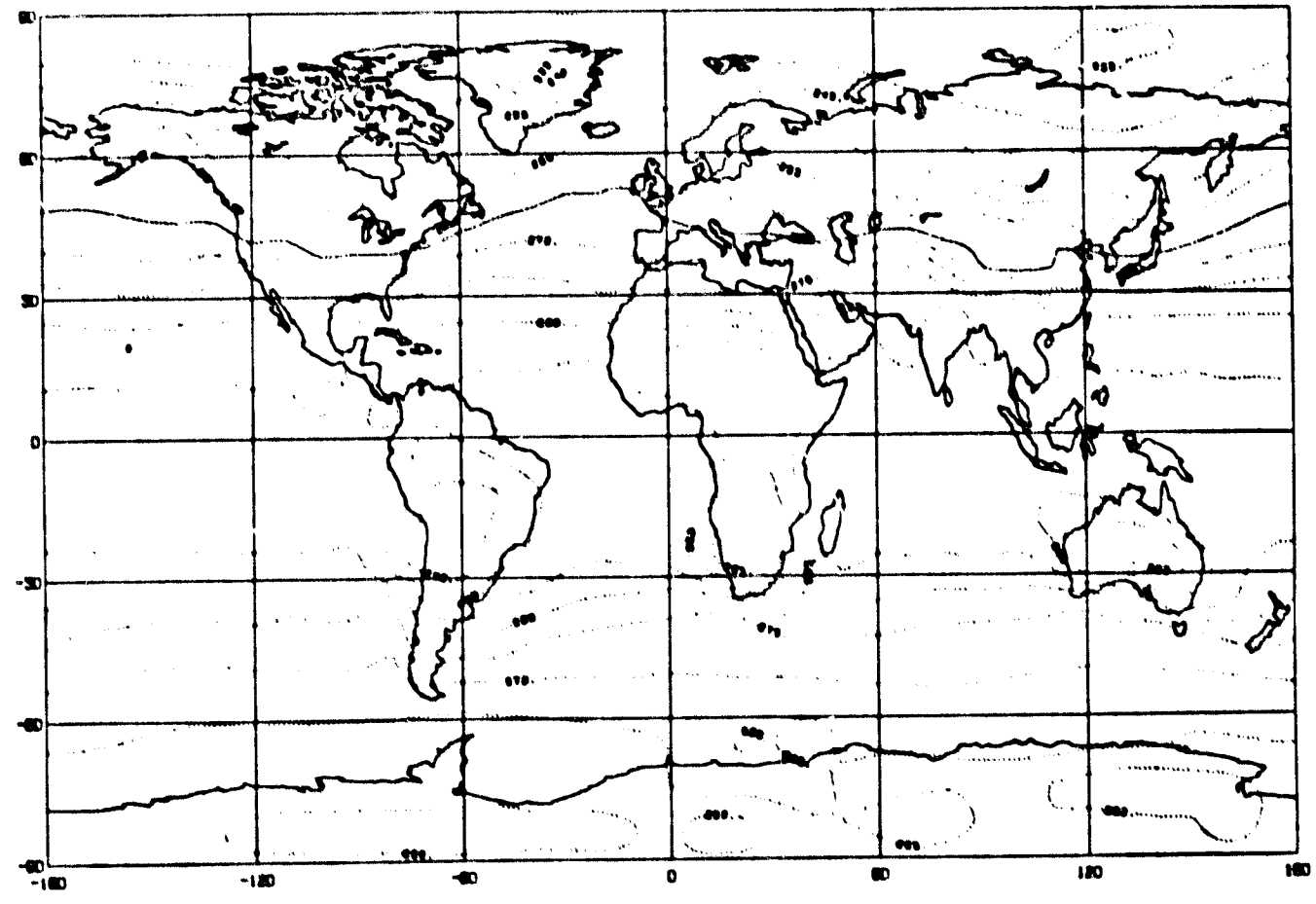

Fig. 3b (Top) Mean layer temperature from 1000-850 mb (T10-8) for run 3 (K).
(Bottom) Mean T8-7 for run 3 (K).

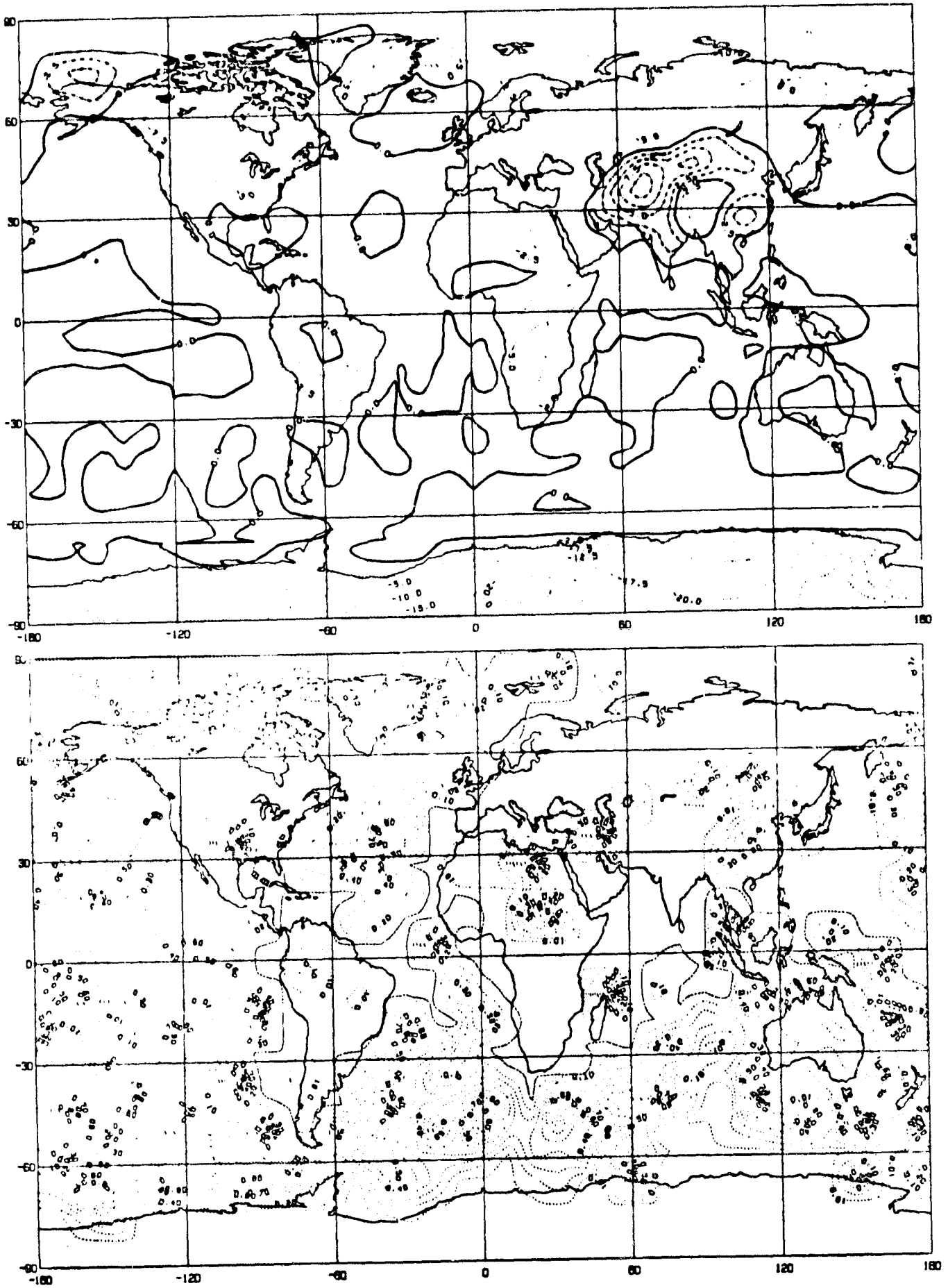

Fig. 3c SAT : (Top) Mean difference for run 3 - run 2 (°C).

(Bottom) Significance level .

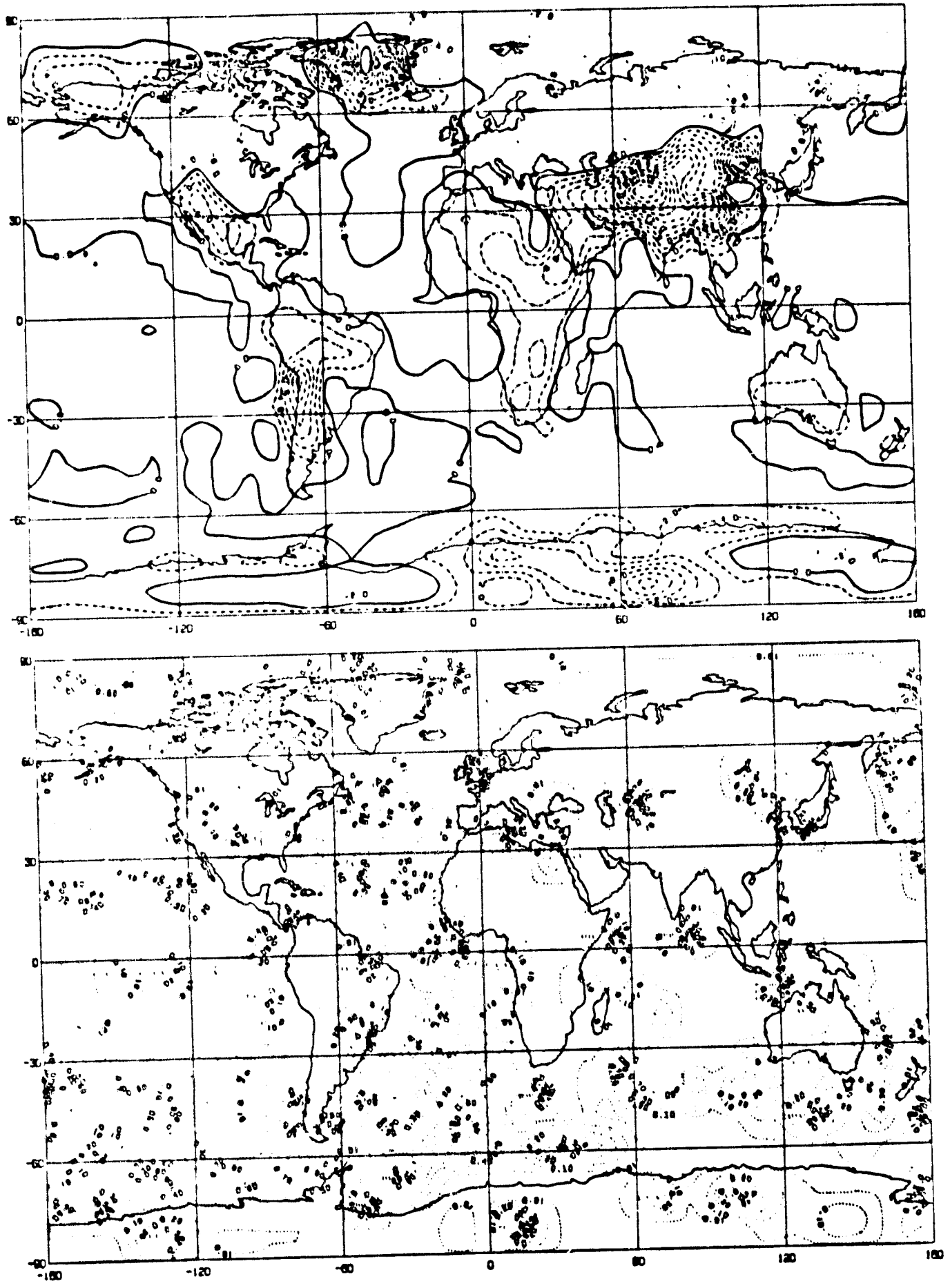

Fig. 3d T10-8: (Top) Mean difference for run 3 - run 2 (K). (Bottom) Significance level .

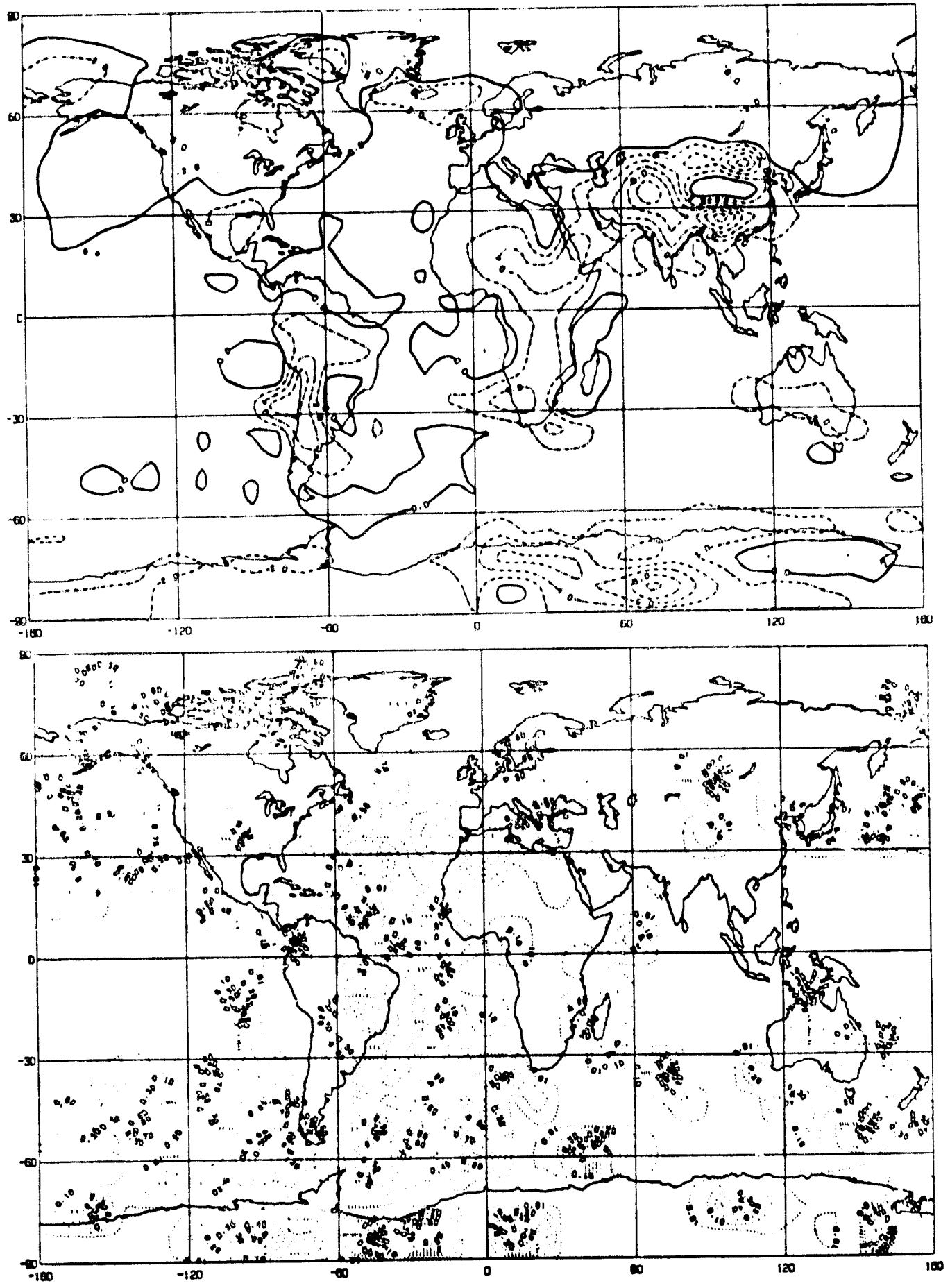

Fig.3e TB-7 : (Top) Mean difference for run 3 - run 2 (K). (Bottom) Significance level .

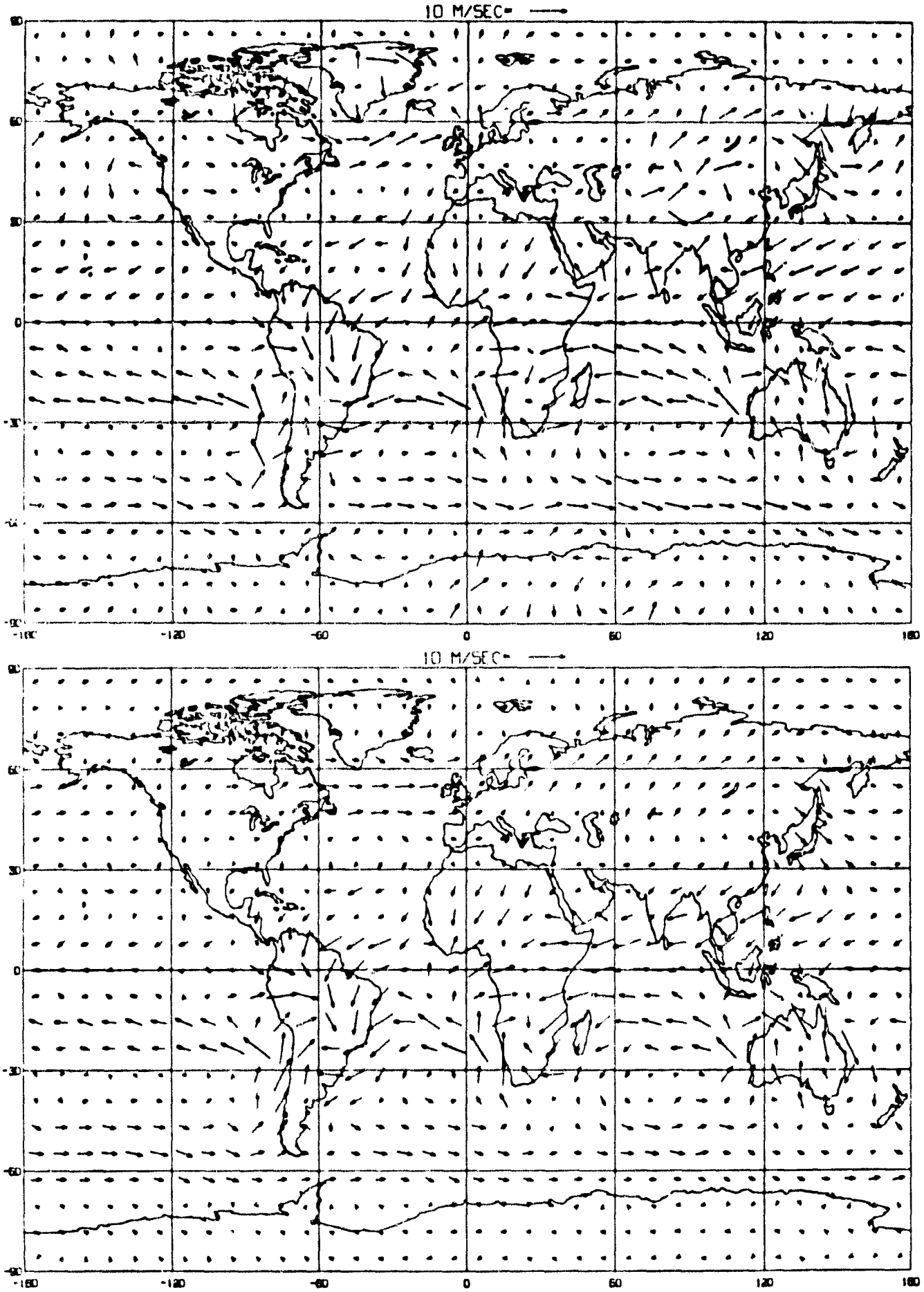

Fig. 3f (Top) Surface wind for run 3 (m/sec).
(Bottom) Surface wind for run 2 (m/sec).

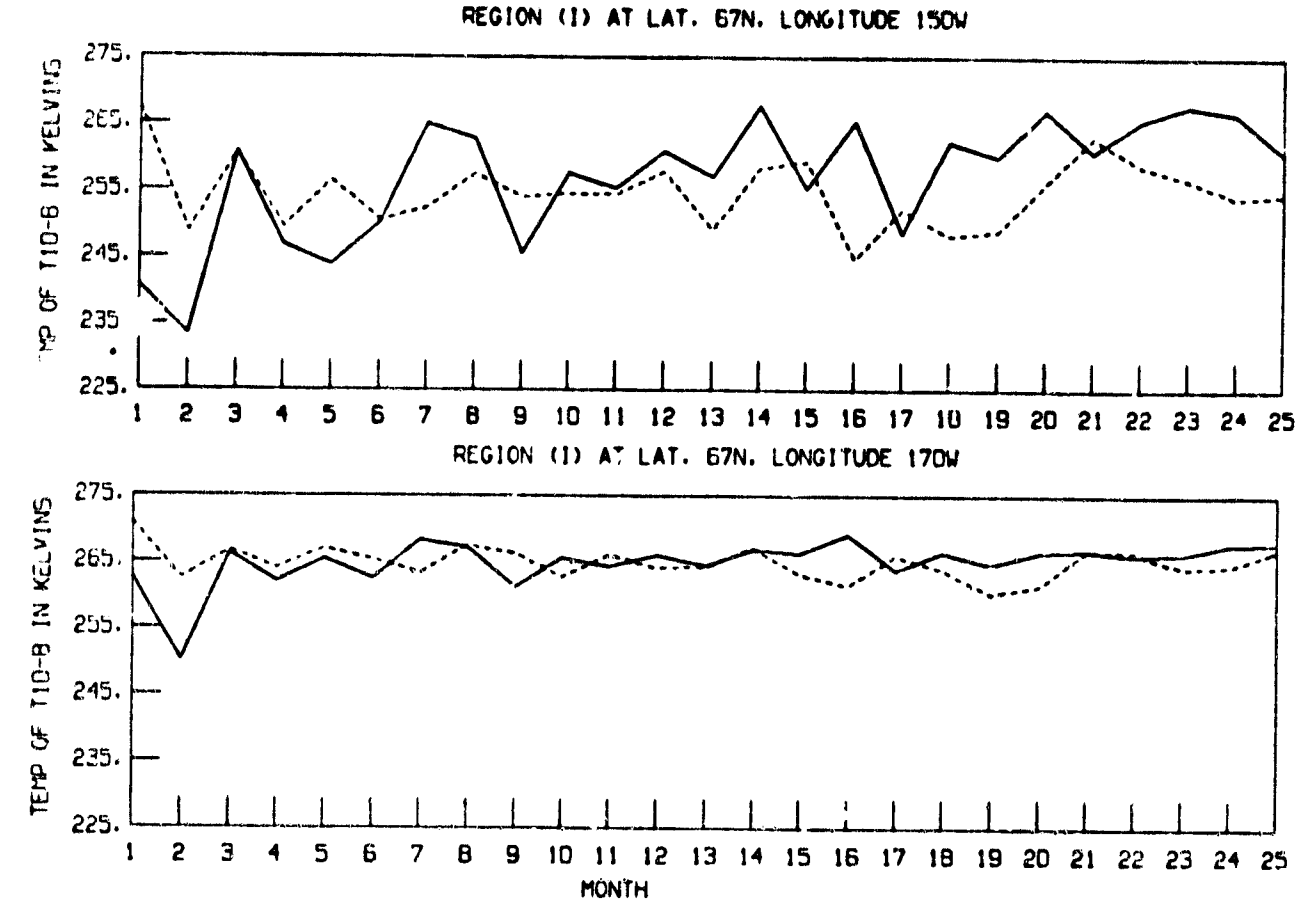

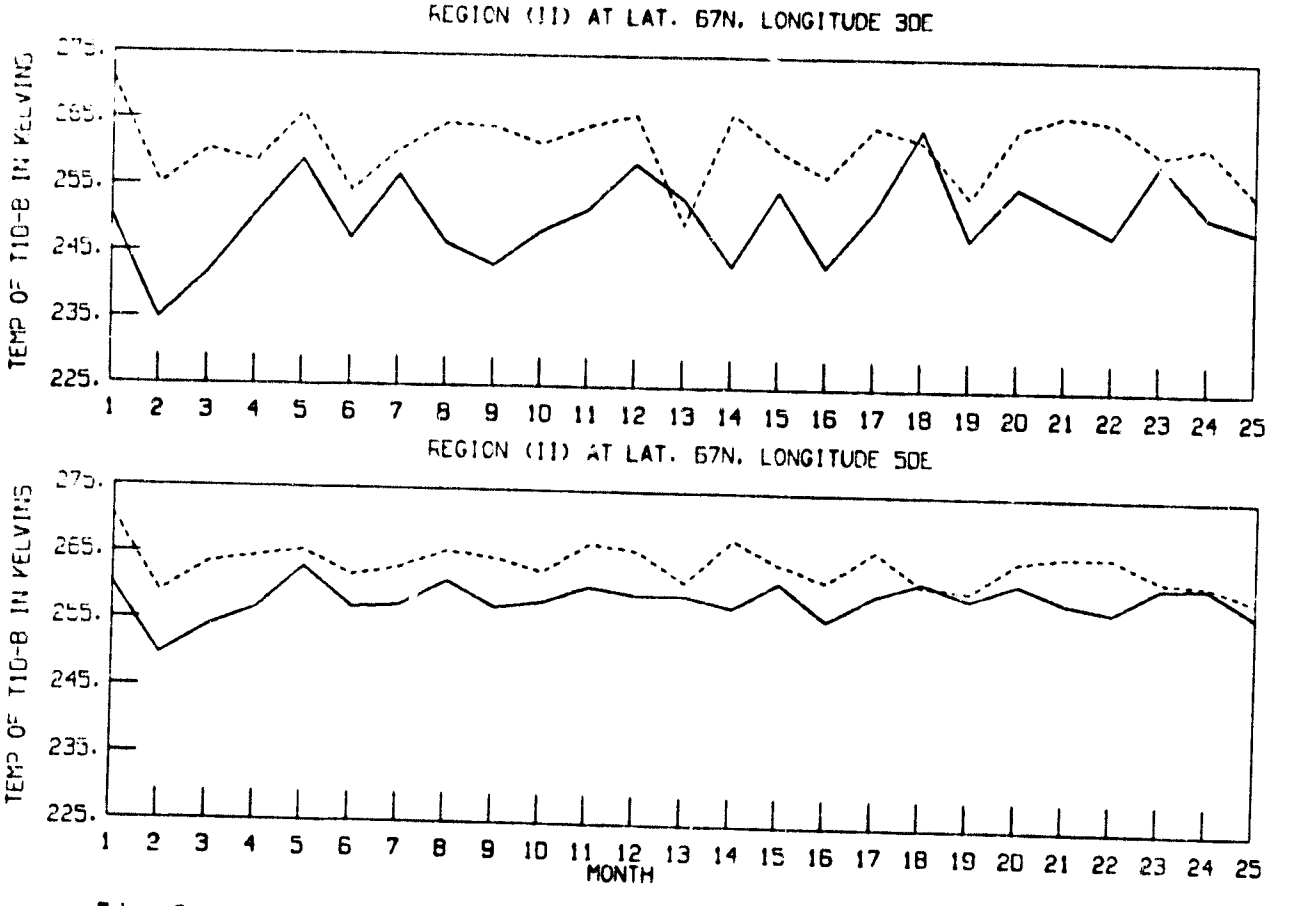

Fig. 3g Time series of T10-8 for runs 2 and 3 in region (i) and region (ii).

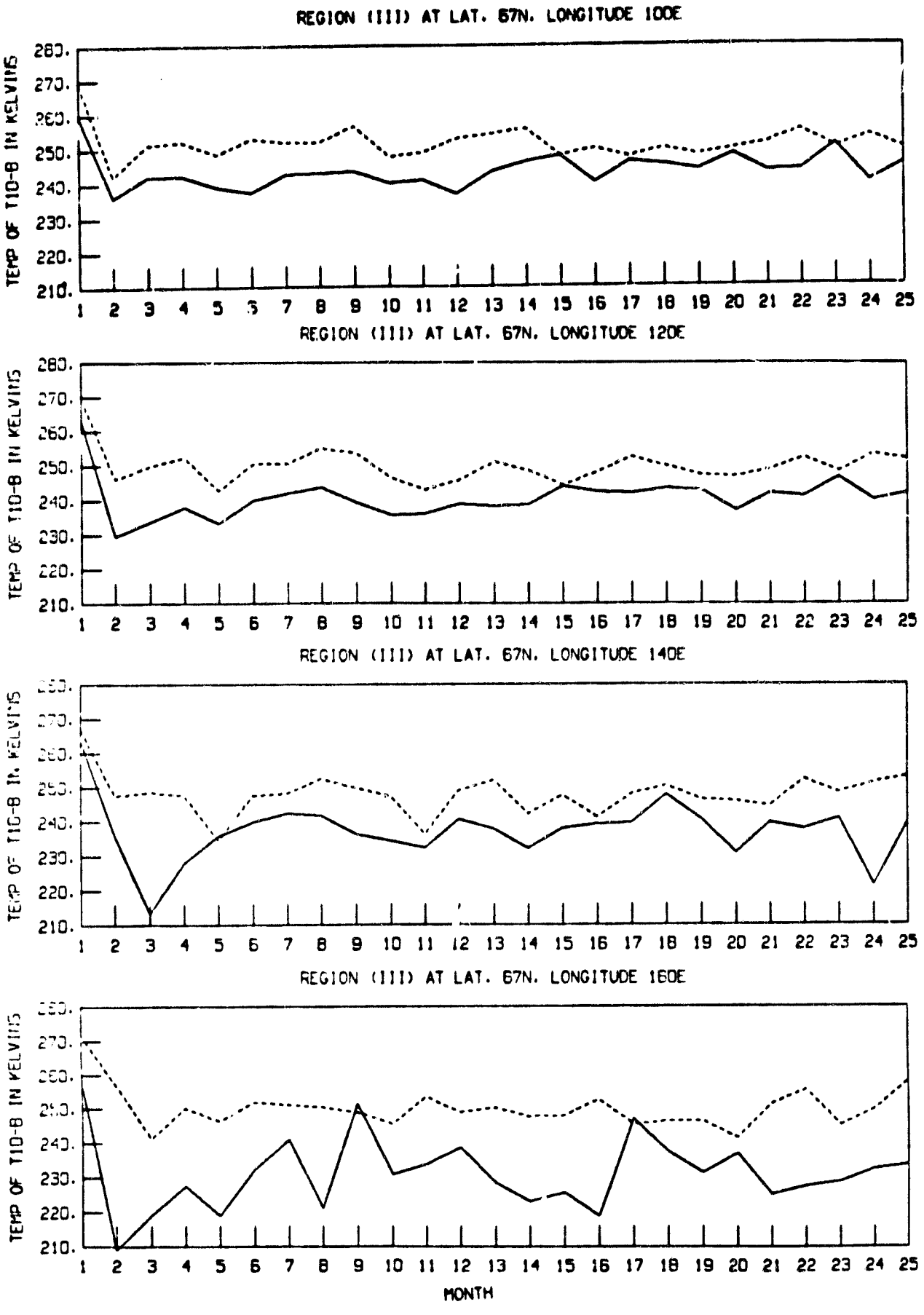

Fig. 3h Time series of T10-8 for runs 2 and 3 in region (iii).

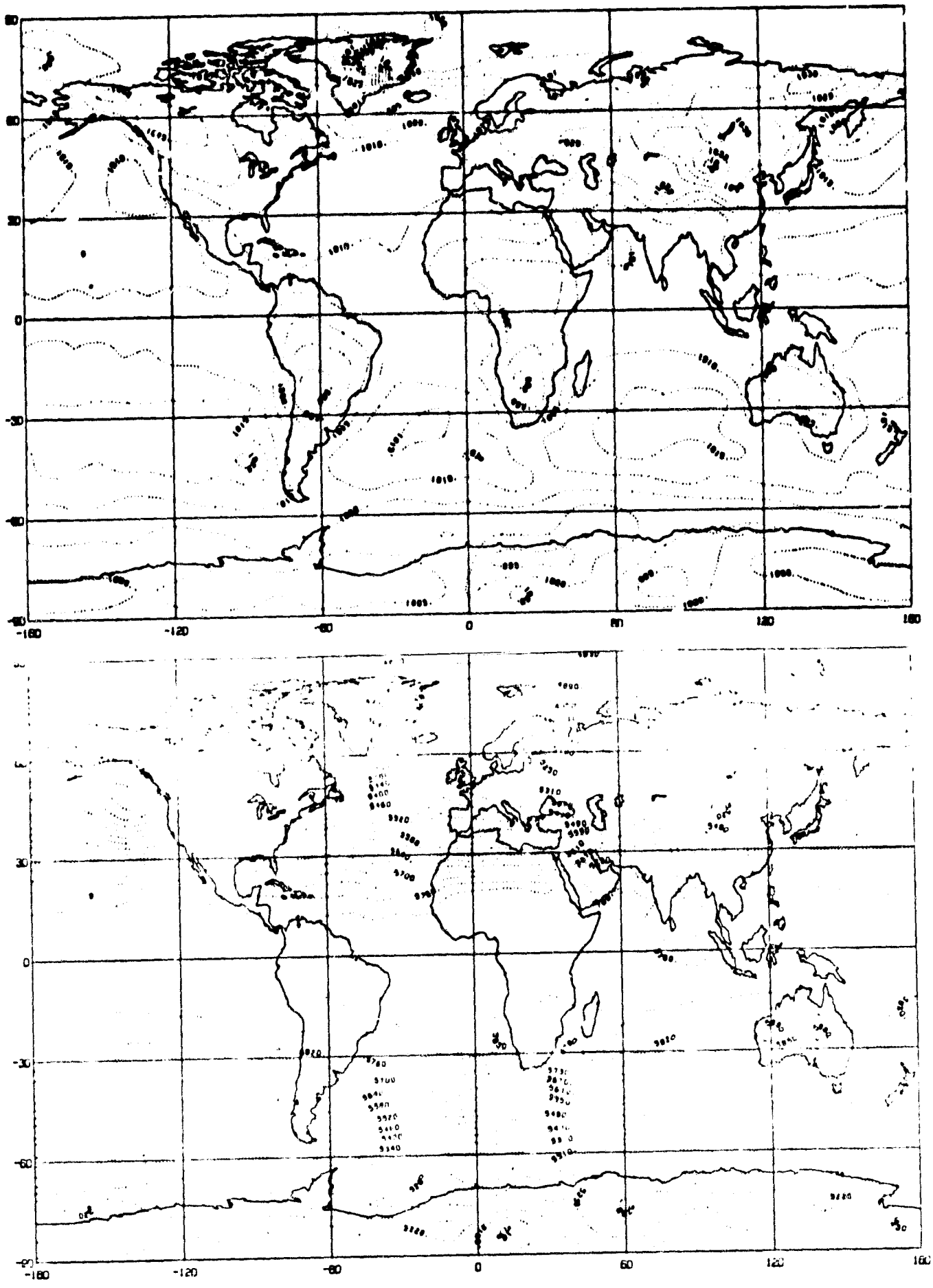

Fig. 3i (Top) Mean SLP for run 3 (mb).
(Bottom) Mean G500 for run 3 (m).

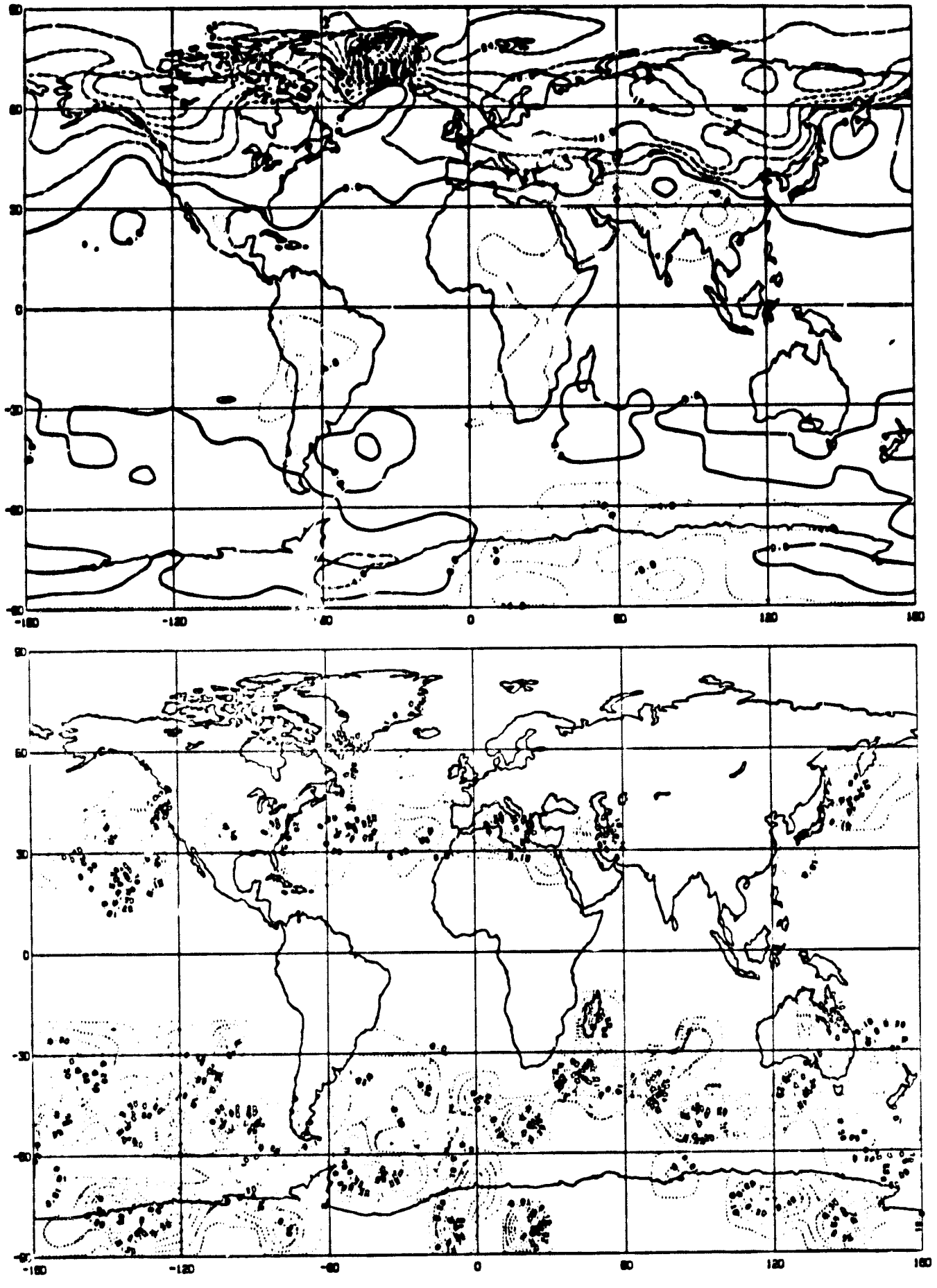

Fig. 3j SLP : (Top) Mean difference for run 3 - run 2 (mb). (Bottom) Significance level .

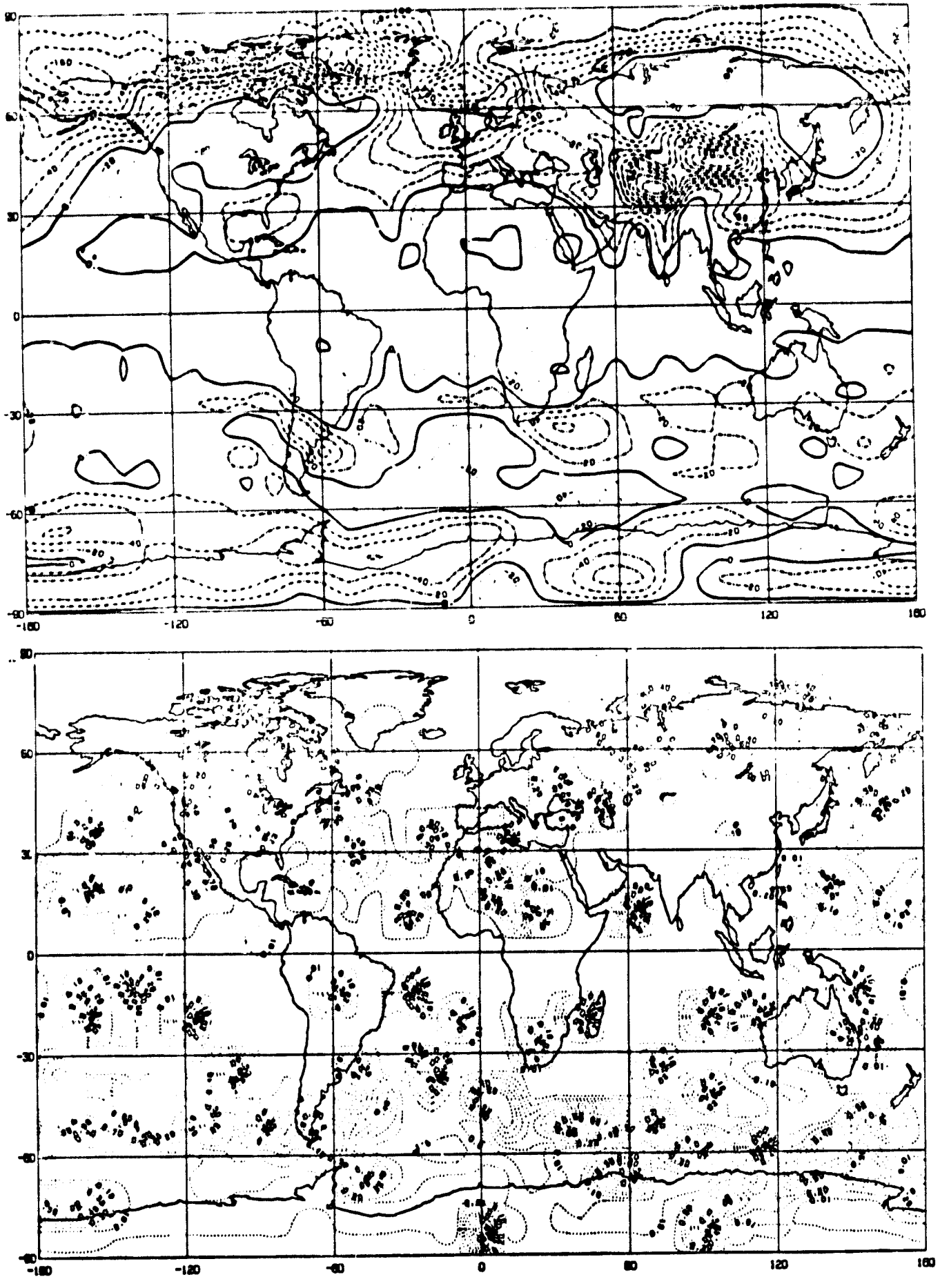

Fig. 3k G500 : (Top) Mean difference for run 3 - run 2 (m).
(Bottom) Significance level .

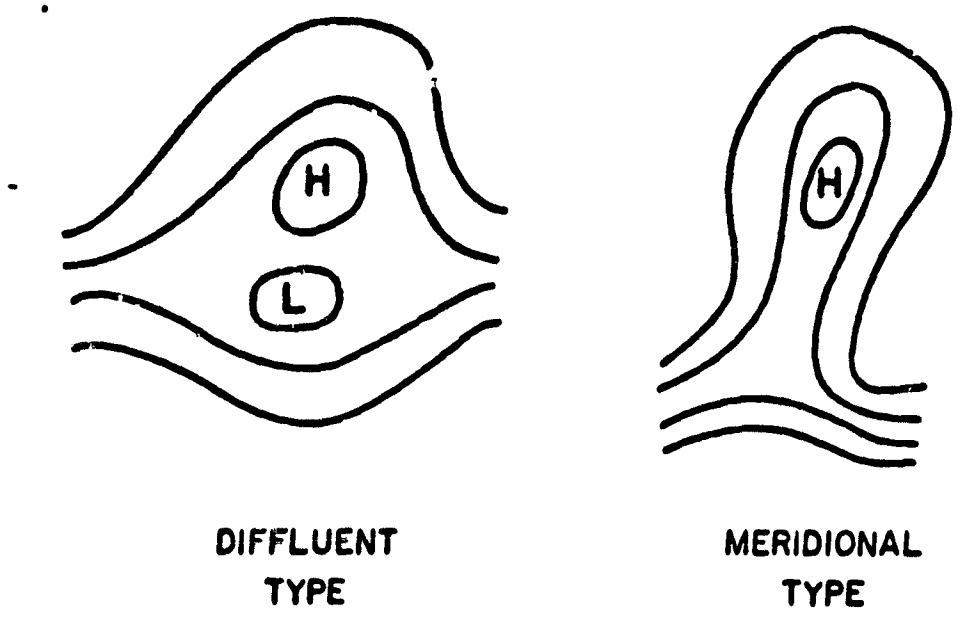

Fig. 31 Schematic representation of the two types of blocking situation, from Kasahara (1980).

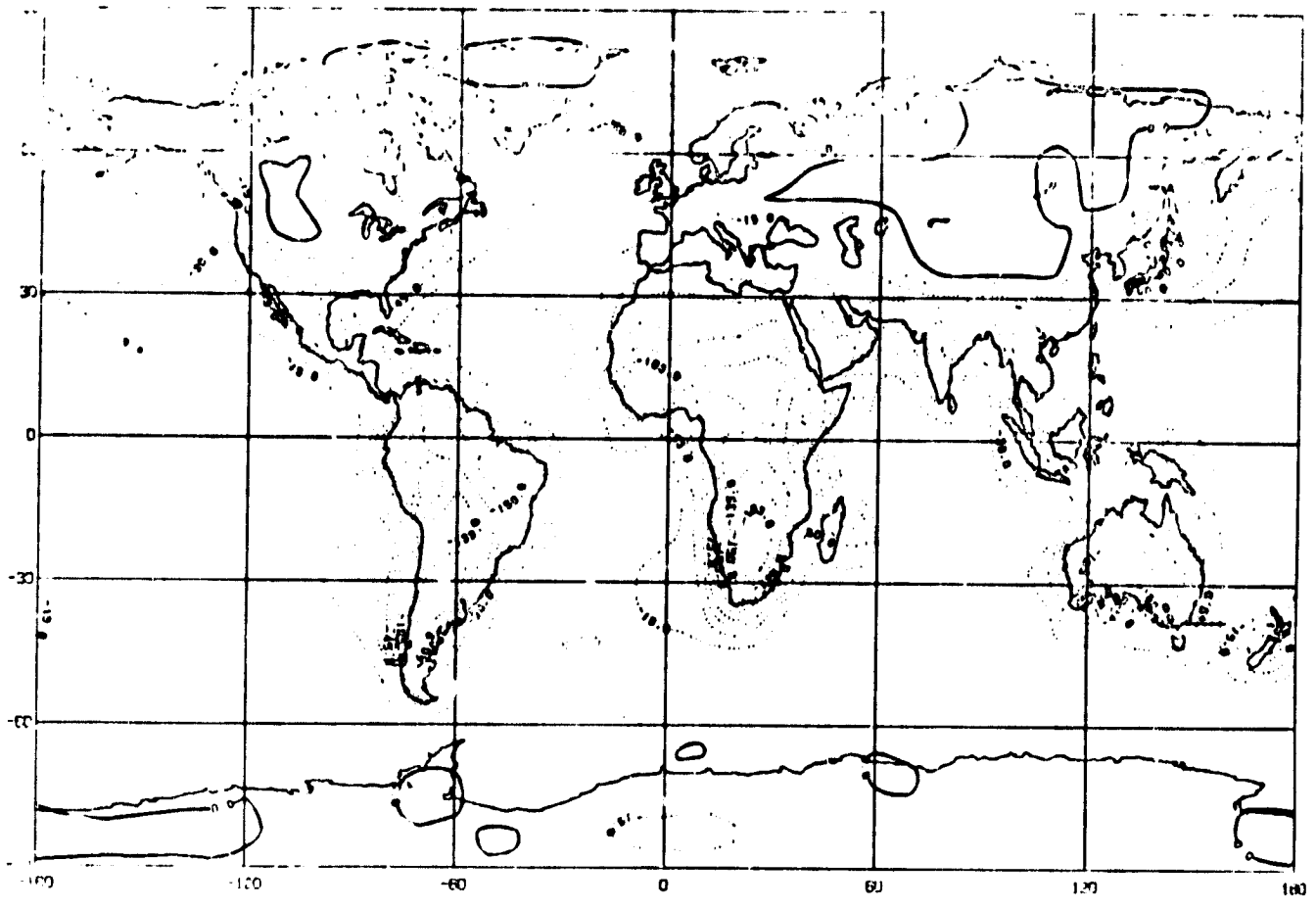

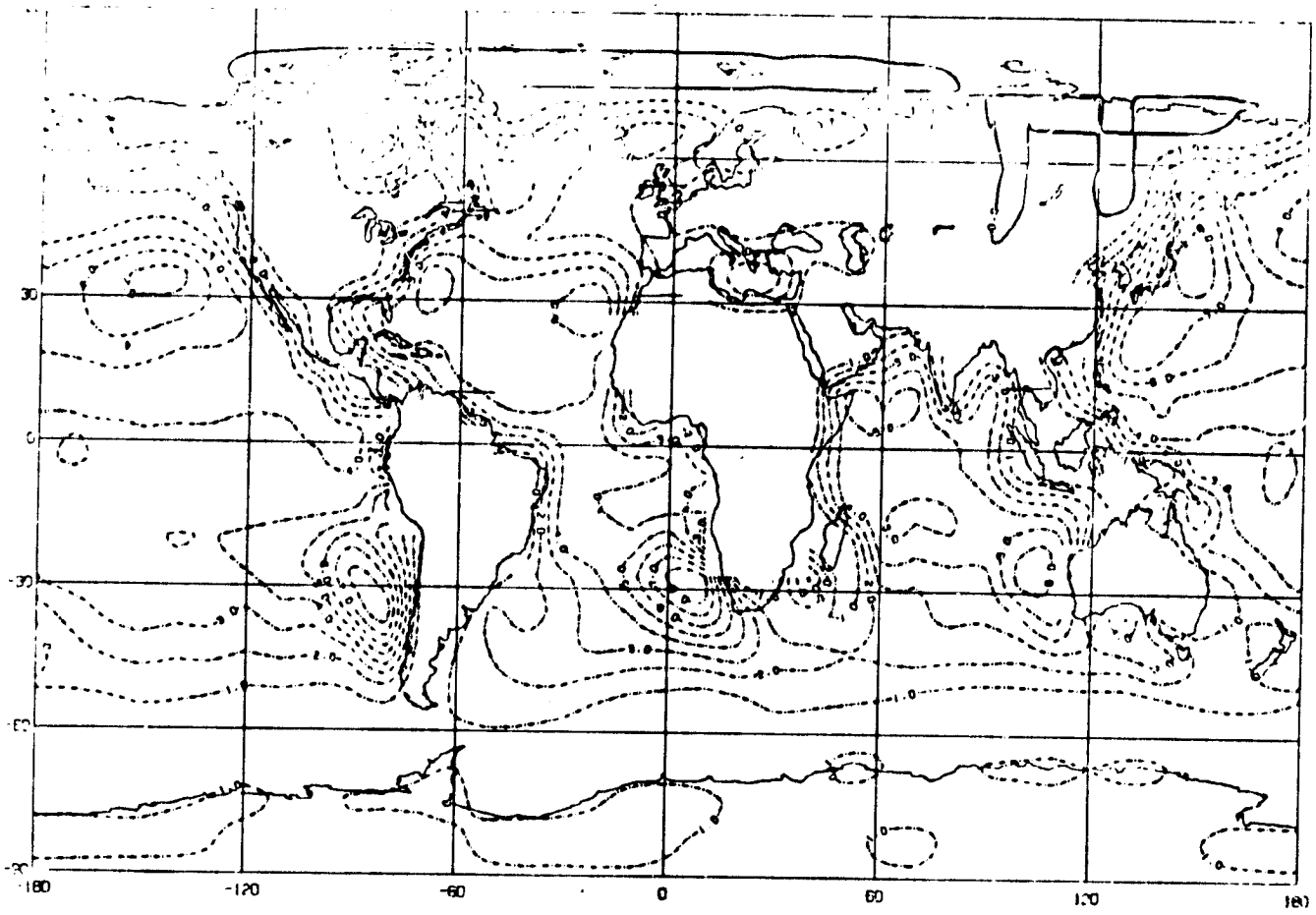

*Fig. 3m (Top) Mean sensible heat flux for run 3 (watts/m**2). (Bottom) Mean evaporation for run 3 (mm/day).*

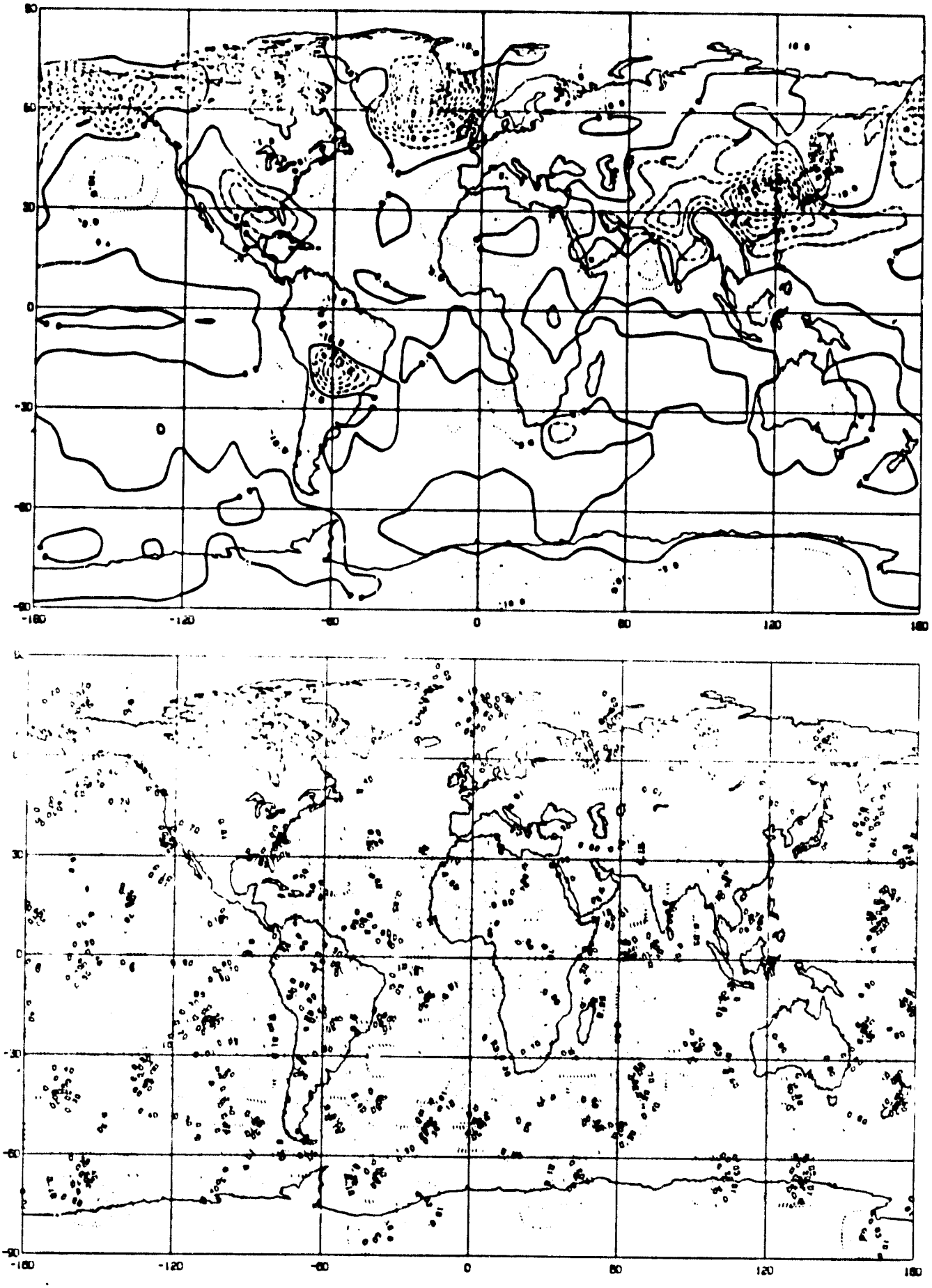

*Fig. 3n Sensible heat flux: (Top) Mean difference for run 3 - run 2 (watts/m**2). (Bottom) Significance level .*

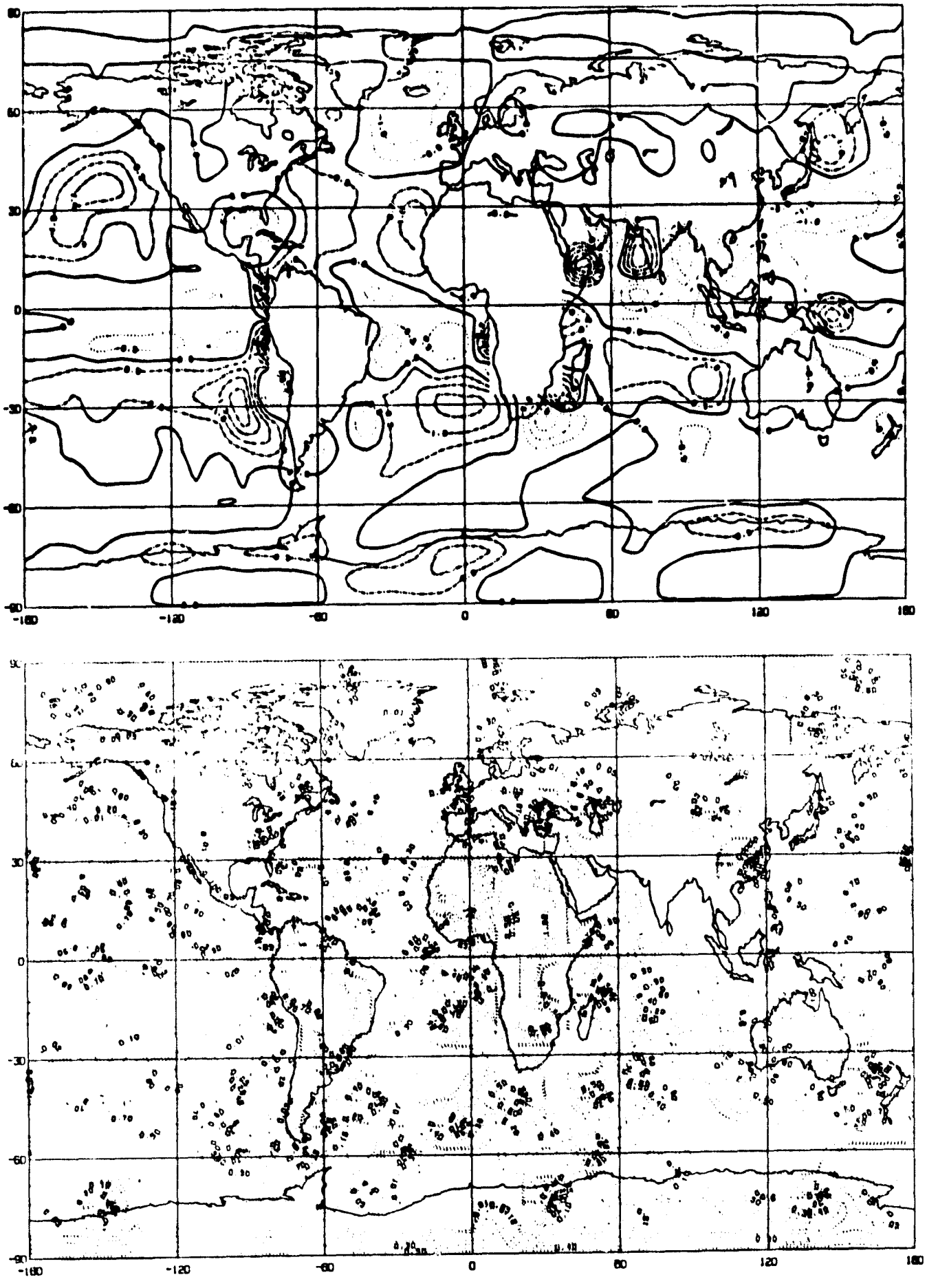

Fig.3o Evaporation : (Top) Mean difference for run 3 - run 2 (mm/day). (Bottom) Significance level .

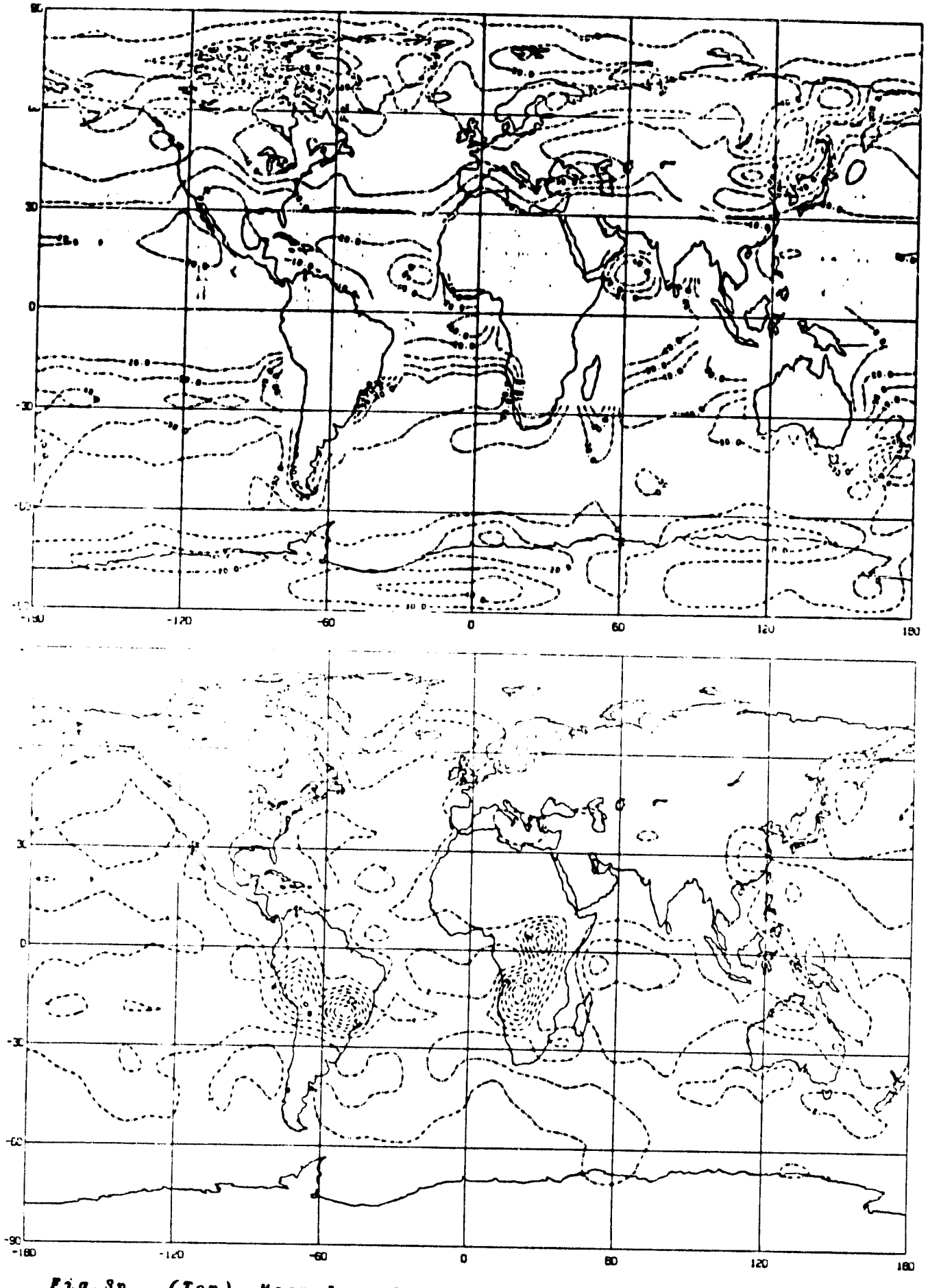

Fig. 3p *(Top) Mean low cloud cover for run 3 (percent). (Bottom) Mean precipitation for run 3 (mm/day).*

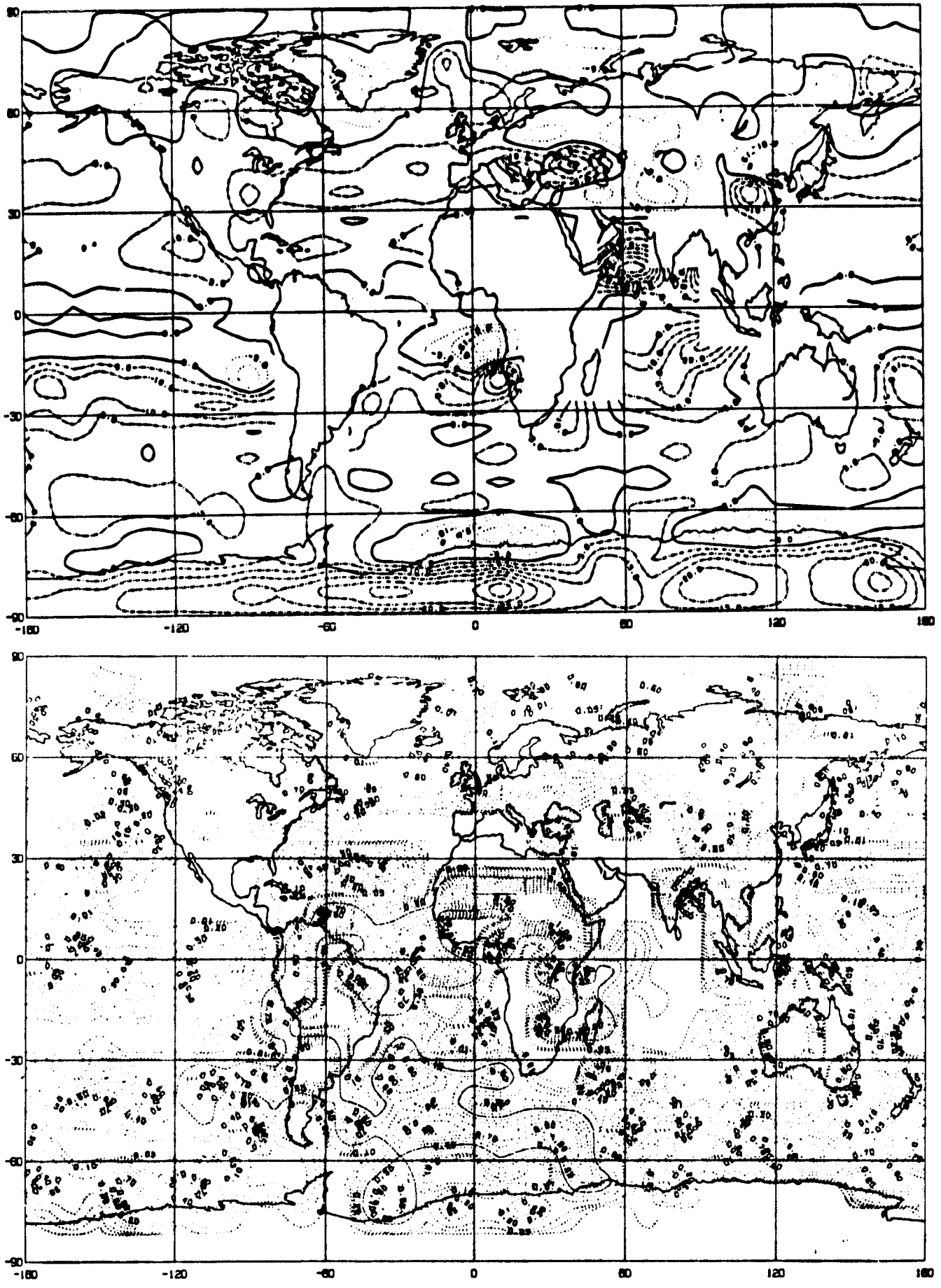

Fig. 3q Low cloud cover: (Top) Mean difference for run 3 - run 2 (percent). (Bottom) Significance level .

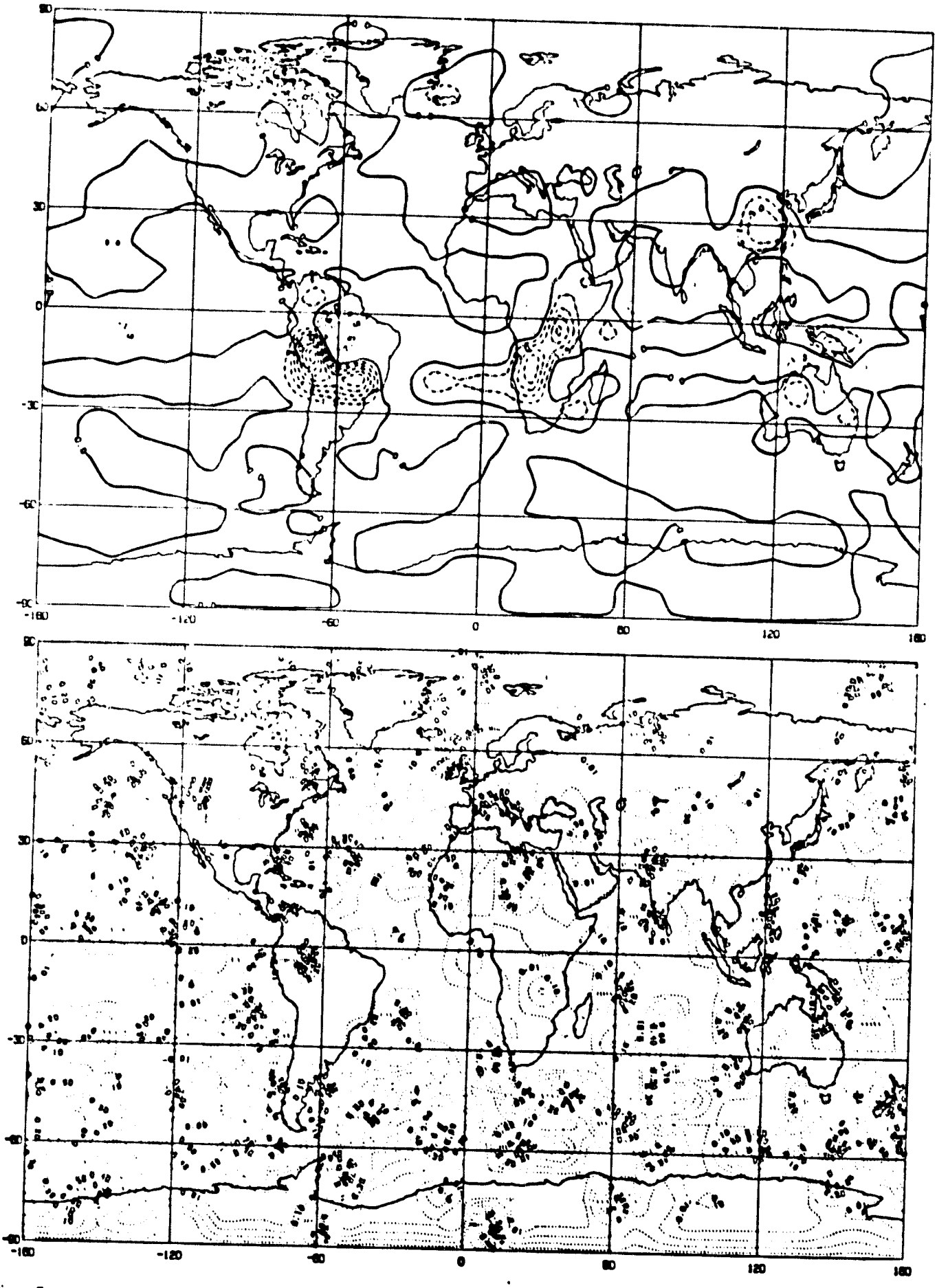

Fig.3r precipitation : (Top) Mean difference for run 3 - run 2 (mm/day).
(Bottom) Significance level .

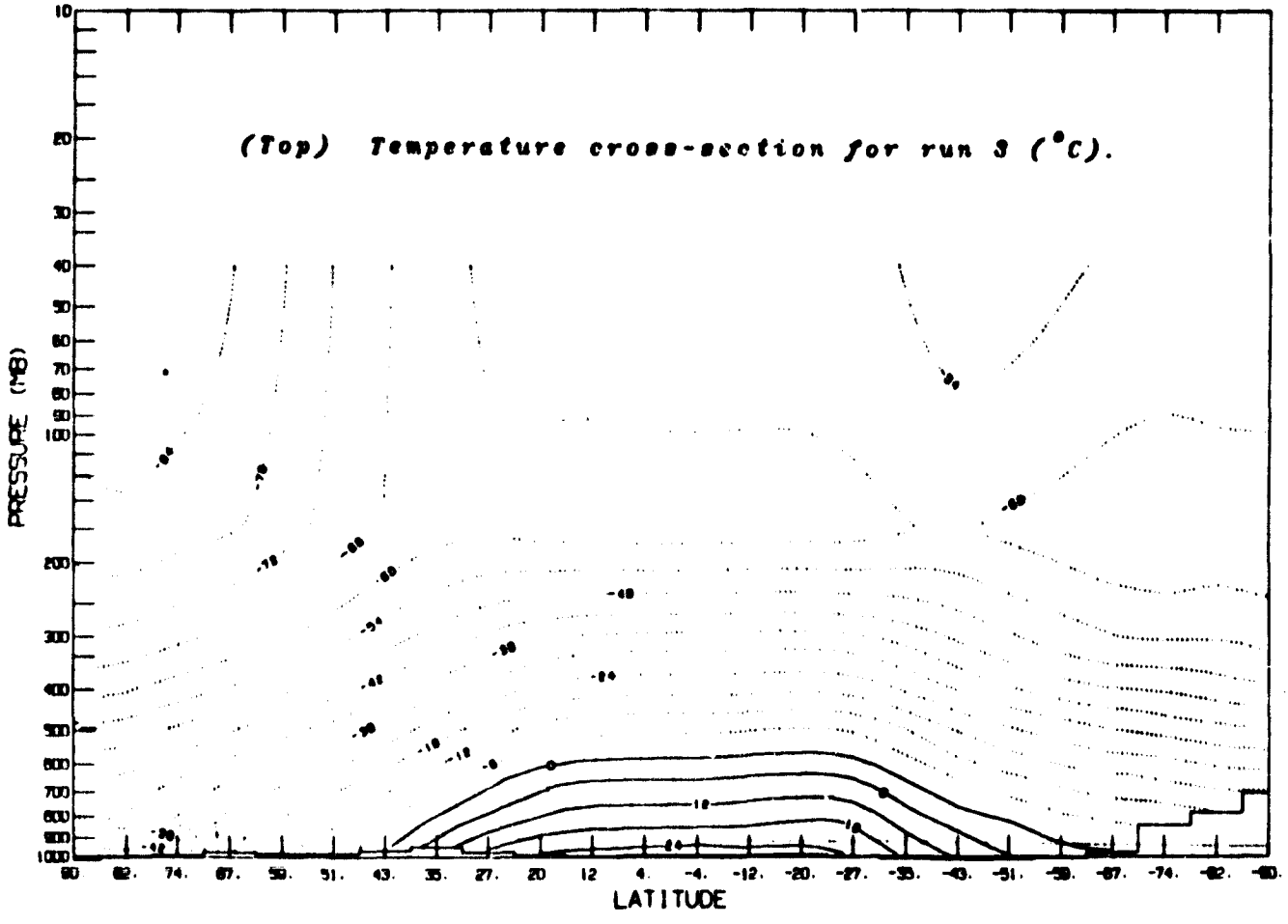
(Top) Temperature cross-section for run 3 (°C).
PRESSURE (MB)
LATITUDE

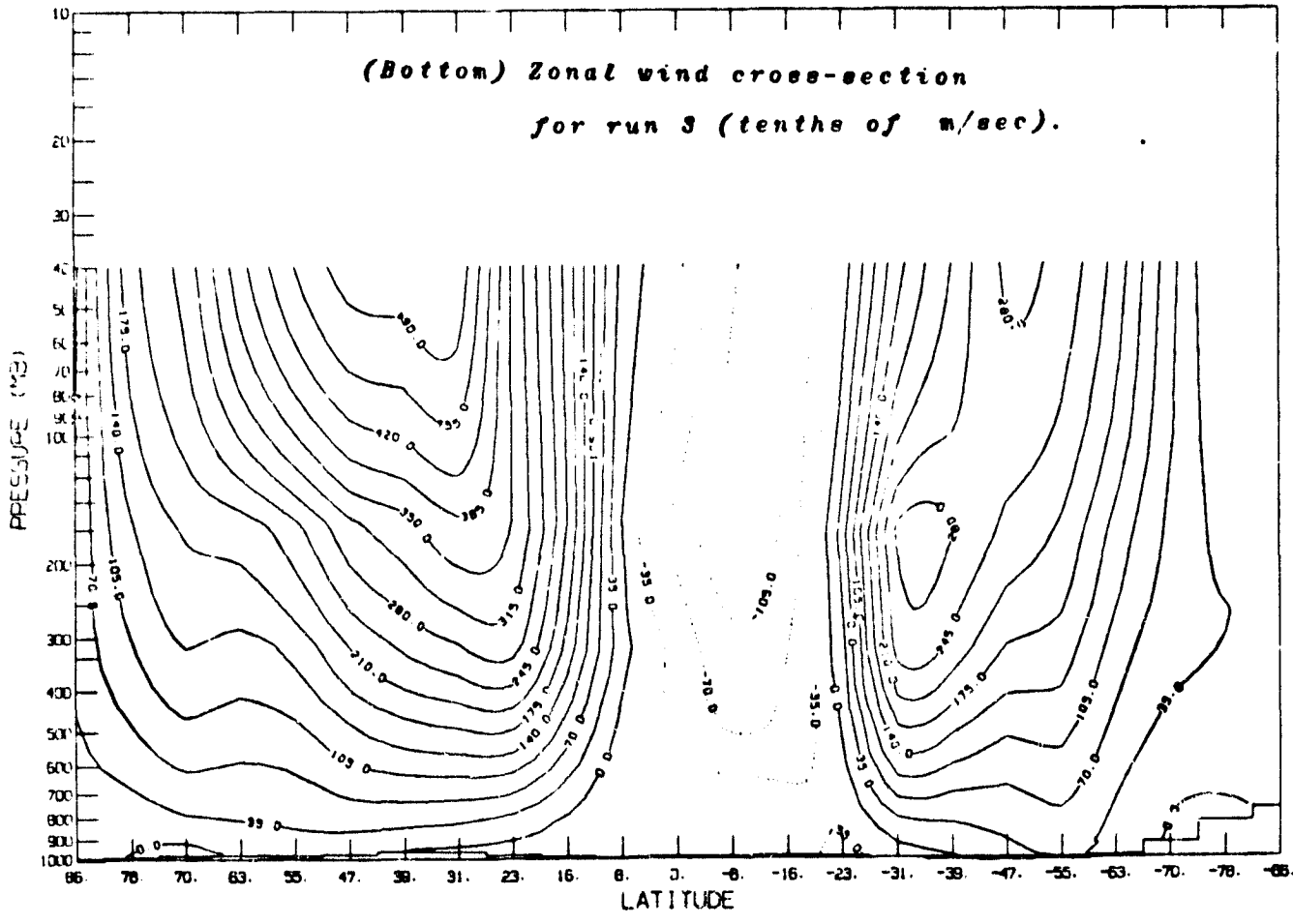
(Bottom) Zonal wind cross-section
for run 3 (tenths of m/sec).
PRESSURE (MB)
LATITUDE

Fig. 3a

Temperature :

(Top) Mean difference for run 3 - run 2 (tenths of °C).

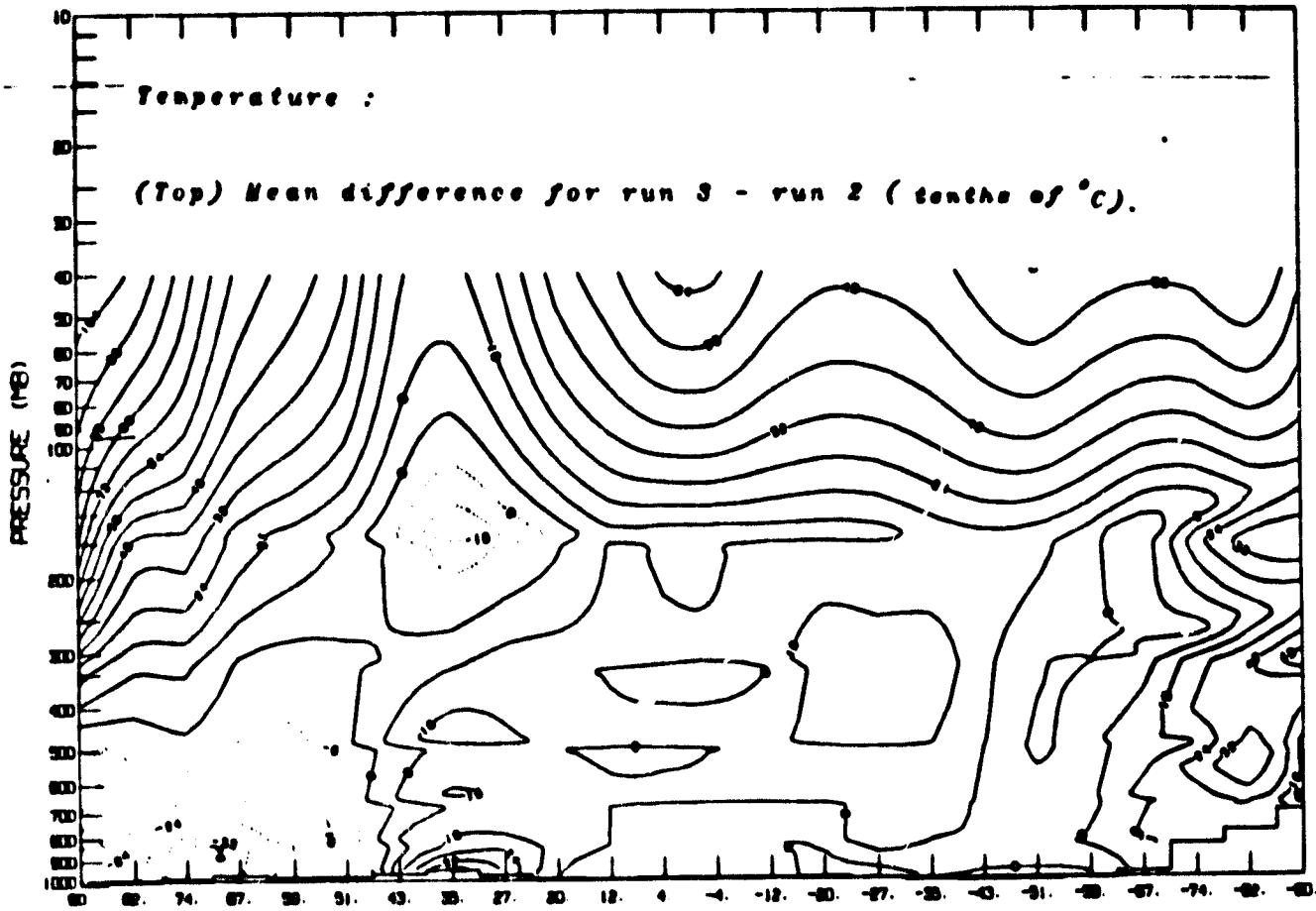

(Bottom) Significance level .

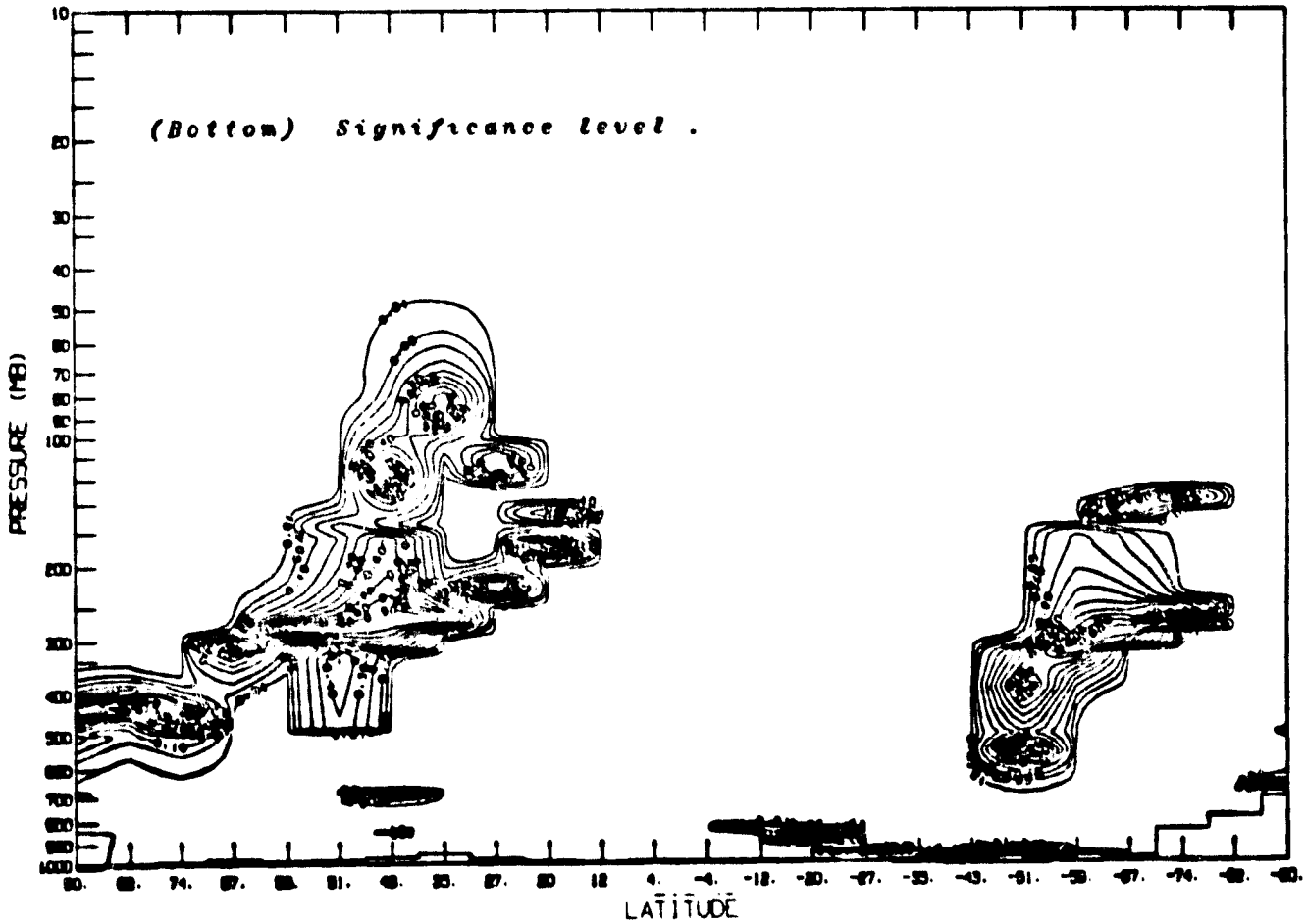

Fig. 3t

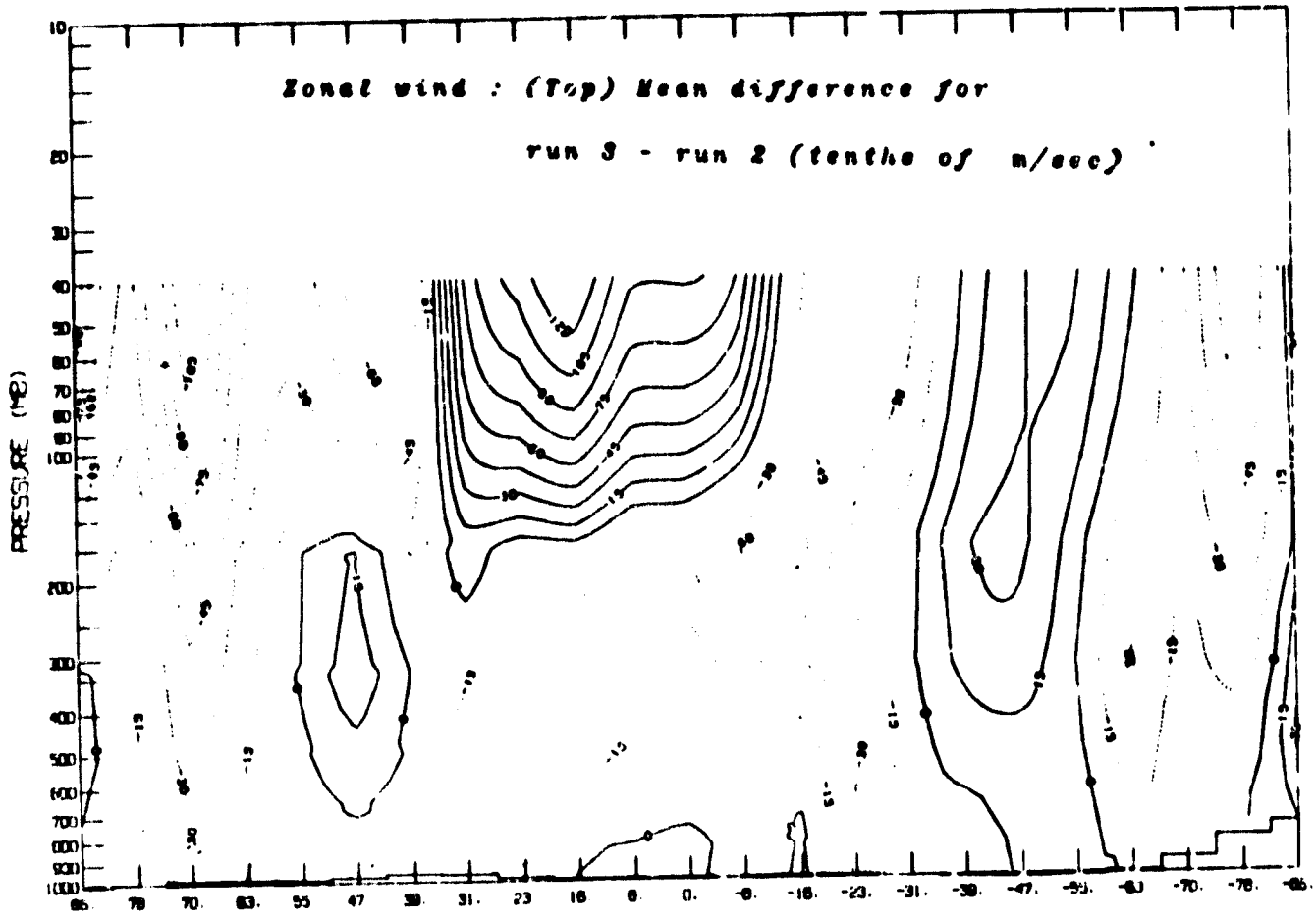
Zonal wind : (Top) Mean difference for
run 3 - run 2 (tenths of m/sec)
PRESSURE (MB)

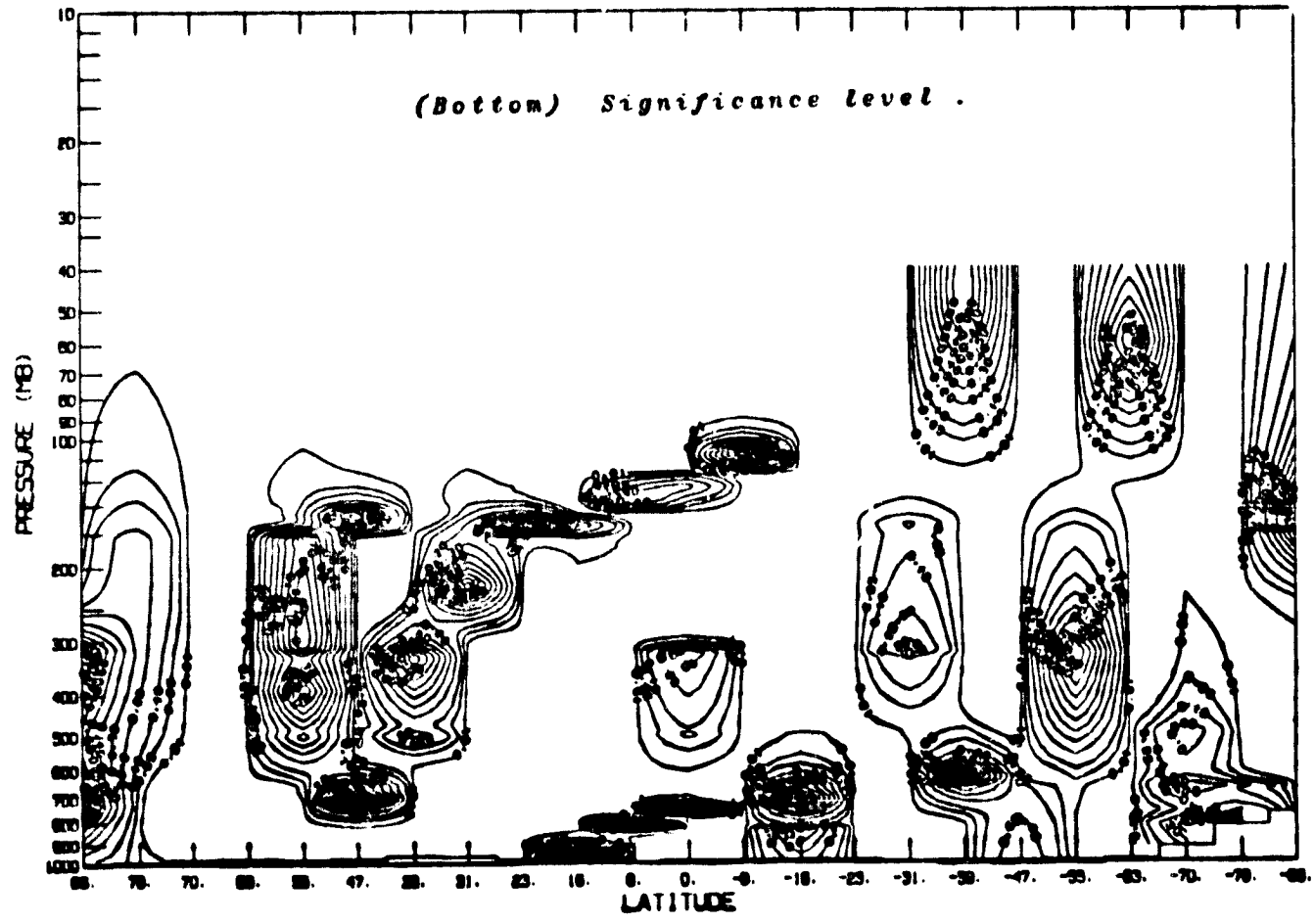
(Bottom) Significance level .
PRESSURE (MB)
LATITUDE

Fig. 3a

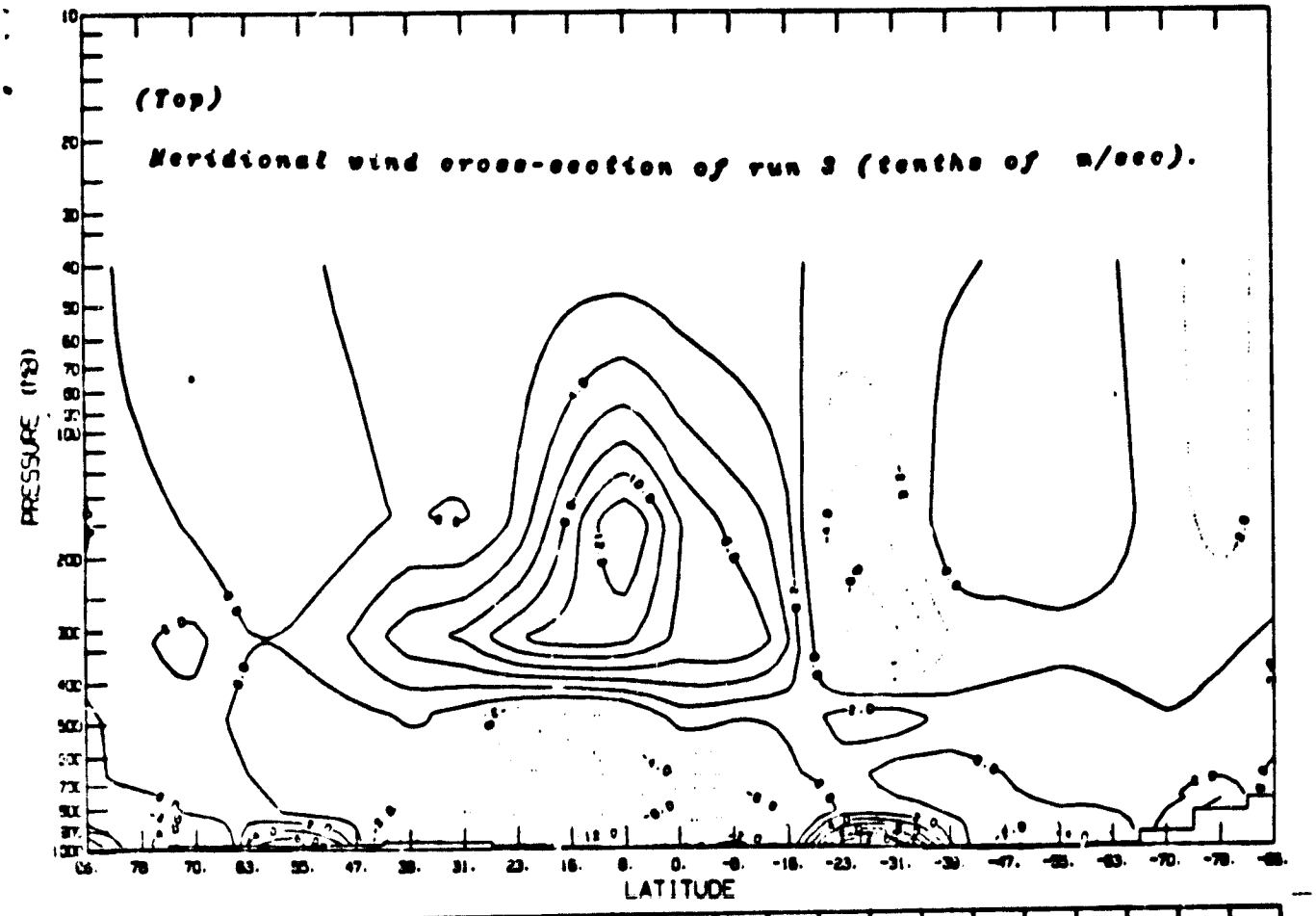
(Top)
Meridional wind cross-section of run 3 (tenths of m/sec).
PRESSURE (MB)
LATITUDE

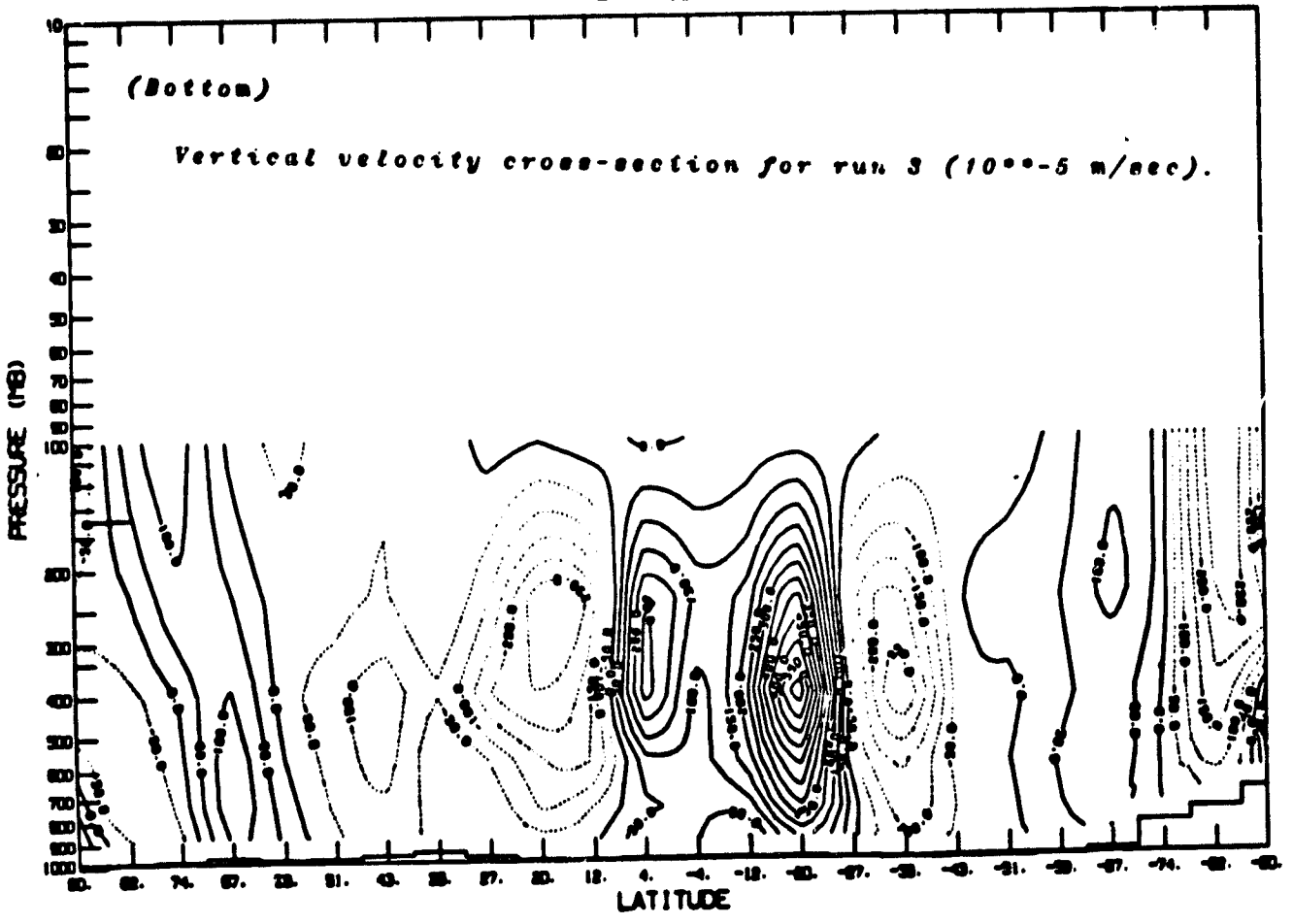
(Bottom)
Vertical velocity cross-section for run 3 (10**-5 m/sec).
PRESSURE (MB)
LATITUDE

Fig. 3v

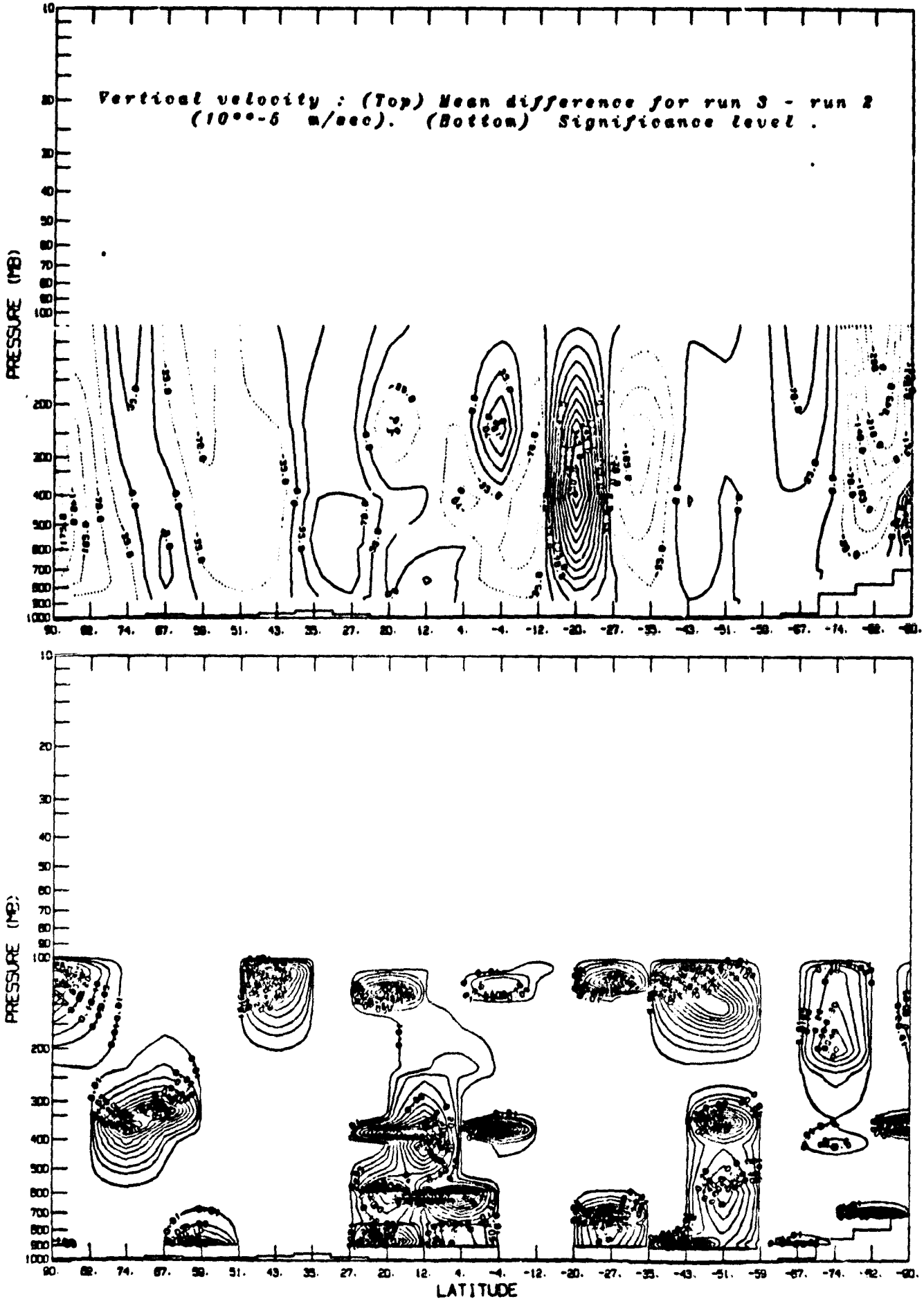
Vertical velocity : (Top) Mean difference for run 3 - run 2
(10**-5 m/sec). (Bottom) Significance level .
PRESSURE (MB)
LATITUDE

Fig. 3x

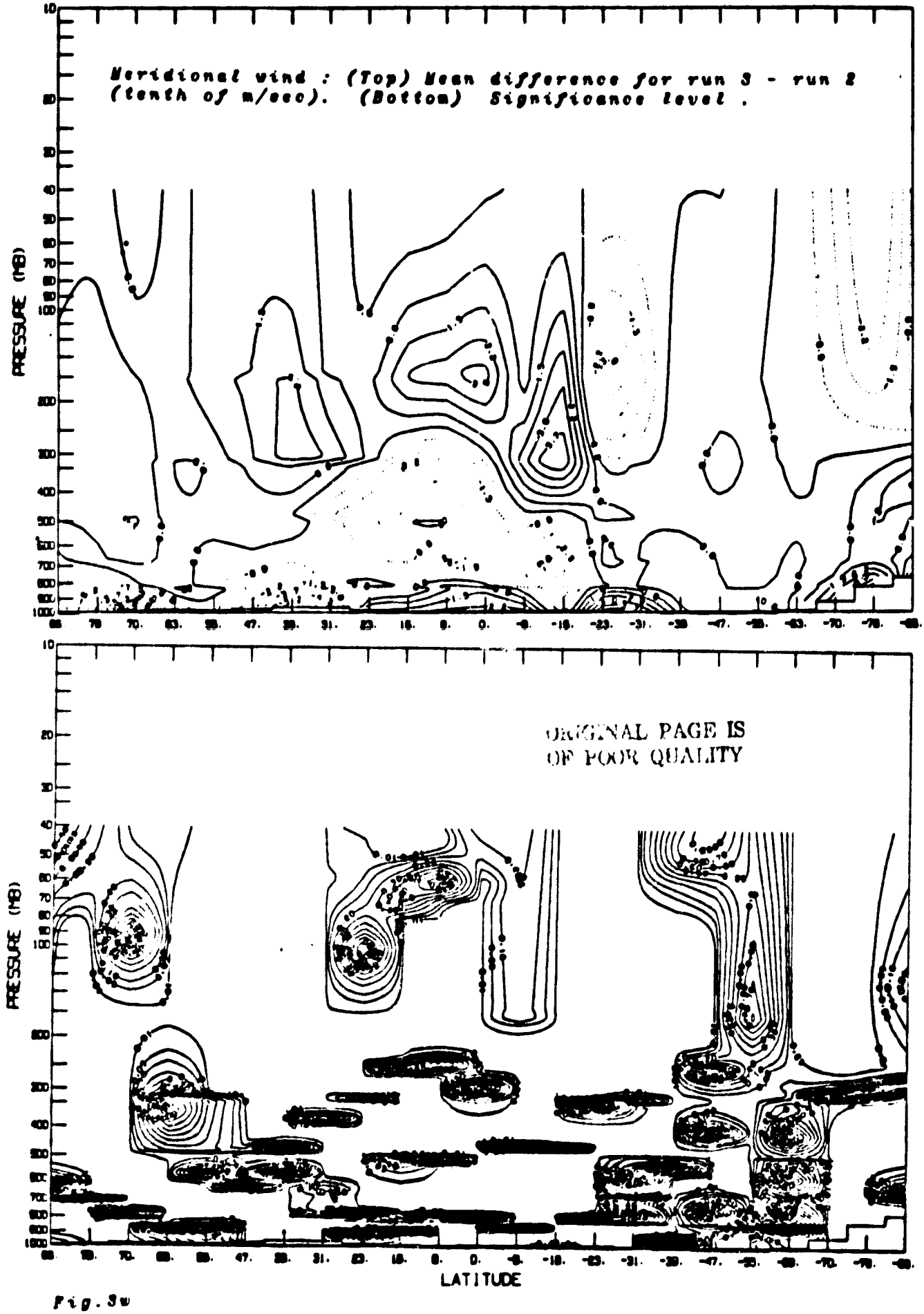

Fig. 3w